

THE UNIVERSITY OF MICHIGAN
COLLEGE OF ENGINEERING
Department of Aeronautical and Astronautical Engineering
Aircraft Propulsion Laboratory

Technical Report

THE INFLUENCE OF A COMPRESSIBLE BOUNDARY ON
THE PROPAGATION OF GASEOUS DETONATIONS

11/1/63 (E. K. Dabora K. Hedhory)
E. K. Dabora

ORA Project 05170

under contract with:

U. S. ARMY RESEARCH OFFICE (DURHAM)
CONTRACT NO. DA-ARO(D)-31-124-G-345
PROJECT NO. 3559-E
DURHAM, NORTH CAROLINA

administered through:

OFFICE OF RESEARCH ADMINISTRATION

ANN ARBOR

December 1963

en8n

UMRQ607

This report was also a dissertation submitted in partial fulfillment of the requirements for the degree of Doctor of Philosophy in The University of Michigan; 1963.

ACKNOWLEDGMENTS

The author is grateful to The University of Michigan Institute of Science and Technology for its financial assistance to conduct feasibility experiments in connection with this work. The major portion of this work, however, was made possible by Grant No. DA-ARO(D)-31-124-G-345 from the U. S. Army Research Office (Durham) whose financial help is gratefully appreciated.

The work reported herein served as my doctoral dissertation and, therefore, I wish to express my indebtedness to the following members of the faculty of The University of Michigan who served on my thesis committee: Professors W. Mirsky, R. B. Morrison (co-chairmen), T. C. Adamson, Jr., S. W. Churchill and J. A. Nicholls. In particular, I wish to express my thanks to Professor J. A. Nicholls, Supervisor of the Aircraft Propulsion Laboratory and Project Supervisor, for his continued guidance and assistance.

Thanks are also due to several members of the Laboratory for their kind assistance at one time or other. In particular, Mr. B. Kerkam, Assistant in Research, was extremely helpful in conducting the experiments and reducing the data.

TABLE OF CONTENTS

	<u>Page</u>
ACKNOWLEDGMENTS.....	ii
LIST OF TABLES.....	v
LIST OF FIGURES.....	vi
NOMENCLATURE.....	ix
ABSTRACT.....	xiii
 I INTRODUCTION.....	 1
II GENERAL CHARACTERISTICS OF GASEOUS DETONATION WAVES.....	 5
2.1 One Dimensional Waves.....	5
2.2 Classification of Detonation Waves.....	9
2.3 Detonation Waves Bounded by an Inert Gas.....	11
a. Effect of an Area Change on the Propagation of a Detonation Wave.....	 11
b. Degree of Confinement and Explosive Deflection Angle.....	 20
c. Shock Angle in the Inert Boundary Gas.....	27
d. Determination of the Detonation Wave Velocity Decrement.....	 33
III CHEMICAL ASPECTS AND QUENCHING CRITERIA.....	36
3.1 Shchelkin's Instability Criterion.....	36
3.2 Belles' Explosion Limit Criterion.....	39
3.3 Patch's Constant Temperature Criterion.....	43
IV EXPERIMENTAL REQUIREMENTS AND ARRANGEMENT.....	46
4.1 Preliminary Experiments.....	46
4.2 Separation of the Explosive from the Inert by a Thin Membrane or Film.....	 51
4.3 Analytical Determination of the Critical Thickness of Thin Films.....	 54
4.4 Preparation of Thin Films and Estimation of Their Thickness.....	 62
4.5 Diffusion Through Thin Films.....	68
4.6 Experimental Arrangement and Procedure.....	74

TABLE OF CONTENTS (CONT'D)

		<u>Page</u>
V	EXPERIMENTAL RESULTS AND DISCUSSION.....	87
5.1	Critical Channel Widths of $H_2 - O_2$ Mixtures When Bounded by Nitrogen.....	87
5.2	Velocity Decrement of Stoichiometric $H_2 - O_2$ When Bounded by Nitrogen and Inferred Reaction Length.....	91
5.3	Behavior of Detonation Waves at Channel Widths Close to the Critical.....	99
5.4	Velocity Decrement of $H_2 - O_2$ Mixtures Bounded by Nitrogen Near Their Respective Critical Channel Widths.....	108
5.5	Estimation of the Reaction Length in the Stoichio- metric Methane Oxygen Mixture.....	113
5.6	Behavior of Detonation Waves When the Density of the Boundary Gas is Much Lower Than That of the Explosive.....	117
5.7	Experimental Interface Angles and Inert Shock Angles.....	124
VI	CONCLUSIONS.....	128
	APPENDIX A - Error Analysis.....	130
	BIBLIOGRAPHY.....	135

LIST OF TABLES

<u>Table</u>		<u>Page</u>
I	Hydrogen-Oxygen Composition Limits.....	45
II	Evaluation of the Functions ϕ_1 and ϕ_2	58
III	Color-Thickness Correlation for Thin Films.....	66
IV	Summary of the Experimental Results Obtained for the Stoichiometric $H_2 - O_2$ Bounded by N_2	98
V	Summary of the Experimental Results Obtained for $H_2 - O_2$ Mixtures Bounded by N_2	111

LIST OF FIGURES

<u>Figure</u>		<u>Page</u>
1	One Dimensional Detonation Wave.....	6
2	Hugoniot Rayleigh Representation of Shock and Detonation Waves.....	6
3	Idealized Flow Model of Detonation Wave - Boundary Interaction.....	13
4	Typical Photograph of the Interaction Process (Reference 31).....	14
5	Idealized Flow Model of Detonation Wave - Boundary Interaction with Finite Reaction Length.....	16
6	Shock Tube Analogy to the Interaction Process.....	22
7	Variation of Non-Dimensional Pressure Ratio, \bar{P} , with the Density Parameter.....	25
8	Variation of Tangent of Interface Angle with the Density Parameter.....	28
9	Wave Refraction at the Interface of Two Media.....	30
10	Relationship of Refracted to Incident Wave as a Function of the Density Parameter.....	32
11	Detonation Wave Velocity Decrement as a Function of the Area Increment.....	35
12	Dependence of the Detonation and the Critical Mach Numbers on Hydrogen-Content in $H_2 - O_2$ Mixtures.....	40
13	Critical Mach Numbers According to Belles' Explosion Limit Criterion.....	42
14	Schematic Drawing of the Test Section Used in the Preliminary Experiments.....	48
15	Photograph of the Test Section Used in the Preliminary Experiments.....	49
16	Detonation Wave Progress of Stoichiometric $H_2 - O_2$ Mixture in Channels of Two Different Widths, Boundary Gas = N_2	50

LIST OF FIGURES (CONT'D)

<u>Figure</u>		<u>Page</u>
17	Detonation Wave Appearance When Confined by a Soap Film.....	53
18	Analogy of the Piston Path in a Shock Tube to the Film Position.....	55
19	Instantaneous Film Velocity vs. Its Acceleration.....	59
20	Film Holder.....	64
21	Dependence of Film Thickness on Collodion Concentration in Amyl Acetate Times Number of Drops.....	67
22	Concentration Distribution Due to Diffusion.....	71
23	Schematic Diagram of Mixing and Charging System.....	75
24	Test Section Assembly.....	77
25	Photograph of the Test Section.....	78
26	Schlieren System and Block Diagram of Instrumentation for Spark Pictures.....	81
27	Schlieren System and Block Diagram of Instrumentation for Streak Pictures.....	84
28	Typical Spark Photographs of a Quenched and an Unquenched Detonation Wave.....	88
29	Critical Channel Widths of $H_2 - O_2$ Mixtures Bounded by Nitrogen.....	90
30	Streak Photographs of a Detonation Wave in Stoichiometric $H_2 - O_2$ ($b = 0.5$ in.).....	93
31	Pertinent Dimensions Helpful for the Interpretation of Streak Photographs.....	94
32	Streak Photographs of a Detonation Wave in Stoichiometric $H_2 - O_2$ ($b = 0.2$ in.).....	95
33	Variation of Detonation Velocity Decrement with Channel Width.....	100
34	Streak Photograph of a Quenching Detonation Wave in Stoichiometric $H_2 - O_2$ with Nitrogen Boundary.....	101

LIST OF FIGURES (CONT'D)

<u>Figure</u>		<u>Page</u>
35	Streak Photograph of a Detonation Wave in Stoichiometric $H_2 - O_2$ and of Attendant Shock Wave in the Nitrogen Boundary (Double Slit).....	103
36	A Guide for the Interpretation of "Double Slit" Streak Photographs.....	104
37	Streak Photograph of a Detonation Wave in Stoichiometric $H_2 - O_2$ with Nitrogen Boundary Showing Spin Characteristics.....	106
38	Streak Photograph of a Detonation Wave in 46.3% $H_2 - 53.7\% O_2$ with Nitrogen Boundary.....	109
39	Streak Photograph of a Detonation Wave in 75% $H_2 - 25\% O_2$ with Nitrogen Boundary.....	110
40	Streak Photographs of a Detonation Wave in Stoichiometric $CH_4 - O_2$ and of Attendant Shock Wave in the Boundary Gas (Double Slit).....	114
41	Spark Photographs of a Detonation Wave in 75% $H_2 - 25\% O_2$ Mixture (b = 0.3 in.) - (a) Hydrogen Boundary, (b) Helium Boundary.....	119
42	Spark Photograph of a Detonation Wave in 33% $CH_4 - 67\% O_2$ with Hydrogen Boundary (b = 0.5 in.).....	120
43	Spark Photograph of a Detonation Wave in 75% $H_2 - 25\% O_2$ Mixture with Hydrogen Boundary Showing an Oblique Shock in the Explosive Resulting from a Leading Shock in the Inert (b = 0.2 in.).....	122
44	Detonation Wave Progress of 75% $H_2 - 25\% O_2$ When Confined by Helium or Hydrogen.....	123
45	Experimental Results of Interface Deflection Angles.....	125
46	Experimental Results of Shock Wave Angles in the Inert Gas.....	126
47	Theoretical Detonation Wave Velocity of $H_2 - O_2$ Mixtures at One Atmosphere and 535°R.....	133

NOMENCLATURE

A	area
\AA	Angstrom units = 10^{-8} cm
a	speed of sound
b	channel width
c_p	specific heat at constant pressure
c_a, c_b	concentration of gas "a" or "b," mole fraction
c_c	volumetric concentration of collodion in amyl acetate
c_n	mass of nitrocellulose/unit volume of collodion
D_{ab}	binary diffusion coefficient
d	channel depth
E	activation energy
e	naperian base
F	function defined by Equation (2.15)
f	mole fraction
h	specific enthalpy
k	constant
k_1, k_2, etc	reaction rate constants
L	perimeter length of drum camera
ℓ_f	film thickness
M	Mach number
m	molecular weight
m, n	integers in Equation (5.4)
n	number of drops
\bar{P}	nondimensional pressure ratio defined in Equation (2.37)

P	permeability
p	pressure
q	specific heat release
R_0	universal gas constant
r	film radius
T	temperature
t	time after passage of wave
\bar{t}	non-dimensional time after passage of detonation wave, Equation (4.10)
t_p	drum period of drum camera
u	velocity in x direction
u_{\max}	maximum velocity in channel
v	specific volume
v	velocity in y direction
\bar{v}	instantaneous non-dimensional velocity, Equation (4.9)
\ddot{v}_f	acceleration of film in y direction
$\ddot{\bar{v}}$	non-dimensional acceleration, Equation (4.8)
$[X]$	third body concentration
\bar{x}	reaction length
x_p	pitch length
z	defined in Equation (4.32)
α	angle of slit with the direction of motion of camera
β, β'	angles of detonation streak with direction of motion of film
$\Gamma(x)$	"Complete" gamma function
$\Gamma(x, y)$	"Incomplete" gamma function defined as $\int_0^y t^{x-1} e^{-t} dt$
γ	ratio of specific heats

δ	deflection angle of interface
ϵ	coefficient defined in Equation (2.21)
ζ	reduced distance
$\bar{\zeta}$	reduced reaction length
θ	wave angle
λ	\bar{v}/\bar{v}_∞
μ	magnification
ν	kinematic viscosity
ν	number of drops/unit volume
ν_{nm}	natural sound frequency
ξ	fractional area increase defined by Equation (2.18)
ρ	density
τ	induction time
ϕ_1	function defined in Equation (2.35)
ϕ_2	function defined in Equation (2.36)
ϕ_3, ϕ_3'	functions defined in Equations (3.8) and (3.10)
χ	see Equation (4.44)
ψ	function defined in Equation (2.23)

Subscripts

1	condition ahead of wave
2	condition behind wave
20	condition immediately behind wave
3	condition behind wave after expansion
c	critical
CJ	Chapman-Jouguet

e	explosive
i	inert
ion	ionization probe
max	maximum
th	theoretical
β	streak pictures

ABSTRACT

The theoretical analysis presented in this work shows that a detonation wave in a gaseous explosive bounded by an inert gaseous medium propagates at a lower velocity than it would have if the explosive were inside a tube with a solid wall. The velocity decrement is found to be dependent primarily on the ratio of the initial densities of the explosive and the inert gases, the reaction length of the explosive and the extent of the explosive normal to the interface. An extension of composition limit criteria shows that there is a limit to the velocity decrement beyond which the detonation is expected to quench and therefore deteriorate into a shock.

Extensive experimental results on $\text{H}_2\text{-O}_2$ mixtures bounded by nitrogen and some results on stoichiometric $\text{CH}_4\text{-O}_2$ bounded by different gases show a general agreement with theory. In the case of $\text{H}_2\text{-O}_2$ mixtures, it is found that a velocity decrement beyond 8-10% leads to quenching. The reaction lengths of the stoichiometric mixtures of $\text{H}_2\text{-O}_2$ and $\text{CH}_4\text{-O}_2$ are found to be .14 in. and .32 in. respectively. In all of the experimental work, the explosive was separated from the boundary gas by a very thin film (250-500 Å) to eliminate any diffusion effects.

Other results relative to the behavior of the detonation wave when the explosive is much denser than the boundary gas and also near the quenching limit are included.

It is concluded that the experimental method described can be used as a new tool for determining some important properties of gaseous detonations.

I. INTRODUCTION

Research on detonation waves has received quite an impetus since the late nineteenth century when Berthelot and Vieille⁽¹⁾ and Mallard and LeChatelier⁽²⁾ published their experimental works identifying the supersonic nature of these waves, and indicating that they constitute a mode of combustion distinct from the slow mode or deflagration. Very shortly thereafter, Chapman⁽³⁾ and Jouguet,⁽⁴⁾ using a hydrodynamic approach, confirmed this observation. In addition, they recognized, independently, that the burned gas behind the wave travels at the local speed of sound relative to the wave. Waves possessing this unique property are now called Chapman-Jouguet waves in their honor.

The present literature on detonation waves and allied subjects covering various aspects of the phenomenon is very extensive as can be seen from the reviews of Morrison, et al.,⁽⁵⁾ Gross and Oppenheim,⁽⁶⁾ Wagner,⁽⁷⁾ and Evans and Ablow.⁽⁸⁾ Experimentally, the study of detonation waves has, up to recent years, been conducted in shock tubes or flame tubes: for example, see the work of Morrison.⁽⁹⁾ In a tube it appears that the only stable type is the CJ wave as shown by Lewis and vonElbe⁽¹⁰⁾ and Scoriah.⁽¹¹⁾

Within the last decade some theoretical studies by Siestrunck, et al.,⁽¹²⁾ and Rutkowski and Nicholls⁽¹³⁾ indicated the possibility of attaining standing detonation waves (i.e., fixed with respect to laboratory coordinates). These waves could be either the CJ type or the strong type where the burned gas travels at subsonic speed relative to the wave.

The first standing detonation wave was realized in 1958, in an under-expanded jet and was reported by Nicholls, Dabora and Gealer.⁽¹⁴⁾ Later on, other researchers such as Gross^(15,16) and Rhodes and Chriss⁽¹⁷⁾ reported on experiments concerned with the establishment of standing detonation waves.

Another aspect of the detonation phenomenon to which considerable attention is given at present is the structure of the wave itself. The pioneering works of Kirkwood and Wood^(18,19,20) and of Hirschfelder and colleagues^(21,22,23) as well as the work of Adamson⁽²⁴⁾ are cited in this regard. White⁽²⁵⁾ used interferometric techniques to study the structure of the wave experimentally. Reviews on this subject can be found in the publications of Oppenheim and Stern⁽²⁶⁾ and Fay.⁽²⁷⁾

The chemical reaction behind the detonation front has been also a subject of study by many investigators. In particular, the hydrogen-oxygen-diluent reaction has been studied in detail: for example, the works of Duff,⁽²⁸⁾ Schott and Kinsey⁽²⁹⁾ and Nicholls.⁽³⁰⁾ The last two works were primarily concerned with the ignition time delay.

Recently, in an effort to obtain a better understanding of the propagation of detonation waves in condensed (liquid or solid) explosives, Sommers⁽³¹⁾ studied, as an analogue, the interaction process between a gaseous detonation wave and an inert confining gas. The analogy stems from the realization that pressures behind detonation waves in condensed explosives are so high that any confining medium would behave much like a compressible material. Sommers succeeded in showing that different confining gases can influence the behavior of

the detonation wave differently, and thus was able to confirm qualitatively what had been observed experimentally in condensed explosives by several investigators such as Campbell et al.,⁽³²⁾ Modard⁽³³⁾ and Nahmani and Manheimer.⁽³⁴⁾

Apart from its usefulness as a tool in gaining an insight into the behavior of condensed explosives, the study of the interaction process between a gaseous detonation and a side inert gas is interesting by itself. The extensive experiments on detonations waves in $H_2 - O_2$ mixtures when confined by an inert gas reported here will show how such studies can lead to estimates of reaction lengths behind detonation waves, and to a check on the reaction mechanism in the same region.

An intriguing application of a detonation wave is its maintenance in an annulus with the front moving in the tangential direction. Detonation can be maintained continuously by exhausting the burned gas through one side and replenishing the annulus by the detonable gas from the other side. This type of detonation traveling in a circular track was reported by Voitschkovskii.⁽³⁵⁾ It has also been studied by Morrison and Cosens⁽³⁶⁾ as a prelude to the design of a rotating detonation wave rocket engine, the feasibility of which is under extensive study at the Aircraft Propulsion Laboratory of The University of Michigan.^(37,38,39) The physical design of such an engine is such that the unburned gas will in general be in contact with the burned gas from the previous cycle. Therefore, one of the problems relevant to the rotating detonation engine is the determination of conditions under which the detonation wave would continue to propagate. The results reported

herein will in part answer this question. The results are also considered relevant to the prevention of detonations that can arise in rocket launching sites due to leakage of fuels and oxidizers, as well as to the design of detonation traps.

II. GENERAL CHARACTERISTICS OF GASEOUS DETONATION WAVES

2.1 One Dimensional Waves

The classical hydrodynamic formulation of the characteristics of a general, steady, one-dimensional wave will be presented briefly here. It is assumed that the wave can be considered as a planar discontinuity, with conditions along the wave being uniform, as represented in Figure 1. Thus the conservation equations can be written as follows:

a. Conservation of mass:

$$\rho_1 u_1 = \rho_2 u_2 \quad (2.1)$$

b. Conservation of momentum:

$$\rho_1 u_1^2 + p_1 = \rho_2 u_2^2 + p_2 \quad (2.2)$$

c. Conservation of energy :

$$\frac{u_1^2}{2} + h_1 + q = \frac{u_2^2}{2} + h_2 \quad (2.3)$$

where q is the heat release (if any) per unit mass due to chemical reaction.

To keep the analysis as general as possible, one can assume that the gases ahead and behind the wave have different molecular weights and ratios of specific heats. However, for simplicity both gases are assumed thermally and calorically perfect. Thus the equation of state is

$$p = \rho \frac{R_o T}{m} \quad (2.4)$$

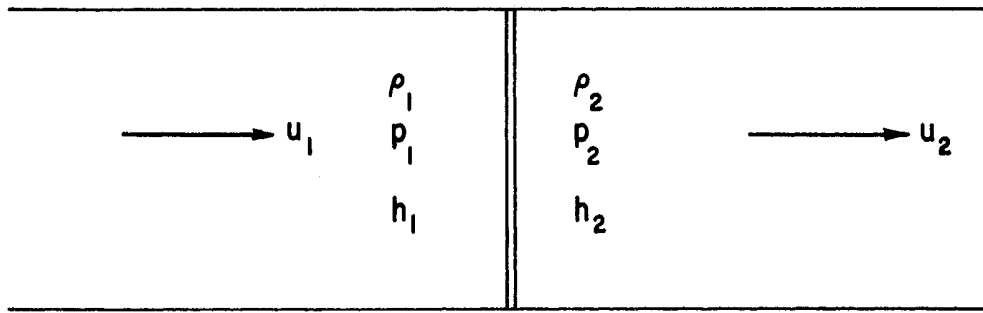


Figure 1. One Dimensional Detonation Wave.

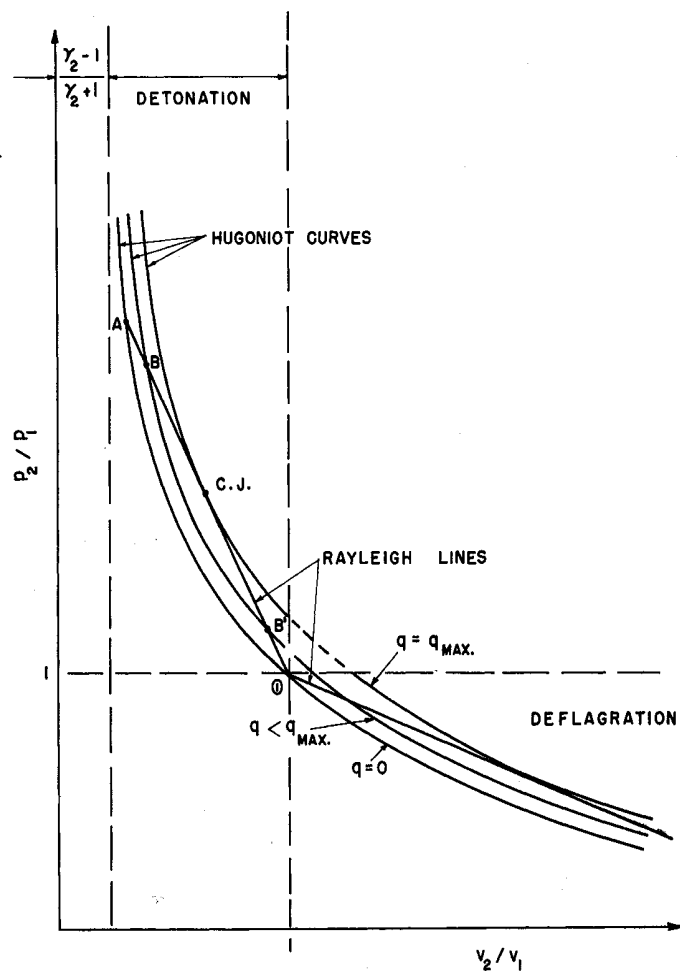


Figure 2. Hugoniot Rayleigh Representation of Shock and Detonation Waves.

and the enthalpy can be written as

$$\begin{aligned} h &= c_p T = \frac{\gamma}{\gamma-1} \frac{R_0}{m} T \\ &= \frac{\gamma}{\gamma-1} \frac{p}{\rho} = \frac{\gamma}{\gamma-1} p v \end{aligned} \quad (2.5)$$

Now if Equations (2.1) and (2.2) are combined, one can readily obtain

$$\frac{\frac{p_2}{p_1} - 1}{\frac{v_2}{v_1} - 1} = - \frac{u_1^2}{p_1 v_1} = -\gamma_1 M_1^2 = - \frac{u_2^2 \rho_2^2}{p_1 \rho_1} \quad (2.6)$$

On a $p v$ diagram this equation represents a straight line with a negative slope for any finite Mach number. This is called the Rayleigh line.

On the other hand, if Equations (2.1), (2.2), (2.3) and (2.5) are combined, the following can be obtained, after elimination of the velocity terms:

$$\left(\frac{2q}{p_1 v_1} + \frac{\gamma_1 + 1}{\gamma_1 - 1} - \frac{\gamma_2 - 1}{\gamma_2 + 1} \right) \left(\frac{\gamma_2 - 1}{\gamma_2 + 1} \right) = \left(\frac{p_2}{p_1} + \frac{\gamma_2 - 1}{\gamma_2 + 1} \right) \left(\frac{v_2}{v_1} - \frac{\gamma_2 - 1}{\gamma_2 + 1} \right) \quad (2.7)$$

This is called the Hugoniot relation, and it can be seen that on a $p v$ diagram it would plot as a family of hyperbolas with a function of q and γ 's as a parameter.

Figure 2 shows a schematic plot of Equation (2.6) (two straight lines) and Equation (2.7) for the adiabatic case and for two cases with heat release. The lower branch of the Hugoniot curves in conjunction with Rayleigh lines of absolute slope less than γ_1 represent the deflagration mode of combustion and is not relevant to our work here. The upper branch and Rayleigh lines of absolute slope greater than γ_1

represent shock or detonation waves. In general, a Rayleigh line intersects the Hugoniot curve at two points which represent the simultaneous solution of Equations (2.6) and (2.7). As examples, point A represents an adiabatic shock wave with p_2/p_1 and ρ_2/ρ_1 greater than unity; point B is the solution for a strong detonation wave, and B' is that for a weak wave both of which occur for a value of q less than the limiting value. Points similar to B' are usually ruled out from entropy considerations, if the detonation process is considered a shock followed by heat release. Finally point CJ is the solution for the Chapman-Jouguet wave and is realized at the limiting value of heat release and is the type of wave observed in flame tubes.

As can be seen from Figure 2, at point CJ, the Rayleigh line is tangent to the Hugoniot curve. If Equations (2.6) and (2.7) are differentiated, we obtain respectively:

$$\frac{\partial(\frac{p_2}{p_1})}{\partial(\frac{v_2}{v_1})} = - \frac{u_2^2 \rho_2}{p_1 \rho_1} \quad (2.8)$$

and

$$\frac{\partial(\frac{p_2}{p_1})}{\partial(\frac{v_2}{v_1})} = - \frac{\frac{p_2}{p_1} + \frac{\gamma_2 - 1}{\gamma_2 + 1}}{\frac{\rho_1}{\rho_2} - \frac{\gamma_2 - 1}{\gamma_2 + 1}} \quad (2.9)$$

Equating (2.8) and (2.9), substituting p_1 from (2.2) and u_1 from (2.1), the solution of u_2 for the CJ point is obtained.

$$u_2 = \sqrt{\frac{\gamma_2 p_2}{\rho_2}} = a_2 \quad (2.10)$$

This means that for a Chapman-Jouguet wave the velocity of the burned gas immediately behind the wave travels at the local sonic speed with respect to the wave. As has been mentioned earlier, this appears to be the most stable type of detonation waves in flame tubes. The question of whether the velocity of sound, a_2 , should be based on frozen or shifting equilibrium is raised in the literature, and for a summary of its implications the reader is referred to the survey article by Gross and Oppenheim.⁽⁶⁾ It is shown there that using either "frozen" or "equilibrium" speed of sound leads to an insignificant difference in the prediction of the detonation velocity; therefore, the "frozen" speed of sound is used in this work.

2.2 Classification of Detonation Waves

The conservation equations together with the perfect gas relation and the definition of the velocity of sound can be combined to give the changes in the thermodynamic properties across the wave in terms of the original Mach number M_1 , q and γ 's. This was done by Adamson and Morrison⁽⁴⁰⁾ for the simple case where no changes in molecular weight and specific heat ratio were considered. Later, Adamson⁽⁴¹⁾ generalized the solutions to cases admitting these changes. These solutions are given here without derivation:

a. Pressure ratio:

$$\frac{p_2}{p_1} - 1 = \frac{\gamma_1 F}{\gamma_2 + 1} \left(M_1^2 - \frac{\gamma_2}{\gamma_1} \right) \quad (2.11)$$

b. Density ratio:

$$\frac{\rho_2}{\rho_1} = \frac{1}{1 - \frac{F}{\gamma_2 + 1} \left(M_1^2 - \frac{\gamma_2}{\gamma_1} \right) \frac{1}{M_1^2}} \quad (2.12)$$

c. Temperature ratio:

$$\begin{aligned} \frac{T_2}{T_1} = \frac{m_2}{m_1} \left[1 - \frac{F}{M_1^2 (\gamma_2 + 1)} \left(M_1^2 - \frac{\gamma_2}{\gamma_1} \right) \right] \times \\ \left[1 + \frac{\gamma_1 F}{\gamma_2 + 1} \left(M_1^2 - \frac{\gamma_2}{\gamma_1} \right) \right] \end{aligned} \quad (2.13)$$

From the latter, one can easily obtain the speed of sound ratio, which will be needed in a later section of this work, as:

$$\left(\frac{a_2}{a_1} \right)^2 = \frac{\frac{\gamma_2 T_2}{m_2}}{\frac{\gamma_1 T_1}{m_1}} = \frac{\gamma_2}{\gamma_1} \left[1 - \frac{F(M_1^2 - \frac{\gamma_2}{\gamma_1})}{M_1^2 (\gamma_2 + 1)} \right] \left[1 + \frac{\gamma_1 F}{\gamma_2 + 1} \left(M_1^2 - \frac{\gamma_2}{\gamma_1} \right) \right] \quad (2.14)$$

The definition of F in the above equations is:

$$F = 1 + \sqrt{1 - \frac{2(\gamma_2^2 - 1)}{(\gamma_1 - 1)} \frac{M_1^2}{(M_1^2 - \frac{\gamma_2}{\gamma_1})^2} \left(\frac{q}{c_{p1} T_1} - \frac{\gamma_1 - \gamma_2}{\gamma_1 (\gamma_2 - 1)} \right)} \quad (2.15)$$

and its implication is as follows:

$F = 1$ represents cases with limiting q , i.e., CJ waves.

$F = 2$ represents cases with $q = 0$, i.e., adiabatic shock waves, (when $\gamma_1 = \gamma_2$).

$2 > F > 1$ represents cases of strong detonation waves.

The solution for the Mach number behind the wave was also given in (41) as

$$M_2^2 = \frac{\gamma_1}{\gamma_2} \left\{ \frac{(\gamma_2 + 1 - F)(M_1^2 - \frac{\gamma_2}{\gamma_1}) + \frac{\gamma_2}{\gamma_1}(\gamma_2 + 1)}{\gamma_1 F(M_1^2 - \frac{\gamma_2}{\gamma_1}) + (\gamma_2 + 1)} \right\} \quad (2.16)$$

It is to be noted that for the CJ case $M_2 = 1$, and therefore, Equation (2.16) yields $F = 1$ so that the propagation Mach number of a Chapman-Jouguet wave can be found from Equation (2.15) by the relation

$$2\left(\frac{q}{c_{p1}T_1} - \frac{\gamma_1 - \gamma_2}{\gamma_1(\gamma_2 - 1)}\right) \frac{\gamma_2^2 - 1}{\gamma_1 - 1} = \frac{(M_1^2 - \frac{\gamma_2}{\gamma_1})^2}{M_1^2} \quad (2.17)$$

Thus if the initial thermodynamic conditions as well as the value of heat release and γ_2 are known, the detonation velocity can be found. In general, however, finding q and γ_2 requires a trial and error solution that involves chemical equilibrium behind the wave as shown, for example, by Lewis and von Elbe,⁽¹⁰⁾ Moyle, et al.,⁽⁴²⁾ Gealer and Churchill,⁽⁴³⁾ Dunn and Wolfson⁽⁴⁴⁾, Eisen, et al.,⁽⁴⁵⁾ and very recently by Zeleznik and Gordon.⁽⁴⁶⁾

2.3 Detonation Waves Bounded by an Inert Gas

a. Effect of an Area Change on the Propagation of a Detonation Wave

When a plane detonation wave propagates in a gaseous explosive column surrounded by an inert gas, an oblique shock is induced in the latter due to the expansion of the burned gas behind the detonation front. This type of interaction is believed to have been first treated by

Doring and Burkhart.⁽⁴⁷⁾ The flow pattern, as it appears to an observer moving with the detonation front, is shown in Figure 3. In this frame of reference, both the detonation and the shock waves appear stationary, and the unburned explosive as well as the surrounding inert gas travel at a velocity, u_1 , into the waves.

Recently Sommers⁽³¹⁾ in his effort to simulate detonation of condensed explosives, devised a means of exposing a gaseous explosive column to an inert gas so that the interaction of the detonation wave with the latter could be observed photographically. Essentially the method consists of letting a stream of explosive gas flow either into a still medium or parallel to a side stream of an inert gas. A detonation is started in the explosive and when it comes in contact with the inert, the interaction process is photographed. Figure 4 is a typical schlieren picture of such an interaction, and it is seen that except for the curvature near the initial interface of both the shock and the detonation fronts, the interaction process follows closely the sketch in Figure 3. It will be shown later that the curvature is primarily due to diffusion between the two gases so that if it is minimized by appropriate means, the curvature will be reduced considerably.

In order to find analytically what effect the expansion of the burned gas and the attendant induced shock in the inert have on the propagation velocity of the detonation wave a model of the interaction process must first be formulated. To begin with, it can be assumed after Zeldovich,⁽⁴⁸⁾ von Neumann⁽⁴⁹⁾ and Doering,⁽⁵⁰⁾ that the detonation wave consists of a shock followed by combustion. Further, since chemical reaction cannot be instantaneous, complete heat release is not immediate

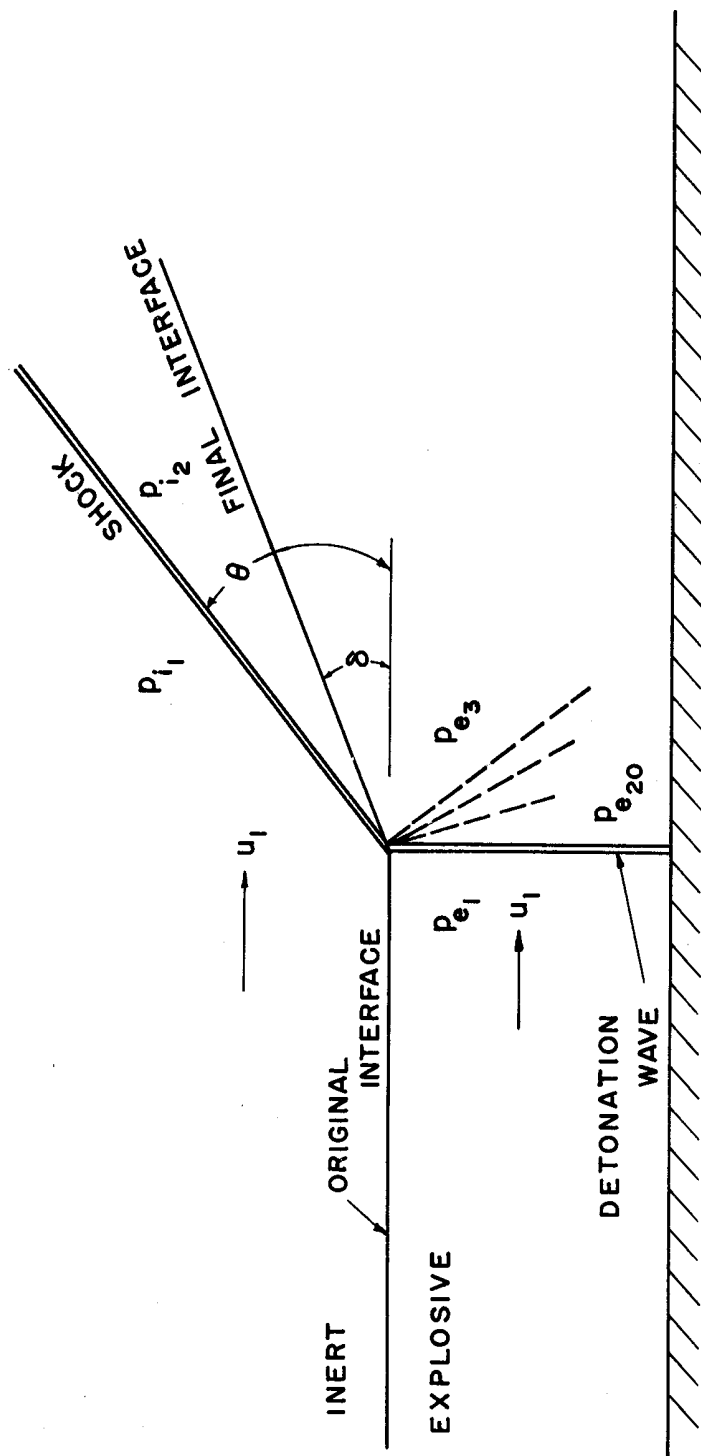
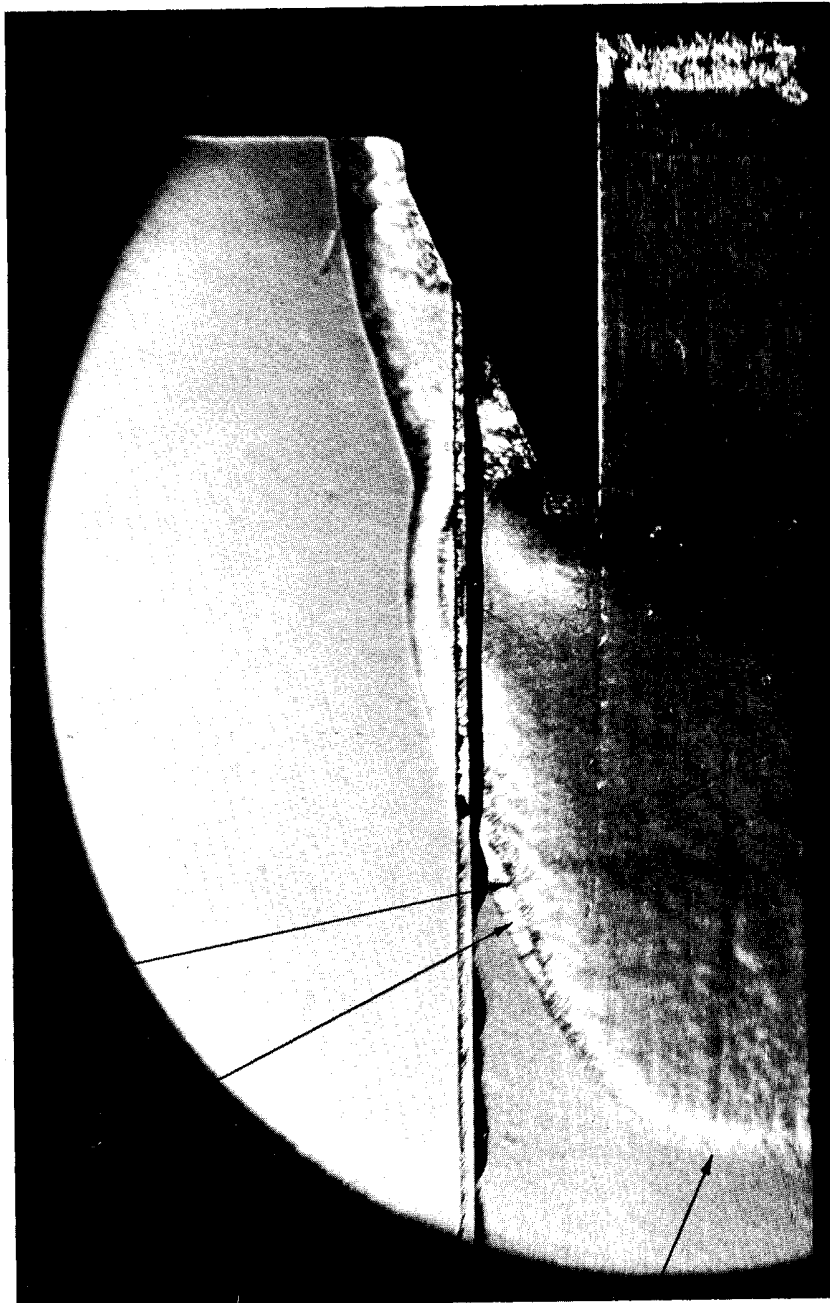


Figure 3. Idealized Flow Model of Detonation Wave - Boundary Interaction.

SHOCK FINAL INTERFACE



DETONATION
WAVE

Figure 4. Typical Photograph of the Interaction Process. (Reference 31)

so that the Chapman-Jouguet plane is at some distance from the shock front. Such a process is illustrated in the $p-v$ plane (Figure 2) as going from ① to A which is the shock, and then back to point CJ through various stages of heat release. It should be pointed out that recent evidence by Hornig⁽⁵¹⁾ and White⁽⁵²⁾ indicates that the ZND model of detonation is essentially correct. The distance between the shock front and the CJ plane, denoted by \bar{x} , will be defined as the reaction length.

In the case where the detonation takes place in a solid tube, the CJ plane should essentially have - except for a boundary layer - the same area as the shock plane. However, when the detonation is exposed to a compressible inert medium the shocked gas, being at higher pressure than the inert, expands so that the CJ plane in this case would have a larger area than the shock front. A detailed analysis of the reaction zone affected by the side relief is extremely difficult to make because the region of interaction would include subsonic and supersonic flow regimes which are further complicated by chemical reaction. Further, the adjustment of the subsonic flow behind the shock front of the detonation wave would most likely cause some curvature in the wave itself, the oblique shock in the inert and the interface.

In order to formulate, then, a model that would be amenable to analysis, the region of curvature is assumed to be very small compared to the total reaction zone - an assumption which is justified only by the experimental evidence shown later. Thus, in the idealized model, shown in Figure 5, the detonation front, the oblique shock and the interface are all assumed to be plane.

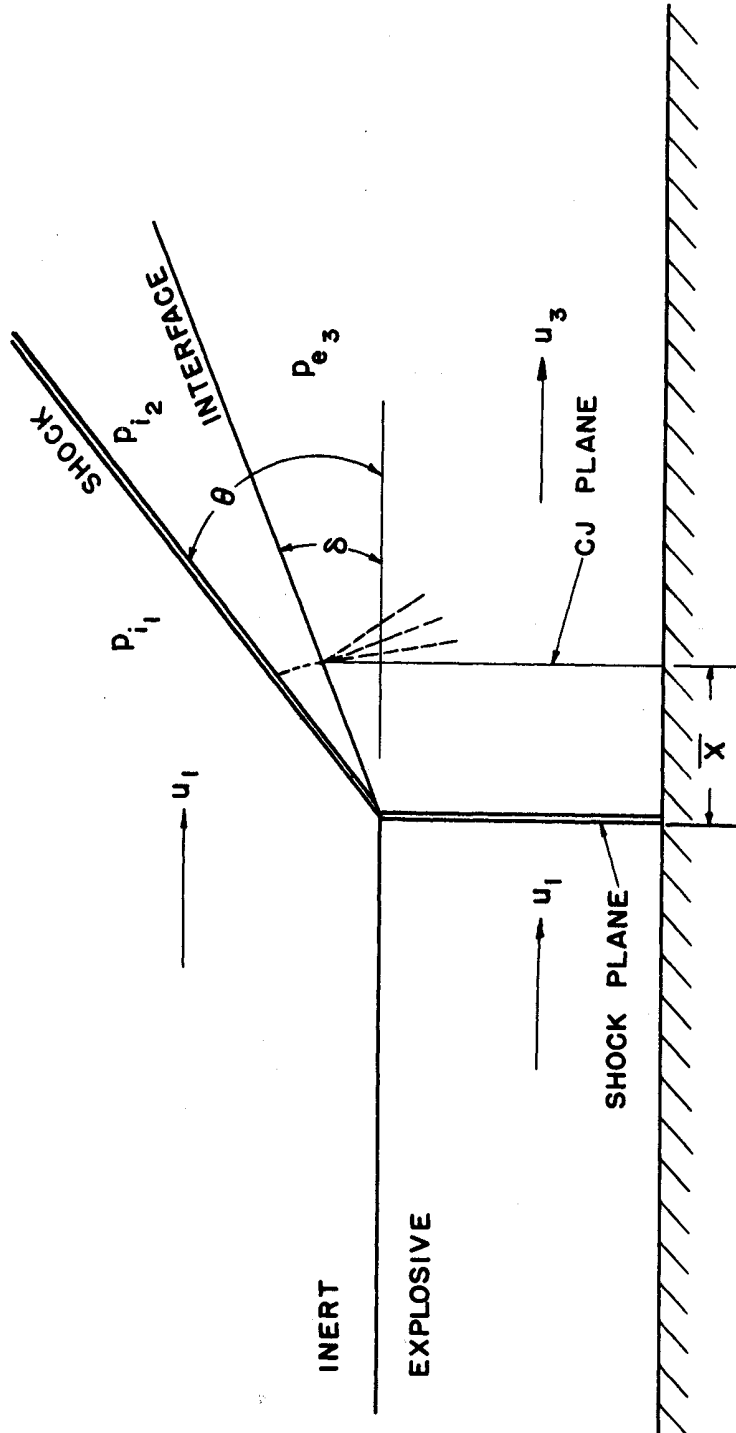


Figure 5. Idealized Flow Model of Detonation Wave - Boundary Interaction with Finite Reaction Length.
(Flow is assumed quasi one-dimensional within reaction zone but two dimensional behind CJ plane.)

The method for calculating the deflection angle of the interface is presented in the next section. However, it is sufficient to point out again, that due to this deflection, each stream-tube, originating at the front of the detonation wave, would experience an area increase at the CJ plane. ✓ The problem then is to find the effect of this area increase on the propagation velocity. The analysis that will follow will make use of reasoning similar to that of Fay⁽⁵³⁾ who investigated the effect of boundary layer on the detonation velocity in solid tubes. If the shock front area is A_1 and the CJ plane area is A_2 which is different from A_1 , then

$$A_2/A_1 = 1 + \xi \quad (2.18)$$

where ξ is the average fractional change in the area of each stream tube.

The conservation equations thus become:

(1) Conservation of mass:

$$\rho_1 u_1 = \rho_2 u_2 (1 + \xi) \quad (2.19)$$

(2) Conservation of momentum:

$$\rho_1 u_1^2 + p_1 = (\rho_2 u_2^2 + p_2)(1 + \xi) - \int_0^\xi p \, d\xi \quad (2.20)$$

and the conservation of energy equation remains the same as Equation (2.3). To evaluate the integral term in Equation (2.20) requires detailed knowledge of the variation of the pressure behind the shock front along the interface within the reaction zone. However, one can define the integral as:

$$\int_0^\xi p \, d\xi = p_2 \epsilon \xi \quad (2.21)$$

and note from Equation (2.11) that p_2/p_1 for a shock ($F = 2$) is about twice that of a detonation wave ($F = 1$) when M_1 is large. Thus, the value of ϵ is between 2 and 1. It will be shown later that it is about 1.15.

Using the same general assumptions as in Sections 2.1 - 2.2, Equations (2.3), (2.19), (2.20), (2.21) together with the definition of the speed of sound can be combined to give:

$$2\left(1 + \frac{q}{c_{p1}T_1}\right) = \left(\frac{\gamma_2}{\gamma_1}\right)^2 \left(\frac{\gamma_1 - 1}{\gamma_2^2 - 1}\right) \left[\frac{1}{1 - \frac{\xi\epsilon}{(1 + \gamma_2)(1 + \xi)}} \right]^2 \frac{(\gamma_1 M_1^2 + 1)^2}{M_1^2} - (\gamma_1 - 1) M_1^2 \quad (2.22)$$

Introducing a new function ψ defined by

$$1 + \psi = \left[\frac{1}{1 - \frac{\epsilon\xi}{(1 + \gamma_2)(1 + \xi)}} \right]^2 \quad (2.23)$$

Equation (2.22) can be reduced to the following:

$$2\left[\frac{q}{c_{p1}T_1} - \frac{\gamma_1 - \gamma_2}{\gamma_1(\gamma_2 - 1)}\right] \frac{\gamma_2^2 - 1}{\gamma_1 - 1} = \frac{(M_1^2 - \frac{\gamma_2}{\gamma_1})^2}{M_1^2} + \frac{\psi \gamma_2^2 (M_1^2 + \frac{1}{\gamma_1})^2}{M_1^2} \quad (2.24)$$

This equation is different from Equation (2.17) by only the last term which represents the effect of area change. For large M_1 , ($M_1 \geq 5$), Equation (2.24) can be reduced further to:

$$2\left[\frac{q}{c_{p1}T_1} - \frac{\gamma_1 - \gamma_2}{\gamma_1(\gamma_2 - 1)}\right] \frac{\gamma_2^2 - 1}{\gamma_1 - 1} = M_1^2 (1 + \psi \gamma_2^2) \quad (2.25)$$

If the heat release is assumed to remain the same whether there is an area change or not, the right hand side of (2.25) remains essentially

constant. It should be added that physically this is a reasonable assumption in that chemical equilibrium is expected to remain the same at the CJ plane whether there is an area change or not. This is so, because the influence of an area increase would be a decrease in both pressure and temperature at that plane, and if the heat release is controlled by dissociation at this point, the pressure and temperature effects would tend to cancel each other. As a check on this assumption, calculations on the stoichiometric $H_2 - O_2$ mixture at a pressure and a temperature of 20% less than atmospheric were performed using the method of Zeleznik and Gordon,⁽⁴⁶⁾ and it was found that the heat release changed only by 0.2%.

Noting that $\psi = 0$ when $\xi = 0$, one can find, after making use of Equation (2.25), that the decrease in Mach number from the case where there is no area change to the case where ξ is finite can be written as:

$$\frac{M_1(\xi=0) - M_1}{M_1(\xi=0)} = \frac{\Delta M_1}{M_1(\xi=0)} = 1 - \sqrt{\frac{1}{1 + \gamma_2^2 \psi}} \quad (2.26)$$

or in terms of ξ .

$$\frac{\Delta M_1}{M_1(\xi=0)} = 1 - \sqrt{\frac{[1 - (\frac{\epsilon}{1+\gamma_2})(\frac{\xi}{1+\xi})]^2}{[1 - (\frac{\epsilon}{1+\gamma_2})(\frac{\xi}{1+\xi})]^2 + \gamma_2^2 [2(\frac{\epsilon}{1+\gamma_2})(\frac{\xi}{1+\xi}) - (\frac{\epsilon}{1+\gamma_2})^2 (\frac{\xi}{1+\xi})^2]}} \quad (2.27)$$

which for $\xi \ll 1$ reduces to

$$\frac{\Delta M_1}{M_1(\xi=0)} \approx \gamma_2^2 \left(\frac{\epsilon}{1+\gamma_2}\right) \xi \quad (2.28)$$

For $\gamma_2 = 1.2$ which is a reasonable value for the products of combustion in $H_2 - O_2$ detonations, the change in Mach number (or velocity) becomes

$$\frac{\Delta M_1}{M_1(\xi=0)} = .654 \epsilon \xi \quad (2.29)$$

Fay, (53) using numerical calculations for the stoichiometric hydrogen-oxygen, obtained a coefficient of .53 instead of the above .654. In our applications, since ξ can be as high as .25, we shall make use of relation (2.27) rather than (2.28).

b. Degree of Confinement and Explosive Deflection Angle

The determination of the interface deflection angle is necessary for the calculation of the area change. In this section the method of Sommers (31) for calculating this angle is described first and then a more general method is presented in detail.

For his solution Sommers assumes the idealized model of Figure 3 wherein the detonation wave is considered a discontinuity. The burned gas behind it suffers a Prandtl-Meyer expansion from unity Mach number consistent with the CJ condition. It is possible then to find the pressure of the expanded gas for various Prandtl-Meyer angles. On the other hand, from a knowledge of the flow Mach number in the inert boundary, solutions for the pressure behind the wave for any wedge angle can be found. The correct solution to both flows is obtained when both the pressure behind the shock and the wedge angle match the pressure of the expanded gas behind the detonation wave and the Prandtl-Meyer angle respectively.

The method to be presented here is based on a shock tube analogy, and is generalized for any combination of explosive and boundary gases. In the analogy, the gas behind the front of the detonation wave will be comparable to the driver gas, and the inert gas will be equivalent to the driven gas. As illustrated in Figure 6, the familiar $y-t$ plot of the shock and the interface propagation will be similar to the $y-x$ plot in the case at hand, where x is equivalent to $u_1 t$. For the purpose of this analogy, the detonation wave is considered again as a discontinuity so that plane 20 and 3 of Figure 5 are considered merged into one plane.

With the nomenclature of Figure 6, the equation for the pressure ratio across the shock in the inert boundary is, from Reference 54:

$$\frac{p_{e20}}{p_{i1}} = \frac{p_{i2}}{p_{i1}} \left[1 - \frac{(\gamma_{e20} - 1) \frac{a_{i1}}{a_{e20}} \left(\frac{p_{i2}}{p_{i1}} - 1 \right)}{\sqrt{2\gamma_{i1}} \sqrt{2\gamma_{i1} + (\gamma_{i1} + 1) \left(\frac{p_{i2}}{p_{i1}} - 1 \right)}} \right] - \frac{2\gamma_{e20}}{\gamma_{e20} - 1} \quad (2.30)$$

Now, p_{e20}/p_{i1} can be written as

$$\frac{p_{e20}}{p_{i1}} = \frac{p_{e20}}{p_{e1}} \cdot \frac{p_{e1}}{p_{i1}} \quad (2.31)$$

and

$$\frac{a_{i1}}{a_{e20}} = \frac{a_{i1}}{a_{e1}} \cdot \frac{a_{e1}}{a_{e20}} = \left(\frac{\gamma_{i1} p_{i1}}{\gamma_{e1} p_{e1}} \cdot \frac{\rho_{e1}}{\rho_{i1}} \right)^{1/2} \cdot \frac{a_{e1}}{a_{e20}} \quad (2.32)$$

Further, from Equations (2.11) and (2.14) respectively

$$\frac{p_{e20}}{p_{e1}} = \phi_1 M_{e1}^2 \quad (2.33)$$

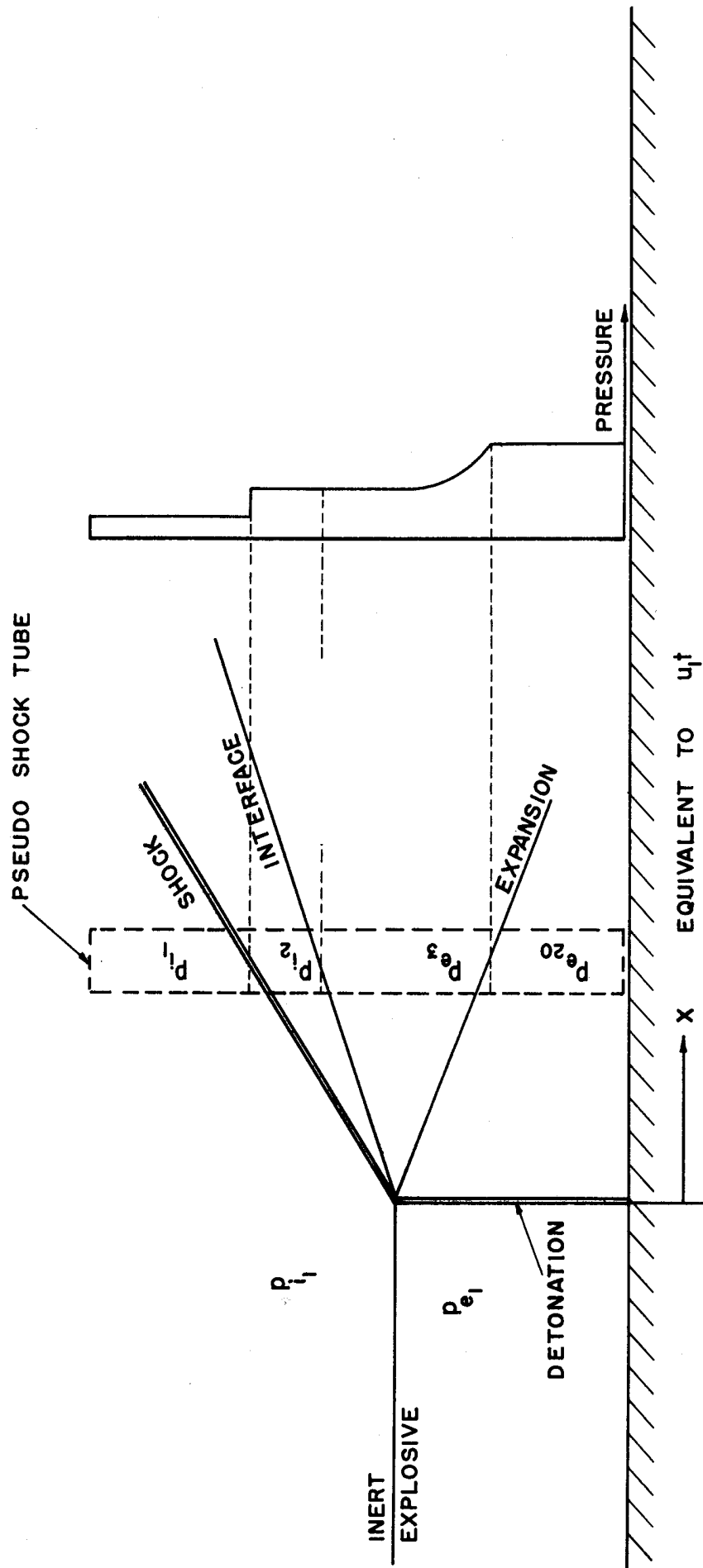


Figure 6. Shock Tube Analogy to the Interaction Process.

and

$$\frac{a_{e20}}{a_{e1}} = \phi_2 M_{e1} \quad (2.34)$$

where:

$$\phi_1 = \frac{\gamma_{e1} F}{\gamma_{e20} + 1} + \frac{1}{M_{e1}^2} \left(1 - \frac{\gamma_{e20} F}{\gamma_{e20} + 1} \right) \quad (2.35)$$

and

$$\begin{aligned} \phi_2 = \frac{1}{\gamma_{e20} + 1} & \left\{ (\gamma_{e20} + 1 - F) F \gamma_{e20} + \frac{1}{M_{e1}^2} [(\gamma_{e20} + 1)^2 (1 - F) \right. \\ & \left. + 2F^2 \gamma_{e20}] \frac{\gamma_{e20}}{\gamma_{e1}} + \frac{F}{M_{e1}^4} \left(\frac{\gamma_{e20}}{\gamma_{e1}} \right)^2 (\gamma_{e20} + 1 - \gamma_{e20} F) \right\}^{1/2} \end{aligned} \quad (2.36)$$

It is to be noted that for large M_{e1} , the functions ϕ_1 and ϕ_2 are essentially constants and depend primarily on the type of wave considered through F .

If we define:

$$\bar{P} \equiv \frac{1}{M_{e1}^2} \left(\frac{p_{i1}}{p_{e1}} \right) \left(\frac{p_{i2}}{p_{i1}} \right) \quad (2.37)$$

and substitute Equations (2.31), (2.32), (2.33), (2.34), and (2.37) into (2.30), the latter can be rearranged to the following form:

$$\left(\frac{\rho_{e1} \gamma_{e1}}{\rho_{i1} \gamma_{i1}} \right)^{1/2} \left[\frac{\gamma_{i1}}{2(\gamma_{i1} + 1)} \right]^{1/2} \phi_2 \left[1 - \left(\frac{\bar{P}}{\phi_1} \right)^{\frac{\gamma_{e20}-1}{2\gamma_{e20}}} \right] \left[\bar{P} + \left(\frac{\gamma_{i1}-1}{\gamma_{i1}+1} \right) \left(\frac{p_{i1}}{p_{e1}} \right) \frac{1}{M_{e1}^2} \right]^{1/2} = \frac{\gamma_{e20}-1}{\gamma_{e1}} \left[\bar{P} - \left(\frac{p_{i1}}{p_{e1}} \right) \frac{1}{M_{e1}^2} \right] \quad (2.38)$$

For large M_{e1} this equation reduces to

$$\left(\frac{\rho_{i1}\gamma_{i1}}{\rho_{e1}\gamma_{e1}} \right)^{1/2} \left[\frac{2(\gamma_{i1}+1)}{\gamma_{i1}} \right]^{1/2} = \frac{(\gamma_{e20}-1)}{\phi_2\gamma_{e1}} \cdot \frac{\sqrt{\bar{P}}}{\left[1 - \left(\frac{\bar{P}}{\phi_1} \right)^{\frac{\gamma_{e20}-1}{2\gamma_{e20}}} \right]} \quad (2.39)$$

Although it is hard to conceive of practical situations where p_{i1} is different from p_{e1} , the ratio p_{i1}/p_{e1} was kept in Equation (2.36) for generality. It is seen that for a reasonably large M_{e1} and a ratio of p_{i1}/p_{e1} moderately different from unity, the correlating parameter for \bar{P} is essentially $(\rho_{i1}\gamma_{i1}/\rho_{e1}\gamma_{e1})^{1/2}$, since $[\gamma_{i1}/2(\gamma_{i1}+1)]^{1/2}$ changes very little with γ_{i1} . The parameter \bar{P} of course is nothing but the pressure ratio across the wave in the explosive after expansion due to side relief has taken place, normalized in terms of M_{e1}^2 , since $p_{i2} = p_{e3}$.

Equations (2.38) and (2.39) are plotted in Figure 7 for a detonation condition in the explosive and for $\gamma_{e1} = \gamma_{i1} = 1.4$, and $\gamma_{e20} = 1.2$. Further in Equation (2.38), p_{i1}/p_{e1} was taken as unity and $M_{e1} = 5$. Also plotted on the same figure are the results obtained using Sommers method under the same conditions. Good agreement between the two methods is apparent. The plot shows that the higher the density parameter,

$$\left(\frac{\rho_{i1}\gamma_{i1}}{\rho_{e1}\gamma_{e1}} \right)^{1/2} \left[\frac{2(\gamma_{i1}+1)}{\gamma_{i1}} \right]^{1/2} \quad \text{is,}$$

the closer the pressure ratio \bar{P} to the ideal pressure ratio of ϕ_1 ,

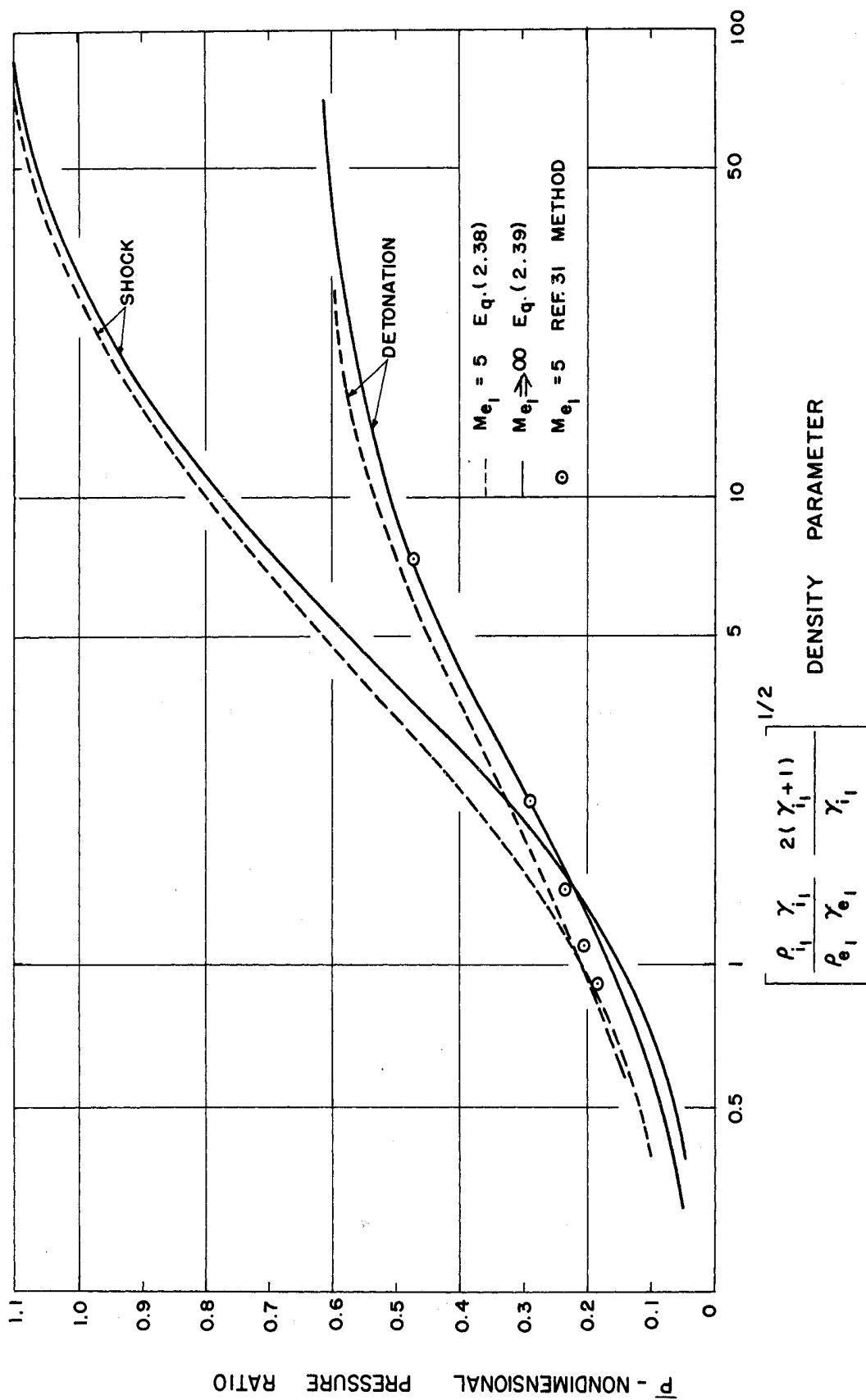


Figure 7. Variation of Non-Dimensional Pressure Ratio, \bar{P} , with the Density Parameter.

indicating that the denser the confining medium is, the better the confinement. This is in agreement with the results of Sommers,⁽³¹⁾ who found that the controlling parameter is the acoustic impedance ratio, $\rho_{i1}a_{i1}/\rho_{e1}a_{e1}$, for it can be shown that in the special case where $p_{i1} = p_{e1}$, $(\rho_i\gamma_{i1}/\rho_{e1}\gamma_{e1})^{1/2}$ is indeed equivalent to $\rho_{i1}a_{i1}/\rho_{e1}a_{e1}$.

In Figure 7, the plots labeled "Shock" are obtained again through Equations (2.38) and (2.39), except that the temperature and the pressure conditions behind the wave in the explosive are taken equivalent to what might be obtained if the detonation wave were a shock at the same Me_1 . In this case γ_{e20} is taken as 1.4. This plot is not intended to imply an actual description of the pressure field, but it is used only as a means of calculating, as shall be done next, the interface angle under widely different conditions.

In order to evaluate the deflection angle, δ , the shock tube analogy is retained. If v_1 is the interface velocity in direction normal to the detonation velocity, then

$$\tan \delta = \frac{v_1/a_{i1}}{u_{e1}/a_{i1}} = \frac{v_1/a_{i1}}{Me_1} \cdot \frac{a_{i1}}{a_{e1}} \quad (2.40)$$

But from Reference 54

$$\frac{v_1}{a_{i1}} = \left(\frac{p_{i2}}{p_{i1}} - 1 \right) \left[\frac{\frac{2}{\gamma_{i1}(\gamma_{i1} + 1)}}{\frac{p_{i2}}{p_{i1}} + \frac{\gamma_{i1} - 1}{\gamma_{i1} + 1}} \right]^{1/2} \quad (2.41)$$

Therefore, writing

$$\frac{a_{i1}}{a_{e1}} = \left(\frac{\gamma_{i1}p_{i1}}{\gamma_{e1}p_{e1}} \cdot \frac{\rho_{e1}}{\rho_{i1}} \right)^{1/2} \quad (2.42)$$

and substituting it and Equations (2.41) and (2.37) into (2.40) we obtain:

$$\tan \delta = \frac{2(\frac{\rho_{e1}\gamma_{e1}}{\rho_{i1}\gamma_{i1}})^{1/2} [\frac{\gamma_{i1}}{2(\gamma_{i1}+1)}]^{1/2}}{[\bar{P} - (\frac{p_{i1}}{p_{e1}}) \frac{1}{M_{e1}^2}]} \frac{[\bar{P} + (\frac{\gamma_{i1}-1}{\gamma_{i1}+1})(\frac{p_{i1}}{p_{e1}}) \frac{1}{M_{e1}^2}]^{1/2}}{1} \quad (2.43)$$

If Equation (2.38) is substituted in the above equation, $\tan \delta$ becomes

$$\tan \delta = \frac{2}{(\gamma_{e20} - 1)} \phi_2 \left[1 - \left(\frac{\bar{P}}{\phi_1} \right)^{\frac{\gamma_{e20} - 1}{2\gamma_{e20}}} \right] \quad (2.44)$$

Since \bar{P} is a function of the parameter,

$$\left[\frac{\rho_{e1}\gamma_{e1}}{\rho_{i1}\gamma_{i1}} \right]^{1/2} \left[\frac{\gamma_{i1}}{2(\gamma_{i1} + 1)} \right]^{1/2},$$

it is possible to find the variation of $\tan \delta$ with this parameter.

This is done in Figure 8 for the same conditions as those of Figure 7.

It can be seen that under the various conditions used, $\tan \delta$ is nearly independent of M_{e1} and as to whether a shock or a detonation is considered in the explosive.

As a way of assessing the range of validity of the shock tube analogy, the results obtained using Sommers' method for $M_{e1} = 5$, $\gamma_{i1} = \gamma_{e1} = 1.4$ and $\gamma_{e20} = 1.2$, are also shown in Figure 8. Excellent agreement is obtained for $\tan \delta$ up to about 0.5. The main conclusion, then, is that the deflection angle depends primarily on the original properties of the explosive and inert gases through the density parameter.

c. Shock Angle in the Inert Boundary Gas

Although it will be seen that the shock angle in the confining gas does not appear explicitly in the evaluation of the propagation

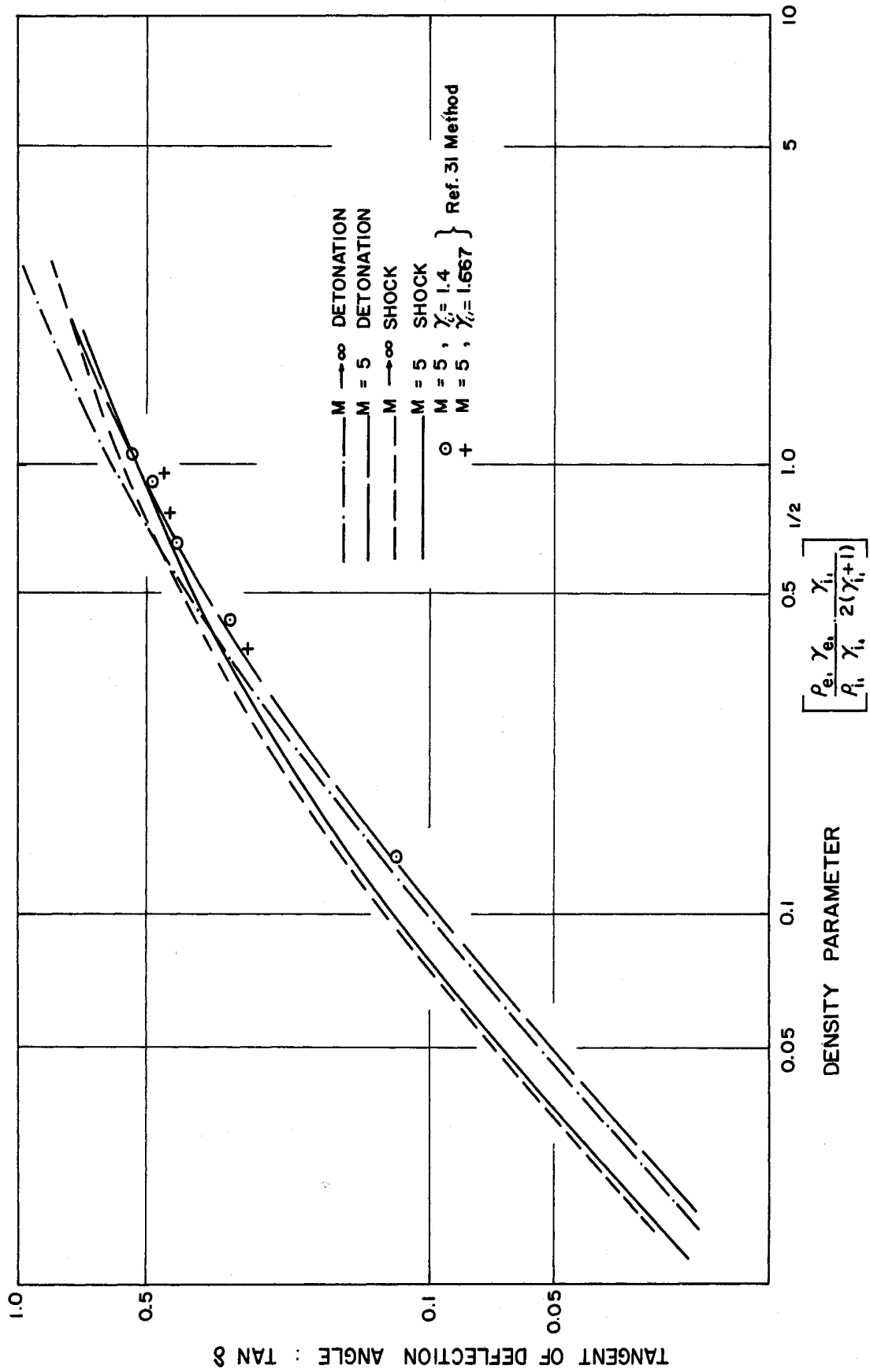


Figure 8. Variation of Tangent of Interface Angle with the Density Parameter.

velocity of the detonation in the explosive, it will nevertheless be solved for next for the sake of completeness of the flow configuration, and because it is one of the prime features that can be observed experimentally.

To this end, let us assume as in Figure 9 that an incident wave travels through the medium e at a velocity $u_{e1}/\sin \theta_{e1}$ in the direction parallel to the interface between two media. The refracted wave travels, of course, at the same velocity but the normal components of the velocities are related by:

$$\frac{u_{i1}}{\sin \theta_{i1}} = \frac{u_{e1}}{\sin \theta_{e1}} \quad (2.45)$$

This is the general refraction law which applies for any type wave, linear or non-linear. It can be written as:

$$\frac{M_{i1} a_{i1}}{M_{e1} a_{e1}} = \frac{\sin \theta_{i1}}{\sin \theta_{e1}} \quad (2.46)$$

Now if we consider a shock wave only in the inert medium i without a change in γ_i , we see from Equation (2.11) that

$$\frac{p_{i2}}{p_{i1}} = 1 + \frac{2\gamma_{i1}}{1 + \gamma_{i1}} (M_{i1}^2 - 1) \quad (2.47)$$

If we substitute (2.42), (2.37) and (2.47) into (2.46), we find that

$$\frac{\sin \theta_{i1}}{\sin \theta_{e1}} = \frac{\gamma_{i1} + 1}{\gamma_{i1}} \cdot \frac{\gamma_{i1}}{\gamma_{e1}} \cdot \left(\frac{\rho_{e1} \gamma_{e1}}{\rho_{i1} \gamma_{i1}} \right)^{1/2} \left[\frac{\gamma_{i1}}{2(\gamma_{i1} + 1)} \right]^{1/2} \left[\bar{P} + \frac{\gamma_{i1} - 1}{\gamma_{i1} + 1} \left(\frac{p_{i1}}{p_{e1}} \right) \frac{1}{M_{e1}^2} \right]^{1/2} \quad (2.48)$$

so that from Equation (2.43)

$$\frac{\sin \theta_{i1}}{\sin \theta_{e1}} = \frac{\gamma_{i1} + 1}{2} \frac{\left[\bar{P} + \frac{\gamma_{i1} - 1}{\gamma_{i1} + 1} \left(\frac{p_{i1}}{p_{e1}} \right) \frac{1}{M_{e1}^2} \right]}{\left[\bar{P} - \left(\frac{p_{i1}}{p_{e1}} \right) \frac{1}{M_{e1}^2} \right]} \tan \delta \quad (2.49)$$

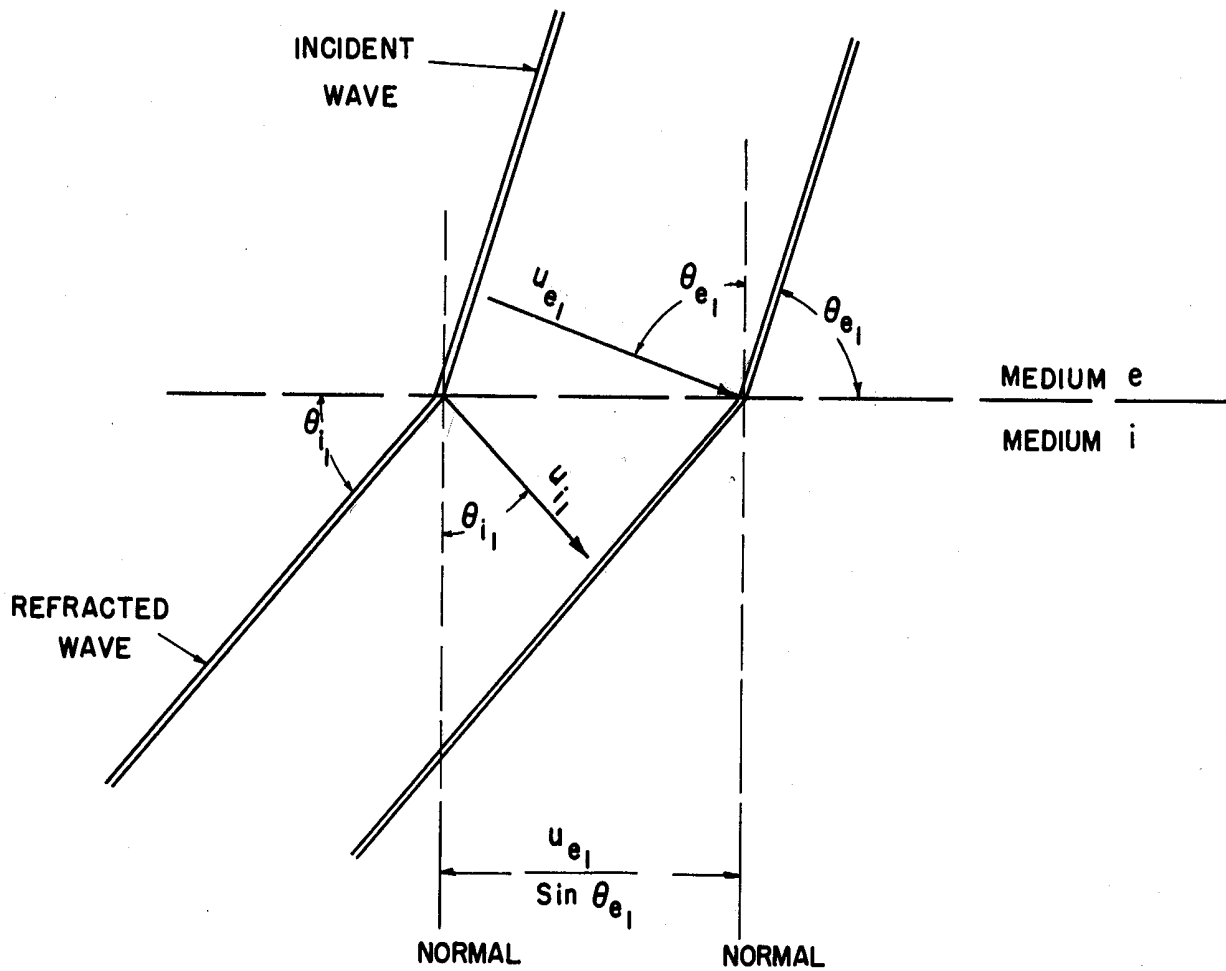


Figure 9. Wave Refraction at the Interface of Two Media.

For the case where the incident wave is normal to the interface

($\theta_{e1} = 90^\circ$), Equation (2.49) reduces to:

$$\sin \theta_{i1} = \frac{\gamma_{i1} + 1}{2} \frac{[\bar{P} + \frac{\gamma_{i1}-1}{\gamma_{i1}+1} (\frac{p_{i1}}{p_{e1}}) \frac{1}{M_{e1}^2}]}{[\bar{P} - (\frac{p_{i1}}{p_{e1}}) \frac{1}{M_{e1}^2}]} \tan \delta \quad (2.50)$$

which for large M_{e1} reduces further to

$$\sin \theta_{i1} = \frac{\gamma_{i1} + 1}{2} \tan \delta \quad (2.51)$$

This is immediately recognized as the relation between wave angle and wedge angle for high Mach numbers and small wedge angles.

Equation (2.48) is plotted in Figure 10 for the case where $\gamma_i = 1.4$ and that where $\gamma_i = 1.667$. In both cases it is assumed that M_{e1} is equal to 5 and a detonation condition prevails behind the wave in medium e. Also shown in the same figure is the solution of Sommers,⁽³¹⁾ for $\sin \theta_{e1} = 1$, and it is seen that the agreement is very good.

An immediate application of Figure 10 is the experimental work of Gvozdeva,⁽⁵⁵⁾ where the refraction of detonation waves was studied. For the case of detonation of ($\text{CH}_4 + 2\text{O}_2$) refracted in air as boundary gas, we note that the parameter

$$\left(\frac{\rho_e \gamma_e}{\rho_i \gamma_i}\right)^{1/2} \left[\frac{\gamma_i}{2(\gamma_i + 1)}\right]^{1/2} = .519 \quad (2.52)$$

Accordingly from Figure 10, $\sin \theta_{i1} / \sin \theta_{e1} = 0.498$. Since $\theta_{e1} = 58^\circ$, one finds $\theta_{i1} = 25^\circ$. Gvozdeva's schlieren photograph shows a shock wave angle θ_{i1} of about 26° , which is in excellent agreement with the theoretical value.

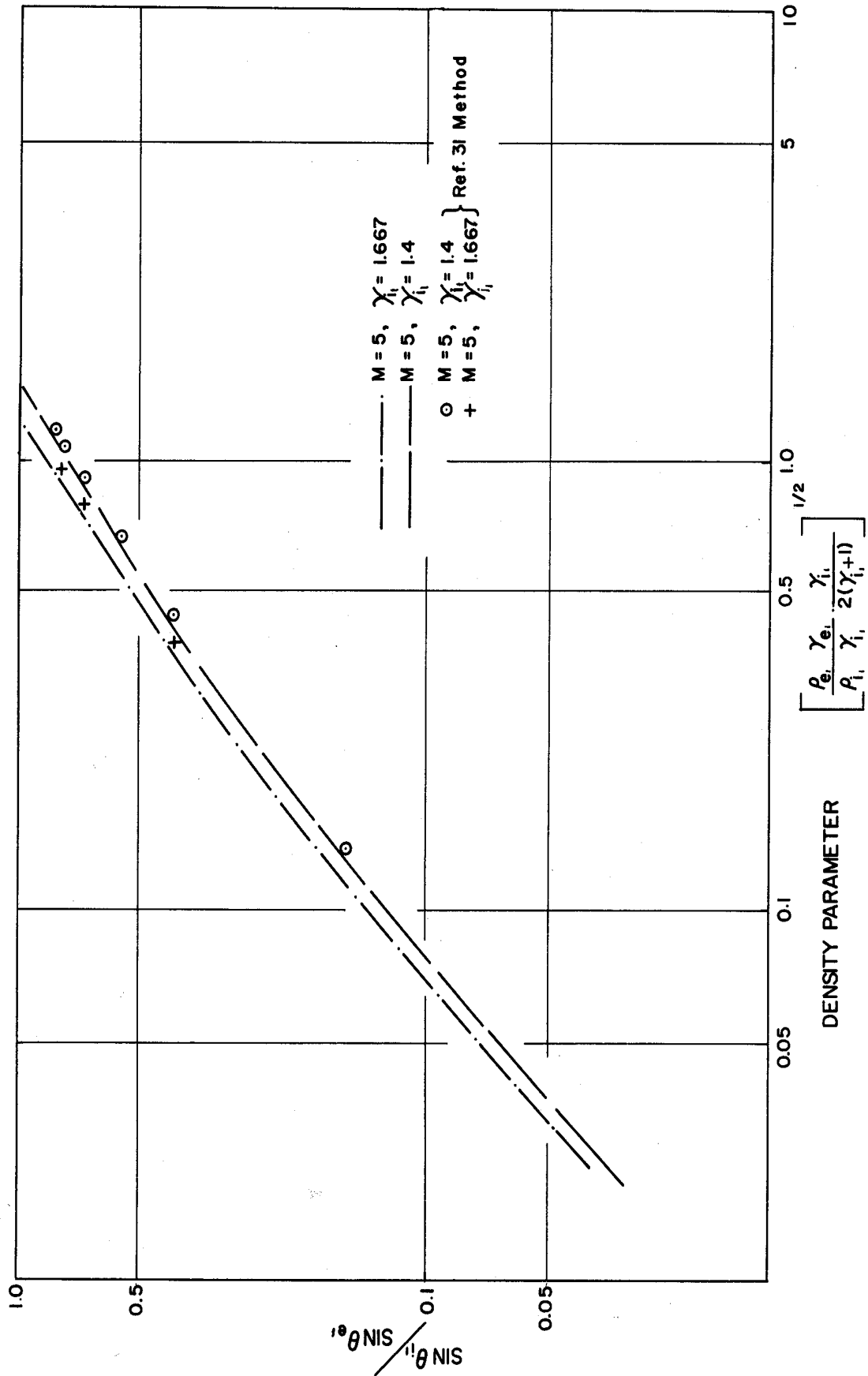


Figure 10. Relationship of Refracted to Incident Wave as a Function of Density Parameter.

d. Determination of the Detonation
Wave Velocity Decrement

With the detonation considered as a discontinuity, one can calculate the deflection angle of the interface as is done in Section 2.3b. In order to determine the detonation wave velocity decrement, the assumption is now made, for the model of Figure 5, that the same deflection angle prevails along the reaction length. This assumption is borne out by the experimental results presented in Chapter V. If one considers a two-dimensional channel of width b , exposed to the inert on one side normal to b , it is easily seen that

$$\xi = \frac{\bar{x} \tan \delta}{b} \quad (2.53)$$

From Equation (2.27), it is seen that the only unknown left is ϵ . An estimate of the value of ϵ can be obtained from the work of Hirschfelder and Curtiss.⁽²¹⁾ In this work, the pressure distribution in the reaction zone of a detonation with an irreversible unimolecular reaction is calculated for the case where the shock and reaction zones are coupled. In terms of their reduced distance which is proportional to \bar{x} and which can be denoted by ζ , it is found that the pressure distribution p could be represented with good fidelity by the following equation:

$$\left(\frac{p}{p_2} - 1\right) = \left(\frac{p_{\max}}{p_2} - 1\right) e^{-k\zeta} \quad (2.54)$$

where p_2 is the CJ pressure. If we define the reduced reaction length $\bar{\zeta}$ as that point where $p = p_{\bar{\zeta}}$ is within one percent of the final value, one obtains

$$\bar{\zeta} = \frac{1}{k} \ln\left(\frac{p_{\max} - p_2}{p_{\bar{\zeta}} - p_2}\right) \quad (2.55)$$

Further, since for a known channel width and a known angle δ , ξ is proportional to ζ , definition (2.21) can be written in the alternative form

$$\int_0^{\bar{\xi}} \frac{p}{p_2} d\zeta = \epsilon \bar{\xi} \quad (2.56)$$

and therefore, after substituting (2.54) into (2.56) and integrating the resulting equation, one gets

$$\begin{aligned} \epsilon &= \left\{ 1 + \frac{1}{k\bar{\xi}} \left(\frac{p_{\max}}{p_2} - 1 \right) (1 - e^{-k\bar{\xi}}) \right\} \\ &= 1 + \frac{\left[\frac{p_{\max}}{p_2} - 1 \right]}{\ln \left[\frac{\frac{p_{\max}}{p_2} - 1}{\frac{p_{\bar{\xi}}}{p_2} - 1} \right]} \left[1 - \frac{\frac{p_{\bar{\xi}}}{p_2} - 1}{\frac{p_{\max}}{p_2} - 1} \right] \end{aligned} \quad (2.58)$$

With $p_{\max}/p_2 = 1.53$ from Reference 21 and $p_{\bar{\xi}}/p_2 = 1.01$, it is found that

$$\epsilon = 1.13 \quad (2.59)$$

With this value of ϵ , a plot of the detonation velocity decrement as a function of the area increment can be made according to Equation (2.27). This is shown in Figure 11 for the case where $\gamma_{e20} = 1.2$. It should be added that the method of obtaining ϵ is considered simply as a good estimate. However, if the exponential character of the pressure variation is retained, it can be shown that ϵ is not very sensitive to either p_{\max}/p_2 or $p_{\bar{\xi}}/p_2$. For example, if $p_{\max}/p_2 = 2$, $\epsilon = 1.21$ and if $p_{\bar{\xi}}/p_2 = 1.10$, $\epsilon = 1.20$.

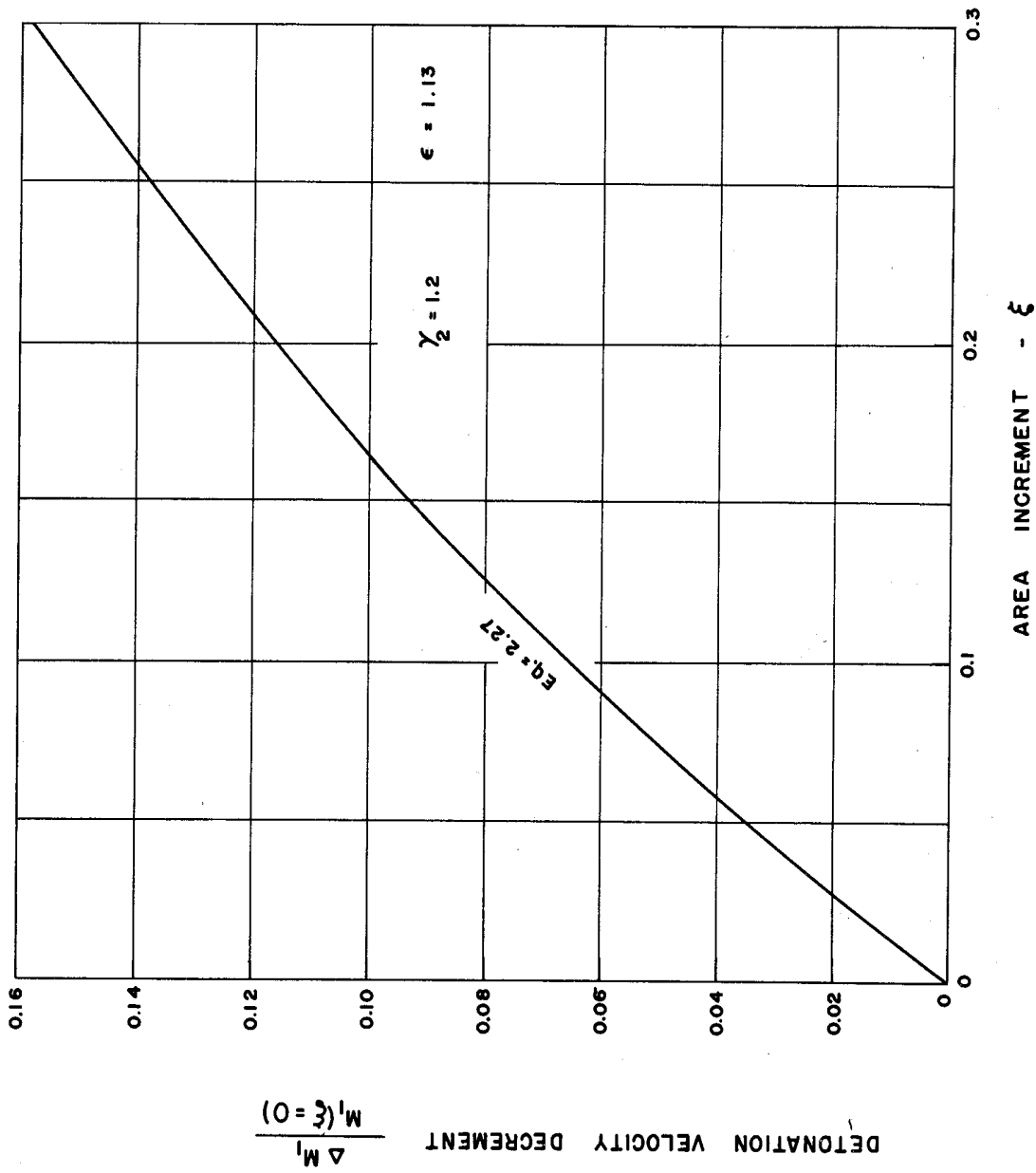


Figure 11. Detonation Wave Velocity Decrement as a Function of Area Increment.

III. CHEMICAL ASPECTS AND QUENCHING CRITERIA

Although Equation (2.27) can predict the velocity decrement in the propagation Mach number of a detonation wave, it does not give any information about whether the detonation would continue to propagate or quench. It is expected, however, that such information could be obtained by a consideration of the nature of the chemical reaction.

The quenching criteria, to be presented here, are based on theories that are used to predict composition limits, and are confined to hydrogen-oxygen mixtures as explosives.

3.1 Shchelkin's Instability Criterion

Shchelkin⁽⁵⁶⁾ examined the stability problem of a detonation wave in the light of an overall reaction rate to arrive at an analytical expression that predicts the onset of a spinning detonation. Since the latter is usually associated with composition limits (i.e., explosive compositions that do not support detonation), it would seem that his solution could be extended to predict limits due to side relief.

Briefly, Shchelkin's theory is as follows. The detonation wave is considered a shock plane followed by a CJ plane after a suitable induction time, τ . This time can be determined from the overall reaction rate when pressure dependence is ignored, as:

$$\tau \sim e^{\frac{E_2}{R_0 T_{e20}}} \quad (3.1)$$

where T_{e20} is the temperature in the shocked gas and E_2 is the activation energy for the overall reaction. (If a disturbance starts in the

CJ plane, the deformation becomes such that some of the gas in the post CJ plane infringes on the unreacted shocked gas. Since the shocked gas is at higher pressure than the reacted gas, it tends to expand to a pressure close to that of the latter, resulting in a temperature decrease. This decrease, of course, tends to increase the induction time. Shchelkin postulated that if this increase is equal or greater than the induction time, instability sets in.

Now

$$\frac{d\tau}{dT_{e20}} \sim - \frac{E_2}{RT_{e20}^2} e^{\frac{E_2}{RT_{e20}}} \quad (3.2)$$

If it is assumed that $d\tau/dT_{e20}$ is constant as the temperature goes from T_{e20} to a temperature T_{e20}^* , consistent with the expansion then the instability criterion becomes:

$$\frac{E_2}{R_0 T_{e20}} \left(1 - \frac{T_{e20}^*}{T_{e20}}\right) \geq 1 \quad (3.3)$$

If the detonation pressure in the CJ plane is p_2 and if the ratio of specific heats in the shocked region is the same as that of the original gas, then, by assuming isentropic expansion, Equation (3.3) can be written as:

$$\frac{E_2}{R_0 T_{e20}} \left[1 - \left(\frac{p_2}{p_{e20}} \right)^{\frac{\gamma_{e1} - 1}{\gamma_{e1}}} \right] \geq 1 \quad (3.4)$$

If the shocked gas has the same molecular weight as the original gas, substitution from Equations (2.11) and (2.13) with the appropriate value of F into (3.4) yields, after denoting the critical Mach number

satisfying the equality sign in (3.4) by M_{1c} :

$$1 - \left\{ \frac{(\gamma_{e1} + 1)}{\gamma_{e2} + 1} \left[\frac{\gamma_{e2} + 1 + \gamma_{e1}(M_{1c}^2 - \frac{\gamma_{e2}}{\gamma_{e1}})}{\gamma_{e1} + 1 + 2\gamma_{e1}(M_{1c} - 1)} \right] \right\}^{\frac{\gamma_{e1} - 1}{\gamma_{e1}}} \\ = \frac{R_0 T_{e1}}{E_2} \left[1 + \frac{2(\gamma_{e1} - 1)(M_{1c}^2 - 1)(\gamma_{e1} M_{1c}^2 + 1)}{(\gamma_{e1} + 1)^2 M_{1c}^2} \right] \quad (3.5)$$

The significance of the above analysis as related to this work is as follows. If the Mach number of propagation of a detonation wave is greater than M_{1c} , it is expected that it would be stable and thus continue to propagate. If, however, the propagation Mach number is smaller than M_{1c} , instability would set in, leading to possible quenching. Thus quenching takes place when

$$\frac{\Delta M_{e1}}{M_{e1}(\xi=0)} \geq \frac{M_{e1}(\xi=0) - M_{1c}}{M_{e1}(\xi=0)} \quad (3.6)$$

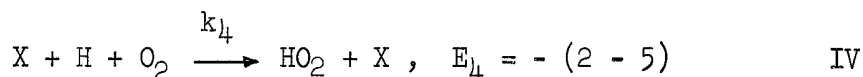
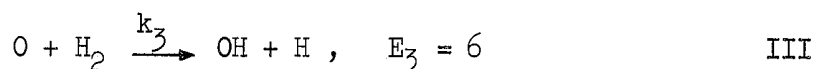
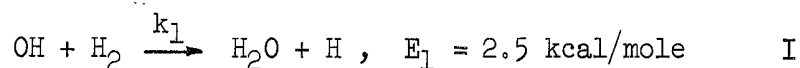
The critical Mach number, M_{1c} , is calculated for the case where the activation energy, $E_2 = 17$ kcal/mole, $\gamma_{e1} = 1.4$, $\gamma_{e2} = 1.2$, and $T_{e1} = 520^\circ\text{F}$. These values are consistent with hydrogen-oxygen mixtures. In particular the value of the activation energy corresponds to reaction II in the next section, which is generally considered to be the controlling reaction. A trial and error method used in Equation (3.5) yields $M_{1c} = 4.09$.

The theoretical detonation Mach numbers for the hydrogen-oxygen mixture without side relief have been recently calculated by Zeleznik and

Gordon, for the stoichiometric mixture⁽⁴⁶⁾ and for other mixtures that extend beyond both the rich and lean ends.⁽⁵⁷⁾ Figure 12 shows a plot of the Mach number as a function of the hydrogen mole fraction with initial conditions of room temperature and pressure. On the same plot the line showing the critical Mach number according to Shchelkin's criterion is included. Thus, the intersections of this line with the detonation curve give the composition limit. Further, since the stoichiometric mixture has the highest Mach number, it would admit the largest decrease in Mach number before quenching.

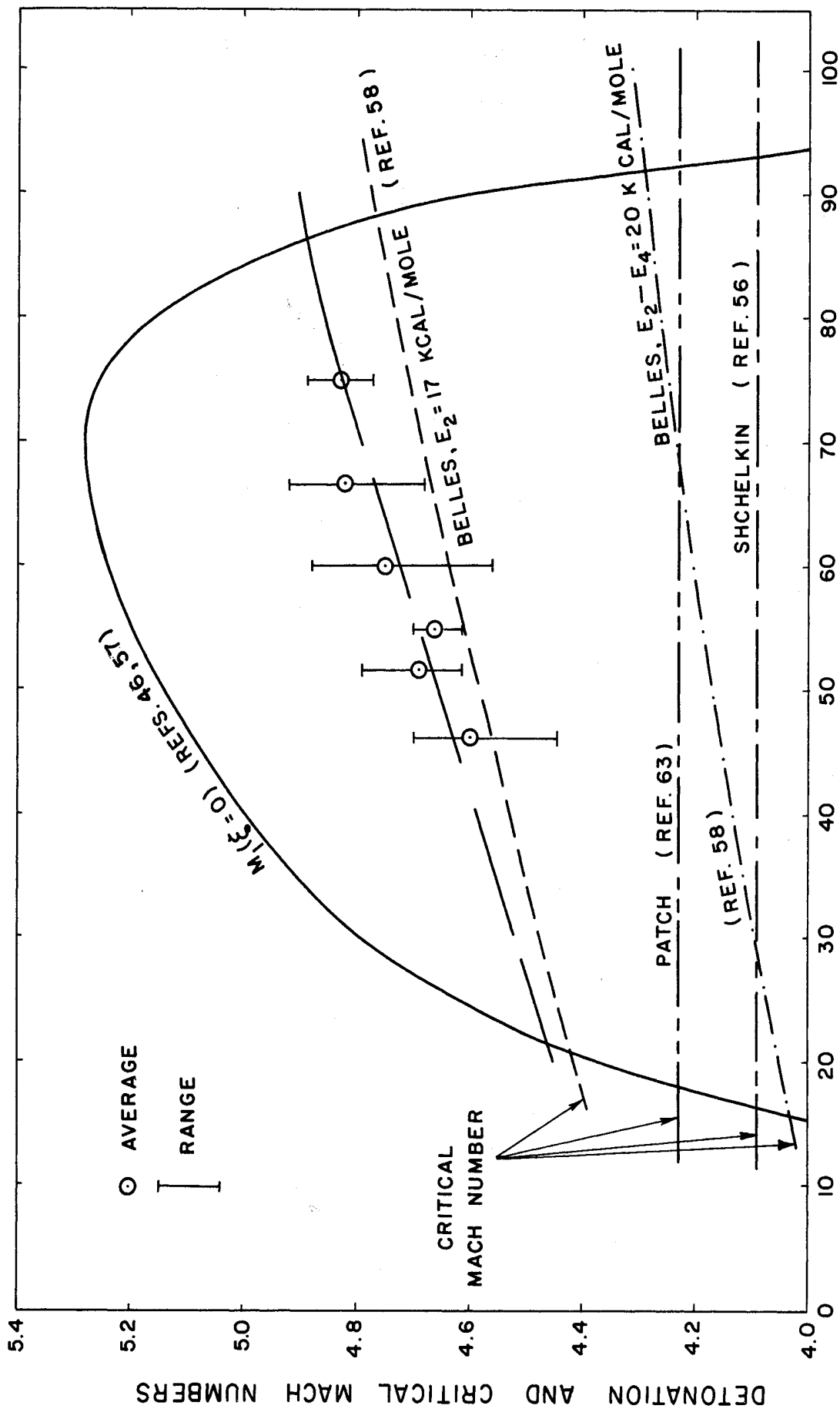
3.2 Belles' Explosion Limit Criterion

Belles⁽⁵⁸⁾ used the well known explosion criterion of hydrogen-oxygen mixtures described by Lewis and vonElbe⁽⁵⁹⁾ to predict the composition limit. The important reactions considered in this scheme are the following:



The steady state approximation for this set of reactions yields the following relation between the chain propagating reaction II and the gas phase chain breaking reaction IV.

$$\frac{2k_2}{k_4[\text{X}]} = 1 \quad (3.7)$$



% HYDROGEN IN H₂ - O₂ MIXTURE

Figure 12. Dependence of the Detonation and the Critical Mach Numbers on Hydrogen-Content in H₂ - O₂ Mixtures.

The values for the rate constants as given by (59) are as follows:

$$k_2 = 10^{-17} \sqrt{\frac{T_{e20}}{830}} e^{-\left(\frac{803}{T_{e20}} - 1\right) \frac{17,000}{803R}} \frac{\text{cm}^3}{\text{sec}}$$

and

$$k_4 = 3.7 \times 10^{-35} \sqrt{\frac{T_{e20}}{803}} \frac{\text{cm}^6}{\text{sec}}$$

If these are substituted into Equation (3.7), one obtains

$$\frac{P_{e20}}{T_{e20}} e^{17,000/RT_{e20}} = \frac{3.11}{f_x} = \phi_3 \quad (3.8)$$

where f_x is an effective mole fraction of third bodies given by (59) as:

$$f_x = f_{H_2} + .35f_{O_2} + .43f_{N_2} + .2f_{Ar} + 1.47f_{CO_2} + 14.3f_{H_2O} \quad (3.9)$$

and where T_{e20} (in °K) and P_{e20} (in atmospheres) are the temperature and pressure respectively in the shocked gas behind the detonation front.

The left hand side of Equation (3.8) is a function of the Mach number, γ_{e1} , the initial pressure and temperature. This function which can be obtained from Equations (2.11) and (2.13) with $F = 2$, is denoted by ϕ_3 . The right hand side of Equation (3.8) is a function of composition only. Plotting ϕ_3 against M_{e1} as in Figure 13 (curve labeled $E_2 = 17$ kcal/mole) where γ_{e1} is taken as 1.4, $T_{e1} = 300^\circ\text{K}$ and $p_1 = 1$ atm, one can obtain the value of M_{e1} for each mixture ratio that satisfies Equation (3.8). This is the Mach number that satisfies the explosion criterion and is considered the critical Mach number below which detonation is not possible. It is plotted in Figure 12 as the curve labeled "Belles, $E_2 = 17$ kcal/mole".

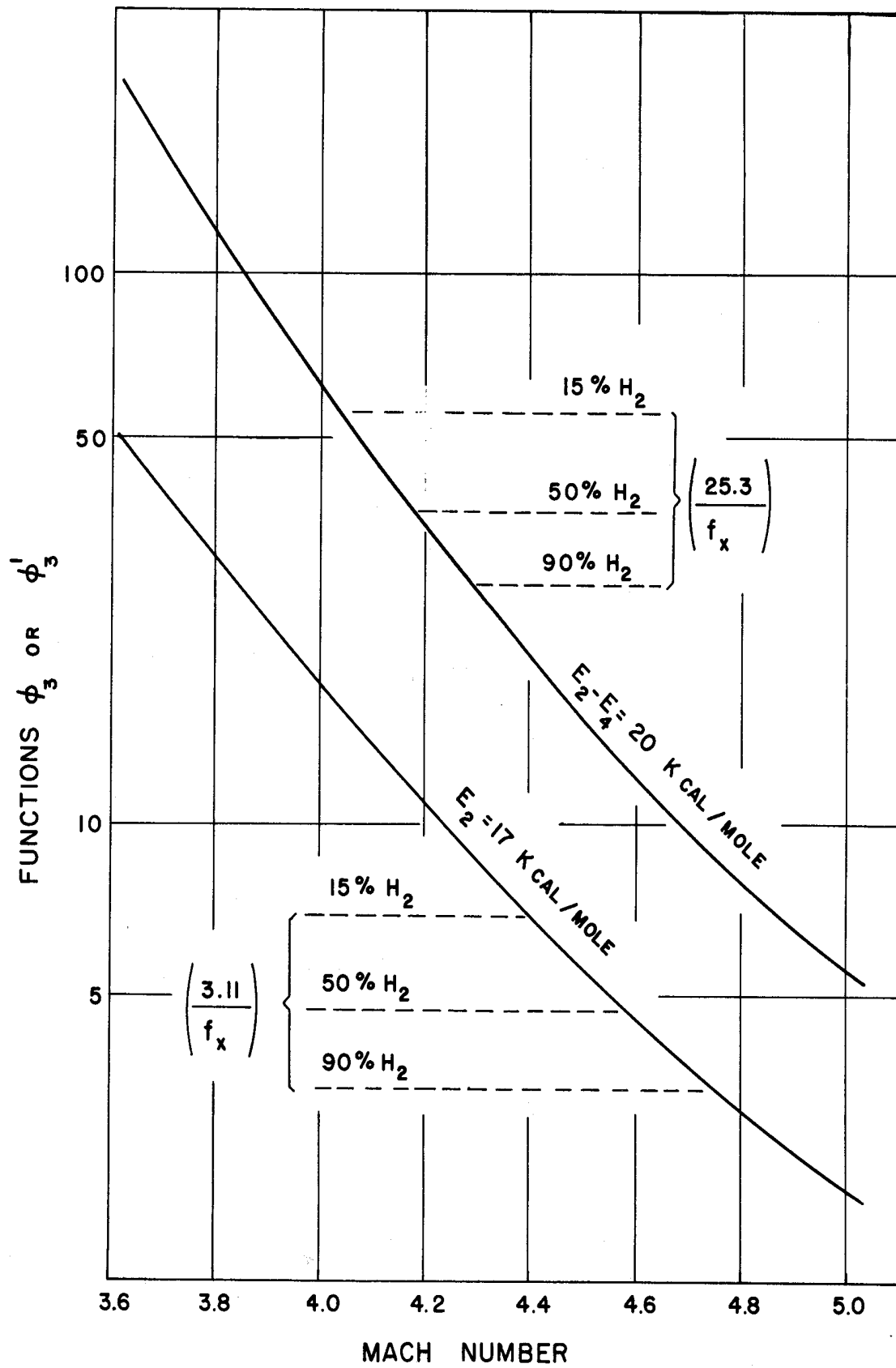


Figure 13. Critical Mach Numbers According to Belles' Explosion Limit Criterion.

More recent data on reaction rate constants indicate that reaction IV has a negative activation energy with $E_4 = - (2 - 5)$ kcal/mole as reported by Clyne⁽⁶⁰⁾ and Baldwin.⁽⁶¹⁾ If the value of $2k_2/k_4 = 72$ mm Hg at 813°K and $E_2 - E_4 = 20$ kcal/mole as quoted by the latter are assumed, then Equation (3.7) becomes

$$\frac{P_{e20}}{T_{e20}} e^{20,000/RT_{e20}} = \frac{25.3}{f_x} = \phi'_3 \quad (3.10)$$

The function ϕ'_3 will be different from ϕ_3 as can be seen from the curve labeled " $E_2 - E_4 = 20$ kcal/mole" in Figure 13. Consequently, the critical Mach number variation corresponding to Equation (3.10) which is plotted in Figure 12 as the curve labeled "Belles, $E_2 - E_4 = 20$ kcal/mole" will also be different. It is apparent that this curve is much lower than that corresponding to Equation (3.8) where old reaction rates are used, and is very close to that of Shchelkin's criterion.

Further, it should be mentioned at this point, that although Belles' analysis is criticized because it extends the explosion limit criterion to regions of pressures and temperatures far removed from static experiments, there is evidence of its validity in the standing detonation wave experiments by Nicholls and Dabora.⁽⁶²⁾

3.3 Patch's Constant Temperature Criterion

Patch⁽⁶³⁾ examined the experimental works of Gordon, et al.,⁽⁶⁴⁾ and of Breton⁽⁶⁵⁾ near the rich and lean limits of hydrogen-oxygen-diluent mixtures for the purpose of deducing a limit criterion. He calculated the theoretical Mach number for mixtures with compositions at the limit corresponding to the values of (64) and (65), from which he deduced the

temperature, T_{e20} , behind the shock at various degrees of relaxation. From his results he concluded that the temperature T_{e20} gave the least standard deviation when rotational relaxation but no vibrational relaxation was considered. The average T_{e20} , he found, was 1314°K when initial conditions were atmospheric. He then proceeded to calculate the theoretical compositions that have a detonation Mach number compatible with the average T_{e20} .

Patch also calculated the theoretical limit composition using Belles' ⁽⁵⁸⁾ explosion limit criterion outlined in the previous section. By comparing the deviation of the theoretical hydrogen mole fraction calculated by the two methods from the experimental mole fraction at the limit, he found that the average of the absolute value of the deviation is smaller in the case of the constant temperature calculation than that of the explosion limit calculation. His conclusion, then, is that a constant ignition temperature independent of composition can adequately predict the composition limits.

On this basis, if one assumes that the same critical ignition temperature is required for all mixture ratios, then the same critical detonation Mach number is necessary. This can easily be found from Equation (2.13) to be $M_{1c} = 4.23$, and is shown on Figure 12 by the straight line labeled "Patch". It is interesting to note that it is close to the critical Mach number calculated by Shchelkin's criterion.

The composition limits as predicted by the above three criteria can now be compared with experimental observation. Table I, below, presents such a comparison. It indicates that all three criteria (except

Belles' with the old chemical kinetic data) predict limits very close to those observed.

TABLE I

HYDROGEN-OXYGEN COMPOSITION LIMITS
Detonation Limits (Mixtures at $T_{el} = 300^\circ\text{K}$ and $p_{el} = 1 \text{ atm.}$)

Criterion	Lean Limit (% H_2)	Rich Limit (% H_2)
Shchelkin($E_2 = 17 \text{ kcal/mole}$)	16.5	93.0
Belles ($E_2 = 17 \text{ kcal/mole}$)	21.0	87.8
($E_2 - E_4 = 20$)	16.8	92.0
Patch ($T_{e20} = 1314^\circ\text{K}$)	18.0	92.2
Observed:		
Gordon, et al. (Reference 64)		92.5
Breton (Reference 65)	15.0	
Lafitte (Reference 66)	15.0	90.0

However, we shall see from the experimental results that quenching due to side relief will follow trends similar to those predicted by Belles' criterion, when old kinetic data are used.

IV. EXPERIMENTAL REQUIREMENTS AND ARRANGEMENT

4.1 Preliminary Experiments

In order to explore in at least a qualitative fashion the ideas embodied by Equations (2.27) and (3.6), it was decided to use a setup similar to that of Sommers⁽³¹⁾ but with some modifications as shall be described presently. The main two ideas that were to be explored are, (1) that the decrease in the detonation velocity when the wave is confined by a compressible medium, should be approximately inversely proportional to the channel width as Figure 11 and Equation (2.53) indicate, and (2) that there should be a point where the decrease can become so high that the detonation would quench and degenerate into a pure shock.

In Sommers' setup, an explosive mixture is realized by metering fuel gas and oxygen into the bottom of a rectangular flame tube of approximately 4 ft in length and .35 in. x .5 in. in cross-section. The explosive mixture flows at very low velocity (order of 10 ft/sec) through the tube and into the test section. At the test section, the explosive jet is bounded by glass plates at the wider sides, and by a solid wall on one narrow side. At the other narrow side the jet flows adjacent to either a quiescent or a flowing boundary inert gas. The explosive mixture is ignited at the bottom of the flame tube, and by a suitable time delay arrangement a schlieren picture of the detonation wave and attendant phenomena at the test section can be taken. Figure 4 is a typical photograph obtained in this manner.

For the purpose of performing the preliminary experiments, the test section is modified as shown schematically in Figure 14. The explosive jet from the flame tube is divided into two columns, usually of different widths. Each column is bounded by a side jet of the inert to be used. The dividing wall is a .010 in. thick brass shim stock, the bottom of which is filed to a wedge. A photograph of the test section is shown in Figure 15.

The idea now is that a detonation wave originating in the flame tube propagates into both channels at the same speed at the beginning of the test section where the explosive is bounded by solid walls. However, when the detonation wave reaches a point where the explosive is exposed to an inert, any effect on the propagation velocity could be noticed. Figure 16 shows a series of photographs taken at different time delays from the instant the detonation wave passes a fixed point in the flame tube. The explosive in this case is stoichiometric H_2-O_2 mixture and the inert is nitrogen. In Figure 16a the detonation front is shown after it has been split by the dividing wall and it is apparent that the wall has a negligible effect. From Figure 16a-16d, one can clearly see that the detonation front travelled faster in the wide channel than in the narrow one. Further, in the wider channel the combustion zone seems to be attached to the front whereas in the narrow channel a "clean" front could be seen followed at an appreciable distance by a "turbulent" region. This is interpreted as a quenched detonation. The "turbulent" zone apparently corresponds to the region where the explosive either

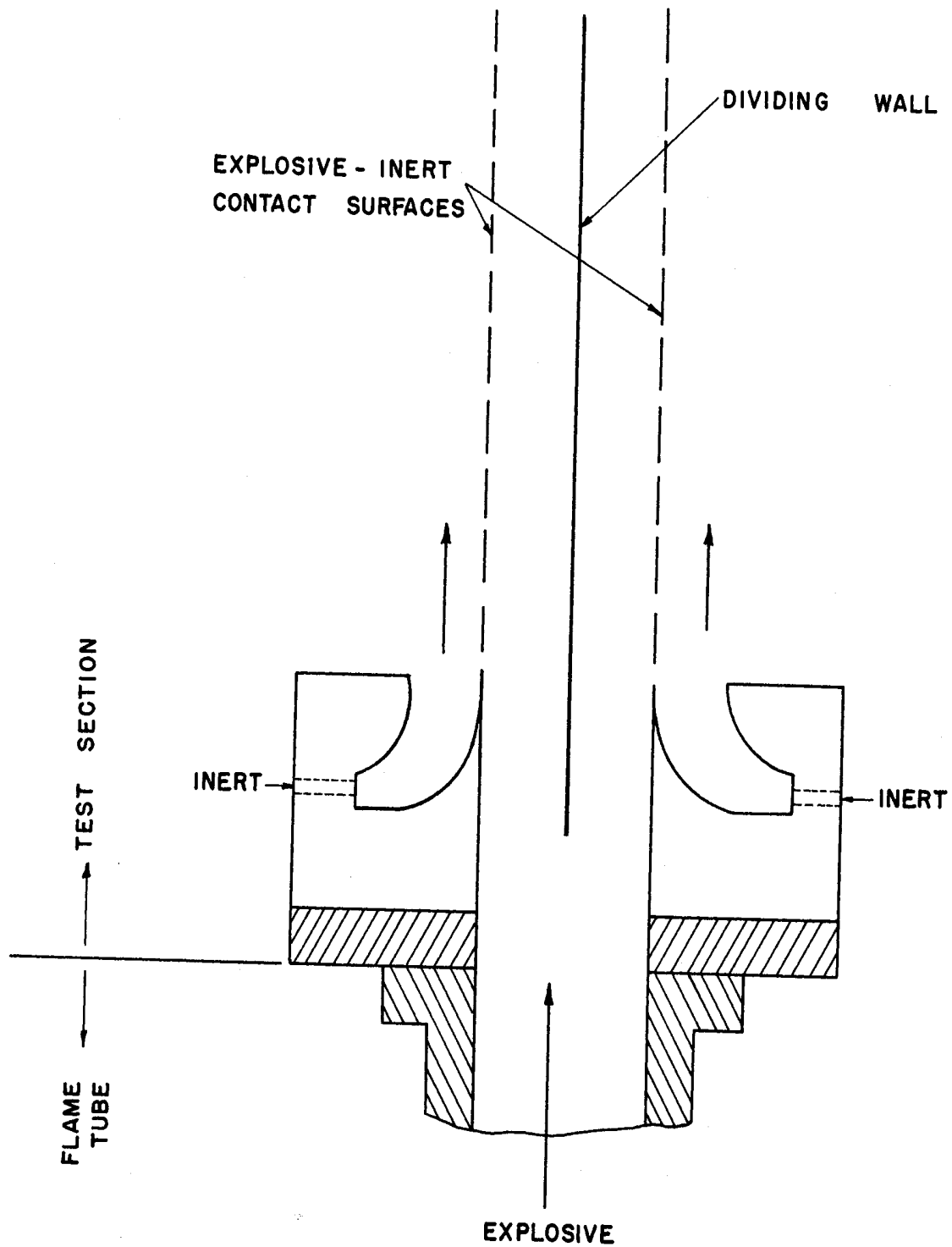


Figure 14. Schematic Drawing of the Test Section Used in the Preliminary Experiments.

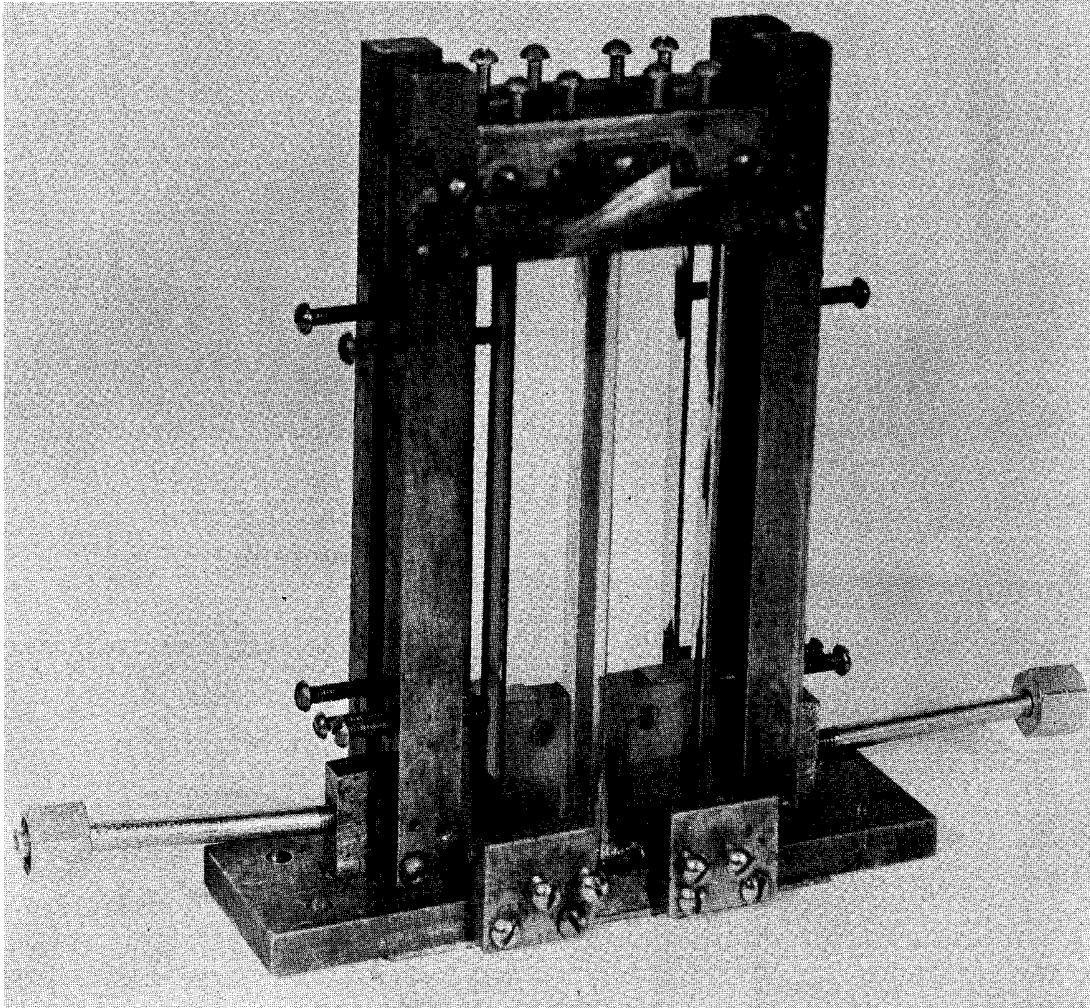
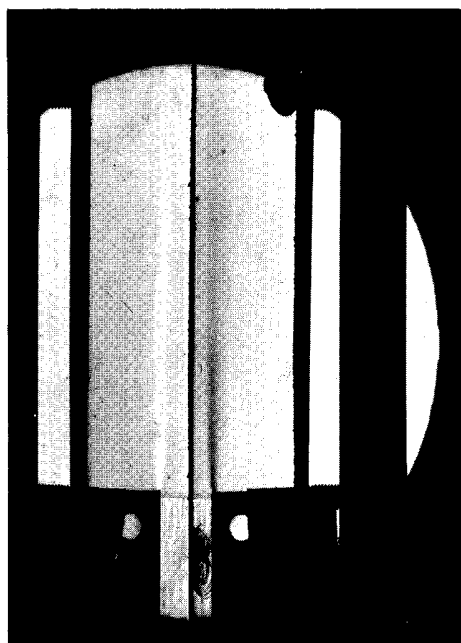
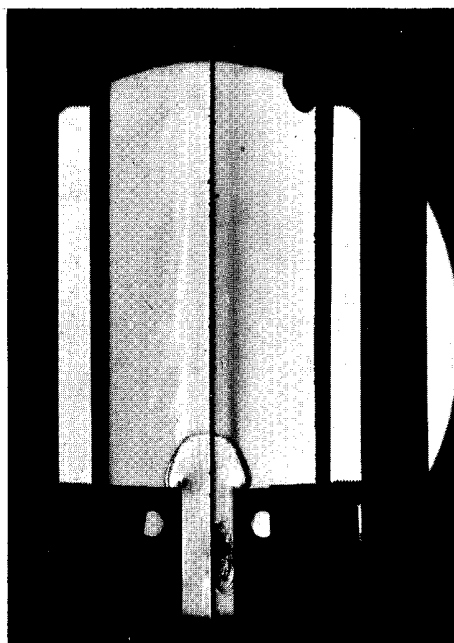


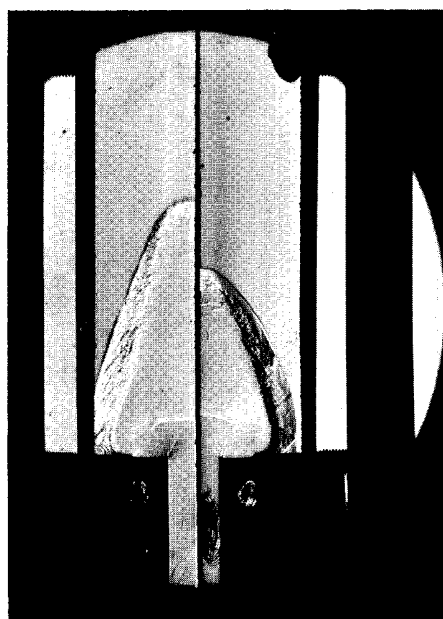
Figure 15. Photograph of the Test Section Used in the Preliminary Experiments.



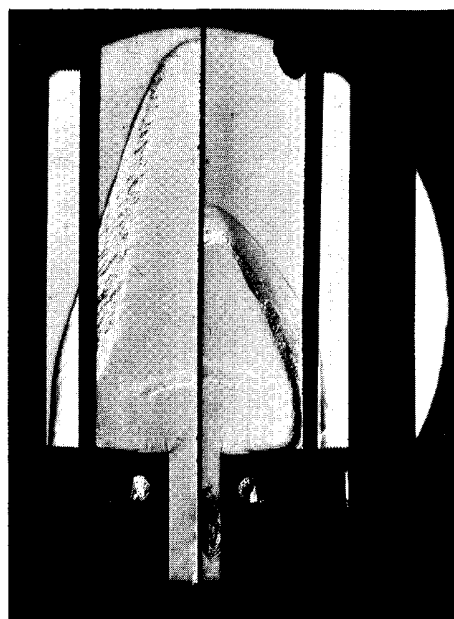
(a) $t = 72.5 \mu\text{sec}$



(b) $t = 77.1 \mu\text{sec}$



(c) $t = 94.6 \mu\text{sec}$



(d) $t = 107.8 \mu\text{sec}$

Figure 16. Detonation Wave Progress of Stoichiometric $\text{H}_2 - \text{O}_2$ Mixture in Channels of Two Different Widths.
(Boundary Gas = N_2)

(Scale: Total width of both channels = .5 in.)
(t = relative time picture was taken)

ceases to burn or is deflagrating. This explanation is further corroborated by x-t plots of the detonations from these and similar photographs, in that the front appears to travel at continuously decreasing velocity in the narrow channel. On the other hand, in the wider channel the velocity seems to reach a new steady-state value somewhat lower than that in the solid tube, at about 10 μ sec after the detonation passes the start of exposure to the inert.

Experiments with mixture ratios other than the stoichiometric indicated the same features just described proving qualitatively the two ideas mentioned at the beginning of this section.

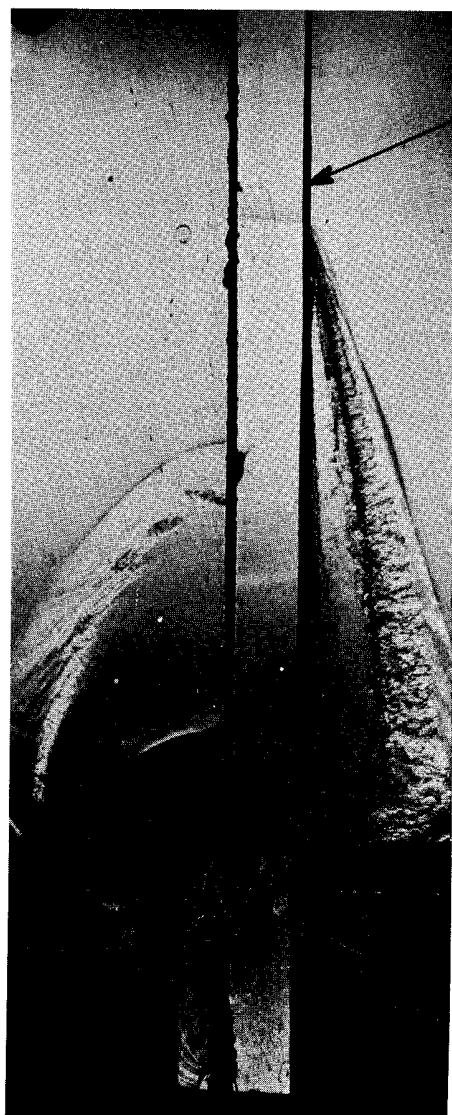
4.2 Separation of the Explosive from the Inert by a Thin Membrane or Film

A close examination of Figure 16 reveals a mixing or diffusion zone between the inert and the explosive. The question arises, then, as to what influence does the diffusion introduce into the problem. For example, could the slowing down of the detonation front be primarily due to diffusion or does the latter have only a minor effect? For his experiment Sommers calculated the diffusion width for the gases he used and found it to be of the order of .1 in. at two inches from the point where the two gases meet. He concluded that since his channel width is .5 in. the effect of diffusion would be negligible.

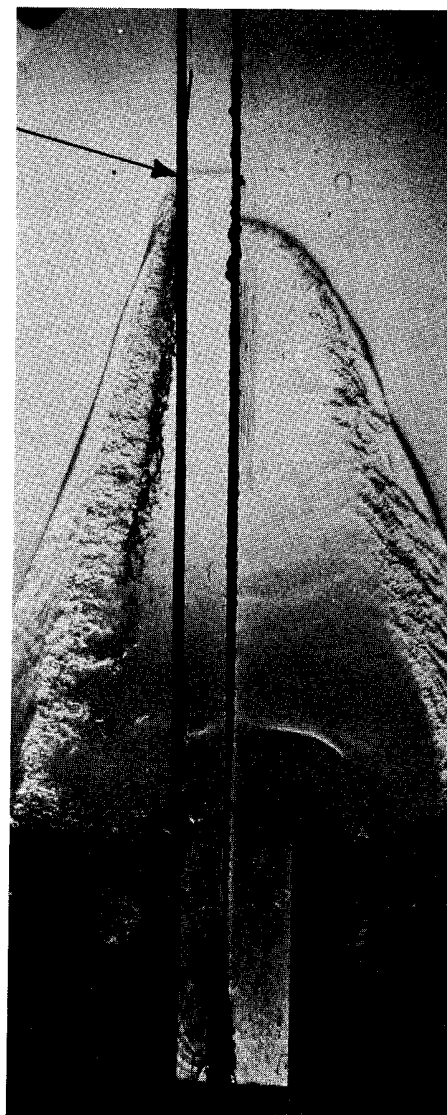
Unfortunately, such a diffusion width becomes too important in our experiments for the simple reason that channel widths less than .5 in. were contemplated. Therefore, methods for eliminating or at least minimizing the diffusion were sought. Separation of the explosive from the inert gas by a thin wall appeared to be the

logical solution. Sommers, early in his work, had used cellophane wrap .0005 in. thick as the dividing wall but he found that such walls offered infinite confinement as far as the detonation wave was concerned. In other words, he found that the detonation wave in a cellophane tube propagated at the same speed as it would have in a tube having thick solid walls. His conclusion was that the presence of any solid wall no matter what its thickness is, would provide infinite confinement for detonations.

Despite this discouraging observation, it was decided that it would be worthwhile to test a thinner membrane and therefore a soap film was tried. The film was obtained by dipping a wire frame into a soap solution and then retracting it. Because of the relatively large area required namely: .35 in. x 3 in., it was found that a thick solution was necessary to obtain a film that would last about two minutes, which was the time necessary to carry out the experiment. Thus, commercial liquid soap with one to one by volume dilution with water was found adequate. After obtaining the soap film on the frame, the frame was inserted into the test section and positioned so as to separate the explosive gas from the boundary inert gas. Figure 17 is typical of the results obtained. In Figure 17a the soap film was on the wider channel and in Figure 17b it was on the narrower channel. In either case, it is clear that the detonation front remained planar and travelled faster in the channel with the soap film. Further, from measurement of detonation velocity in the solid tube ahead of the test section and other necessary data, it appeared that the detonation wave did



(a) Film on wider channel



(b) Film on narrower channel

Figure 17. Detonation Wave Appearance When Confined by a Soap Film.

not change its velocity while travelling in the channel provided with the soap film. These results, then, supported Sommers' conclusion mentioned earlier.

At this stage, the author's attention turned to the work of Gvozdeva⁽⁵⁵⁾ where a study of the refraction of detonation waves from one medium to another was made. The two gaseous media were separated by a thin nitrocellulose film which evidently introduced a negligible effect. From this work and the tests described above, it became apparent that an analytical determination of what constitutes a film of negligible effect is in order. This is presented in the following section.

4.3 Analytical Determination of the Critical Thickness of Thin Films

For the determination of film thickness, one can resort back to the shock tube analogy. Again in this analogy, the driver gas is the gas behind the detonation wave and the driven gas is the inert medium. Further if there is a film between these two gases, it will be analogous to a piston of a gun tunnel. Because the film is thin and reasonably weak, it is assumed that the only resistance it offers to the expansion of the burned gas is that due to inertia. Figure 18 shows schematically the analogy with the film position assuming the "piston" path.

The acceleration, $\overset{0}{v}_f$, of the film in the y direction is governed by the following equation:

$$p_{e3} - p_{i2} = \rho_f \ell_f \overset{0}{v}_f \quad (4.1)$$

The expansion of the gas behind the wave is assumed to take place isentropically so that:

$$\frac{p_{e3}}{p_{e20}} = \left[1 - \frac{\gamma_{e20} - 1}{2} \frac{v_{e3}}{a_{e20}} \right]^{\frac{2\gamma_{e20}}{\gamma_{e20} - 1}} \quad (4.2)$$

and finally the instantaneous velocity of the inert in the y direction is the same as that of Equation (2.41) and is rewritten here for convenience:

$$\frac{v_i}{a_{i1}} = \left[\frac{p_{i2}}{p_{i1}} - 1 \right] \left[\frac{\frac{2}{\gamma_{i1}(\gamma_{i1} + 1)}}{\frac{p_{i2} + \gamma_{i1} - 1}{p_{i1} \gamma_{i1} + 1}} \right]^{1/2} \quad (4.3)$$

The velocity of the film and the velocities of the gases immediately in front or behind it are all the same and therefore can be denoted by v

$$v_f = v_i = v_{e3} = v \quad (4.4)$$

By using the definitions of ϕ_1 , ϕ_2 and \bar{P} of Equations (2.33), (2.34) and (2.37) respectively and noting that:

$$\frac{v_{e3}}{a_{e20}} = \frac{v}{a_{i1}} \cdot \frac{a_{i1}}{a_{e1}} \cdot \frac{a_{e1}}{a_{e20}} \quad (4.5)$$

one can write Equations (4.1) and (4.3) in the following forms respectively:

$$\frac{p_{e3}}{p_{e20}} - \frac{\bar{P}}{\phi_1} = \frac{c}{v} \quad (4.6)$$

and

$$\bar{v} = \frac{2}{\gamma_{el} \phi_2} \left[\frac{\rho_{el} \gamma_{el}}{\rho_{il} \gamma_{il}} \cdot \frac{\gamma_{il}}{2(\gamma_{il} + 1)} \right]^{\frac{1}{2}} \frac{\bar{P} - \frac{p_{il}}{p_{el}} \frac{1}{M_{el}^2}}{\left[\bar{P} + \frac{p_{il}}{p_{el}} \cdot \frac{1}{M_{el}^2} \cdot \frac{\gamma_{il} - 1}{\gamma_{il} + 1} \right]^{\frac{1}{2}}} \quad (4.7)$$

where

$$\frac{0}{\bar{v}} = \frac{d\bar{v}}{dt} \equiv \frac{\rho_f \ell_f^0 v}{p_{el} \phi_1 M_{el}^2} \quad (4.8)$$

$$\bar{v} = \frac{v_{e2}}{a_{e20}} \equiv \frac{v}{a_{el}} \cdot \frac{1}{\phi_2 M_{el}} \quad (4.9)$$

and

$$\bar{t} = \frac{\phi_1 p_{el} M_{el}}{\phi_2 \rho_f \ell_f a_{el}} t \quad (4.10)$$

From Equation (2.43), Equation (4.7) is seen to be:

$$\bar{v} = \frac{\tan \delta}{\phi_2} \quad (4.11)$$

However, $\tan \delta$ in Figure 8 is found to be a function of the density ratio parameter independent of whether a shock or a detonation condition behind the front of the detonation wave is assumed, and weakly dependent on the Mach number for $M_{el} \geq 5$. Hence, the high Mach number approximation can be used in Equation (4.7) to give:

$$\bar{v} = \frac{2}{\gamma_{e1}} \frac{\sqrt{P}}{\phi_2} \left[\frac{\rho_{e1}\gamma_{e1}}{\rho_{i1}\gamma_{i1}} \cdot \frac{\gamma_{i1}}{2(\gamma_{i1} + 1)} \right]^{1/2} \quad (4.12)$$

Substituting this equation and Equation (4.2) into Equation (4.6), one obtains:

$$\left[1 - \frac{\gamma_{e20} - 1}{2} \bar{v} \right]^{\frac{2\gamma_{e20}}{\gamma_{e20} - 1}} - \frac{1}{\phi_1} \left[\frac{\gamma_{e1}\phi_2}{2} \right]^2 \left[\frac{\rho_{i1}\gamma_{i1}}{\rho_{e1}\gamma_{e1}} \cdot \frac{2(\gamma_{i1} + 1)}{\gamma_i} \right] \bar{v}^2 = \frac{0}{\bar{v}} \quad (4.13)$$

At this point the values of ϕ_1 and ϕ_2 for the shock or the detonation conditions are calculated using the values of γ_{i1} , γ_{e1} , γ_{e20} and p_{i1}/p_{e1} shown in Table II below in Equations (2.33) and (2.34).

TABLE II
EVALUATION OF THE FUNCTIONS ϕ_1 AND ϕ_2

M_{e1}	F	$\left(\frac{p_{i1}}{p_{e1}}\right)$	γ_{i1}	γ_{e1}	γ_{e20}	ϕ_1	ϕ_2
5	2(shock)	1	1.4	1.4	1.4	1.160	.481
$\rightarrow \infty$	2(shock)	any	1.4	1.4	1.4	1.1667	.441
5	1(deton)	1	1.4	1.4	1.2	.654	.560
$\rightarrow \infty$	1(deton)	any	1.4	1.4	1.2	.636	.545

As is expected, the values of ϕ_1 and ϕ_2 depend primarily on whether shock or detonation conditions is assumed but not on the Mach number for $M_{e1} \geq 5$.

Equation (4.13) is plotted in Figure 19 for both shock and detonation conditions with ϕ_1 and ϕ_2 corresponding to very large M_{e1}

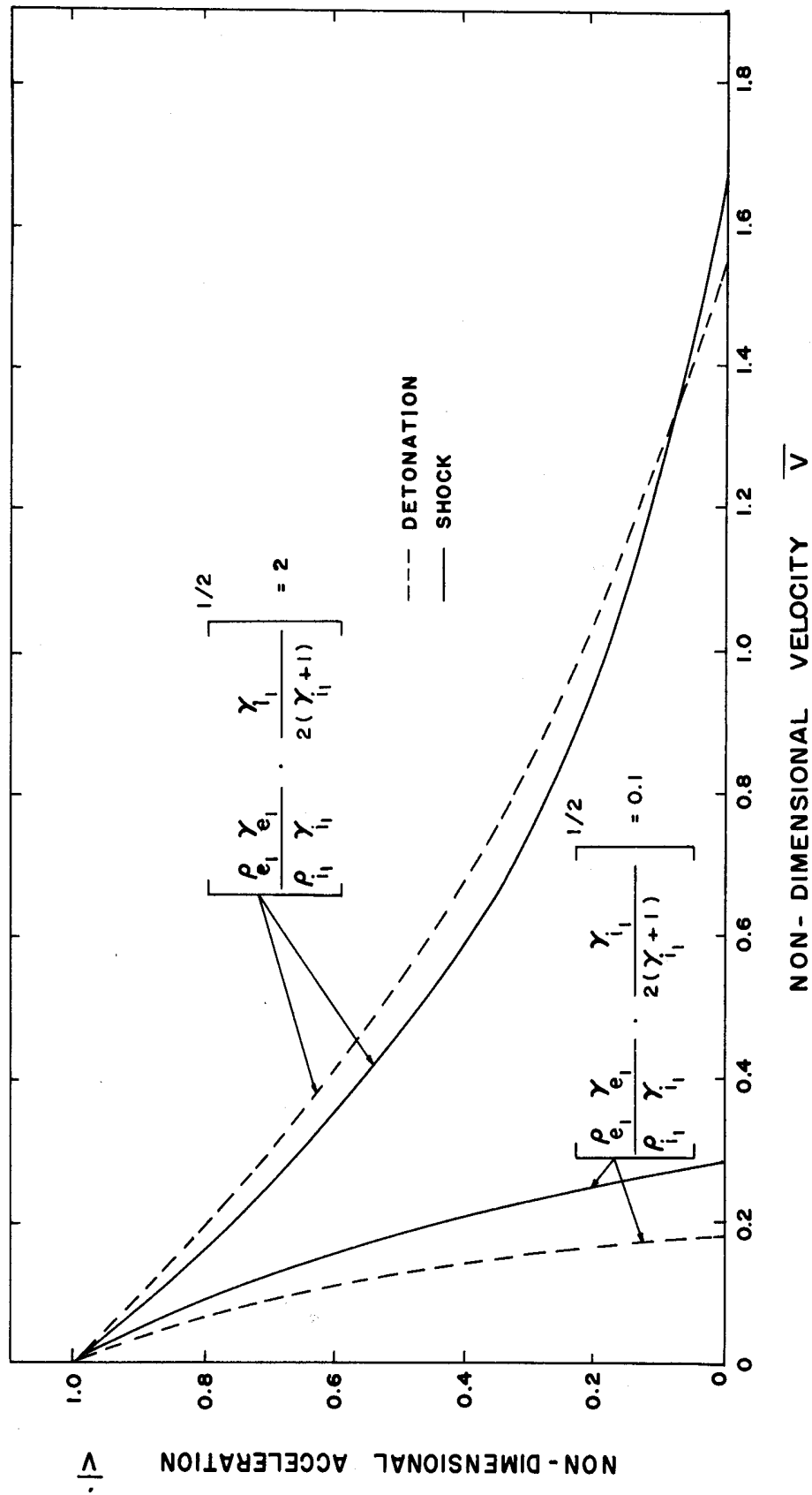


Figure 19. Instantaneous Film Velocity vs. Its Acceleration.

and with γ 's corresponding to Table II. Further, two values of the density ratio parameter appearing in the equation are considered, namely

$$\left[\frac{\rho_{e1}\gamma_{e1}}{\rho_{i1}\gamma_{i1}} \cdot \frac{\gamma_{i1}}{2(\gamma_{i1} + 1)} \right]^{1/2} = .1 \text{ or } 2.$$

These values are chosen because they bracket the values for the combination of gases that are used experimentally.

From Figure 19 it is seen that the variation of the non-dimensional acceleration can reasonably be expressed as a linear function of the non-dimensional velocity, i.e.,

$$\frac{0}{\bar{v}} = 1 - \frac{\bar{v}}{\bar{v}_{\infty}} \quad (4.14)$$

where \bar{v}_{∞} is the velocity at $\frac{0}{\bar{v}} = 0$.

Equation (4.14) can be integrated by separation of variables to obtain the time t_{λ} , required for the velocity to reach a certain fraction, λ , of the final velocity. Thus

$$\int_0^{\lambda \bar{v}_{\infty}} \frac{d\bar{v}}{1 - \frac{\bar{v}}{\bar{v}_{\infty}}} = \int_0^{\bar{t}_{\lambda}} d\bar{t} \quad (4.15)$$

or

$$\bar{v}_{\infty} \ln \left(\frac{1}{1-\lambda} \right) = \bar{t}_{\lambda} \quad (4.16)$$

Setting this time to be a fraction, σ , of the reaction time, one obtains after noting that the reaction time = \bar{x}/u_{e1} and using Equation (4.10):

$$\frac{l_f}{\bar{x}} = \frac{\sigma \phi_1 \rho_{el} M_{el}}{\phi_2 \bar{v}_{\infty} \rho_f a_{el} u_{el} \ln \left(\frac{1}{1-\lambda} \right)} \quad (4.17)$$

or

$$\frac{l_f}{\bar{x}} = \frac{\sigma \phi_1}{\bar{v}_{\infty} \gamma_{el} \phi_2 \ln \left(\frac{1}{1-\lambda} \right)} \cdot \frac{\rho_{el}}{\rho_f} \quad (4.18)$$

With the values of ϕ_1 and ϕ_2 shown in Table II, it can be seen that the most stringent case is that for a detonation condition behind the wave. Further, when ρ_e is smaller than ρ_i then \bar{v}_{∞} is also small and when ρ_e is larger than ρ_i , v_{∞} is large. By considering these effects and after setting $\sigma = .1$ and $\lambda = .99$, one obtains for the most conservative case

$$\begin{aligned} \frac{l_f}{\bar{x}} &= \frac{.1 \times .636}{.185 \times 1.4 \times .545 \times 4.6} \cdot \frac{\rho_{el}}{\rho_f} \\ &= .0978 \frac{\rho_{el}}{\rho_f} \approx .1 \frac{\rho_{el}}{\rho_f} \end{aligned} \quad (4.19)$$

The inertia of films with thickness given by this equation would be felt only within one-tenth of the reaction length. For the purpose of this study, this is considered the critical thickness beyond which the effect of the film is no longer deemed negligible. For film material, such as nitrocellulose, having a density of 1.58 gms/cm^3 and for an explosive (80% H_2 - 20% O_2) density of $3.57 \times 10^{-4} \text{ gms/cm}^3$ at N.T.P. and a reaction length of about 0.3 cm.,

$$l_f = 6.8 \times 10^{-6} \text{ cm} = 680 \text{ \AA} \quad (4.20)$$

This result explains why cellophane whose thickness is two orders of magnitude higher can act as infinite confinement.

It is to be noted that although Equation (4.19) predicts that the film thickness should be proportional to the operating pressure, the fact that the reaction length is inversely proportional to the pressure for a second order reaction cancels its dependence on pressure.

4.4 Preparation of Thin Films and Estimation of Their Thickness

Thin films with thicknesses of the order required for our purposes have been used in electron microscopy as supporting membranes for the specimens being observed. There are several materials that can be used, but apparently the two most common materials are Formvar (polyvinyl formal) or Collodion (cellulose tetranitrate dissolved in ether and alcohol). The film is usually prepared by first obtaining a solution of the material in an appropriate volatile solvent and carefully placing a few drops of the solution on the surface of distilled water in a Petrie dish of about 20 cm in diameter. The solution spreads over the surface, the solvent evaporates, and one is left with a thin film floating on the water surface. Various techniques for removing the film are used and the interested reader is referred to a book by Hall⁽⁶⁷⁾ which contains a chapter on the subject of films.

The material adopted for use in the experiments of this study is Collodion dissolved in amyl-acetate. It was found after some experimentation that three drops of 15% solution were adequate for they provided a film of acceptable thickness yet they allowed a reasonable time before the solvent completely evaporates -- a situation that renders the removal of the film subject to frequent breakage.

To prepare the film for use, three drops of the solution are placed on the water surface in rapid succession. These are easily seen to spread over most of the dish surface. As the solvent evaporates there appear broad diffraction color bands over the whole surface. As soon as they disappear a steel frame-film holder whose dimensions are shown in Figure 20, is introduced near the edge of the dish until all of the opening is submerged in the water under the film. The film holder is lifted gently at an angle until the edge of the film starts adhering to the surface of the holder near the top of the opening. When the holder is lifted further its two outer edges usually start cutting the film. However, sometimes the cuts need to be started by a sharp razor or knife. The holder is now moved to the center of the dish, as it is lifted, until the film covers the opening adhering to both the flat and chamfered parts of the edges of the holder. During this operation care is taken that no fold back of film occurs and that no wrinkles are present. As soon as the frame is removed the flat part of the edge is blotted out so that the film rests essentially on the chamfered portion. Sometimes a few water drops cling to the film and are allowed to

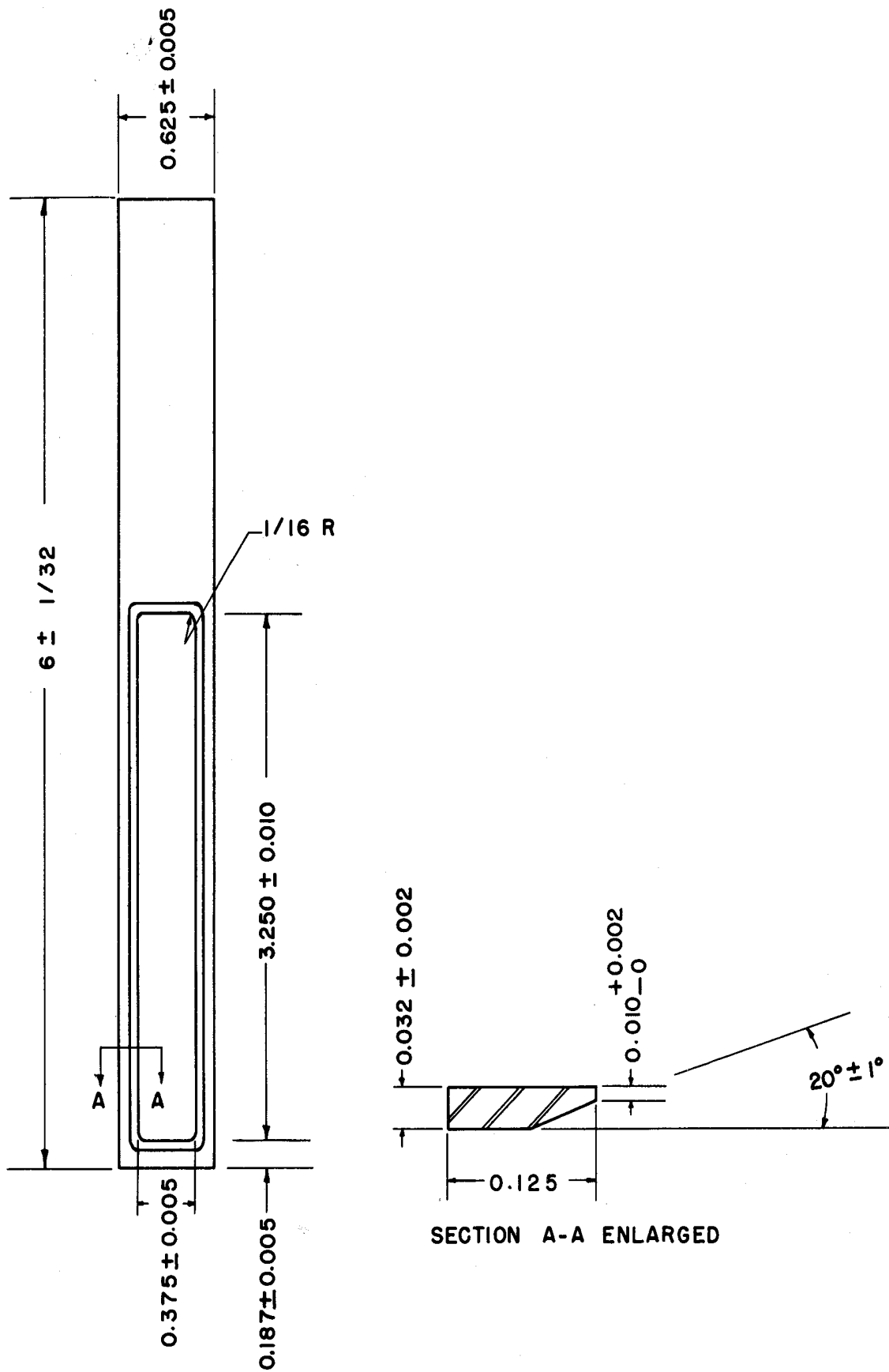


Figure 20. Film Holder.

evaporate before using the film. This is done either by letting the water naturally evaporate or by passing dry nitrogen on either side of the film when the film holder is placed in the test section.

The film obtained in this manner is usually colorless or silvery grey. Its thickness can be estimated by two methods. The first method is based on calculating the residue volume and assuming it is evenly distributed over the water surface. Thus:

$$l_f = \frac{c_n c_c n}{\pi v r^2 \rho_f} \quad (4.21)$$

where c_n = mass of nitrocellulose/unit volume of collodion

$$= .04 \text{ gms/cm}^3$$

c_c = volumetric concentration of collodion in amyl acetate

$$= .15$$

n = number of drops used = 3

v = number of drops/unit volume = 30 cm^{-3}

r = film radius = 7.5 cm

ρ_f = nitrocellulose density = 1.58 gms/cm^3

With the above values one finds that

$$l_f = 2.15 \times 10^{-6} \text{ cm} = 215 \text{ \AA}$$

The second method of evaluating the film thickness is based on a study by Peachy⁽⁶⁸⁾ who gives a correlation between the interference color of thin sections and their thickness when observed under white light. For films with index of refraction = 1.5 the correlation is as shown in Table III below:

TABLE III

COLOR-THICKNESS CORRELATION FOR THIN FILMS
(index of refraction = 1.5)⁽⁶⁸⁾

<u>Thickness Range</u>	<u>Interference Color</u>
< 600 ⁰ Å	Gray
600 - 900	Silver
900 - 1500	Gold
1500 - 1900	Purple
1900 - 2400	Blue
2400 - 2800	Green
2800 - 3200	Yellow

The index of refraction of nitrocellulose is 1.514, and therefore the above table can be considered applicable. On this basis the color of films made from two different solutions and varying number of drops was observed and their thickness was estimated. Some averaging was necessary as apparently the films were not uniform in thickness. The result is shown in Figure 21 from which the thickness of films used in this study can be estimated to be about 230 ⁰Å. This result is in agreement with the result of the previous method. In addition, it is apparent that such films satisfy the requirements set in the previous section.

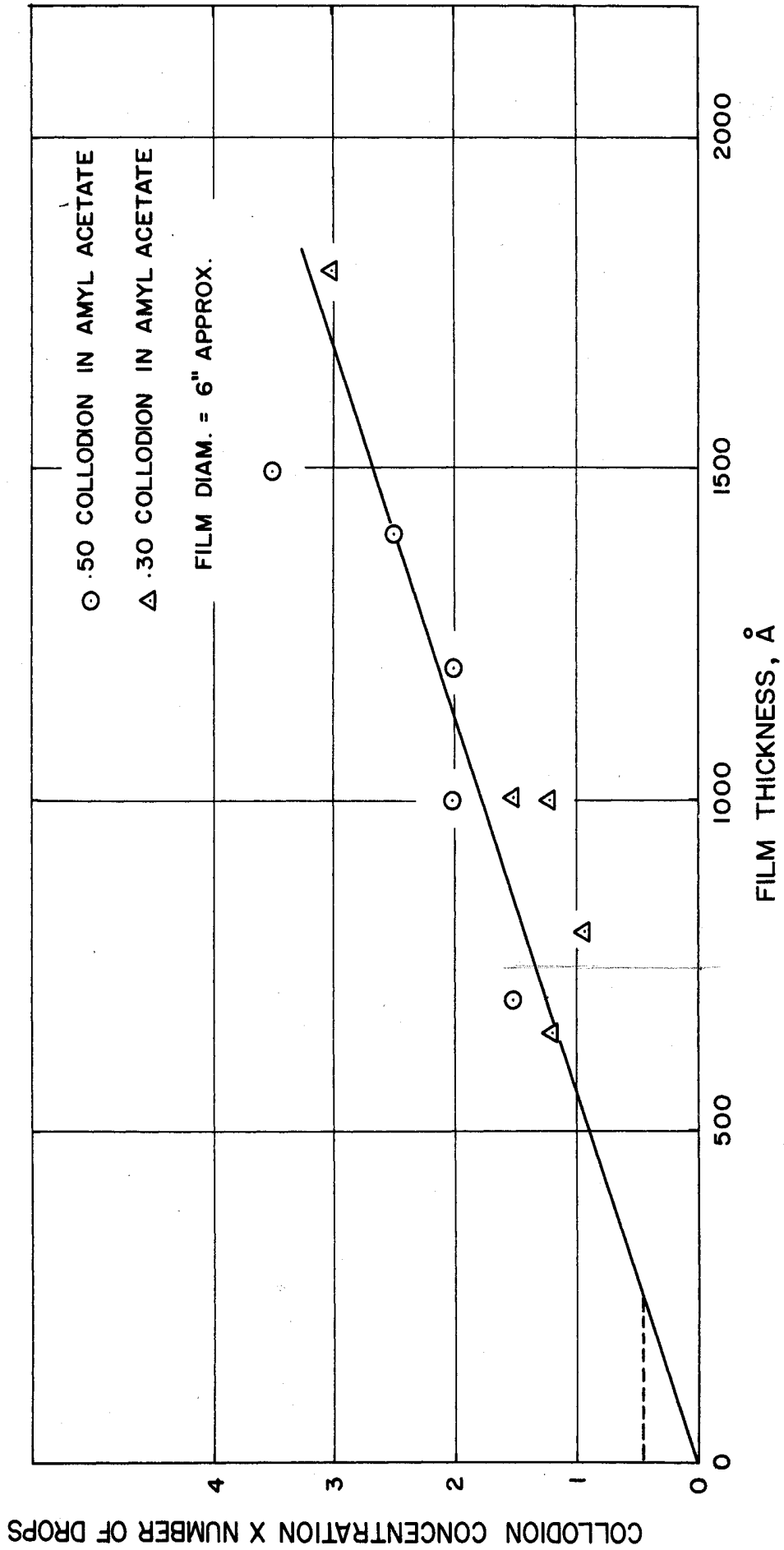


Figure 21. Dependence of Film Thickness on Collodion Concentration in Amyl Acetate Times Number of Drops.

4.5 Diffusion Through Thin Films

A film with thickness of the order of that mentioned in the previous two sections is not expected to eliminate completely the diffusion between the gases it separates. However, it is plausible to assume that it represents a definite barrier to the diffusion, and therefore, the question arises as to how good a barrier it is.

To answer this question, imagine two semi-infinite compartments one beside the other and each of which contains a different gas at the same temperature and pressure. The distribution of the two gases in the two compartments as a function of time is to be found for the following two cases: one, when at time zero the wall between the compartments is removed completely and two, when the wall is replaced by a thin film.

If the two gases are denoted by "a" and "b" in compartments 1 and 2 respectively, use of Fick's second law gives, at $t \geq 0$

$$\frac{\partial c_a}{\partial t} = D_{ab} \frac{\partial^2 c_a}{\partial y^2} \quad (4.22)$$

For the first case, the boundary conditions are as follows:

$$c_{a1} = c_{a2} \quad \text{for } y = 0, \quad t > 0 \quad (4.23)$$

and

$$\frac{\partial c_{a1}}{\partial y} = \frac{\partial c_{a2}}{\partial y} \quad \text{for } y = 0, \quad t > 0 \quad (4.24)$$

$$c_a = 1 \quad \text{for } y > 0 \quad t = 0 \quad (4.25)$$

$$c_a = 0 \quad \text{for } y < 0 \quad t = 0 \quad (4.26)$$

For the second case, the boundary conditions are the same except the condition (4.23) is replaced by

$$D_{ab} \frac{\partial c_{a1}}{\partial y} + \frac{P}{\ell_f} (c_{a2} - c_{a1}) = 0, \text{ for } y = 0, \quad t > 0 \quad (4.27)$$

where P is the permeability of species "a" in the film. This condition expresses the assumptions that no accumulation of species "a" in the film takes place and that its distribution is linear within the film.

It can readily be seen that the diffusion problem above is analogous to the heat conduction problem between two semi-infinite solids of the same material but having two different temperatures initially. The first case above is similar to the case where at time zero the two solids are brought together without contact resistance, and the second case is similar to that when there is a contact resistance such as a gaseous film.

The solution for Equation (4.22) under the appropriate boundary conditions can be found in the treatise of Carslaw and Jeager⁽⁶⁹⁾ and is presented below.

For the first case:

$$c_a = \frac{1}{2} \left[1 + \operatorname{erf} \frac{y}{2\sqrt{D_{ab}t}} \right] \text{ for } y > 0 \quad (4.28)$$

and

$$c_a = \frac{1}{2} \operatorname{erf} \frac{|y|}{2\sqrt{D_{ab}t}} \text{ for } y < 0 \quad (4.29)$$

and for the second case:

$$c_a = \frac{1}{2} \left\{ 1 + \operatorname{erf} \frac{y}{2\sqrt{D_{ab}t}} + \left[\exp \left(z^2 - \frac{y^2}{4D_{ab}t} \right) \right] \operatorname{erfc} z \right\}$$

for $y > 0$ (4.30)

and

$$c_a = \frac{1}{2} \left\{ \operatorname{erf} \frac{|y|}{2\sqrt{D_{ab}t}} + \left[\exp \left(z^2 - \frac{y^2}{4D_{ab}t} \right) \right] \operatorname{erfc} z \right\}$$

for $y < 0$ (4.31)

where

$$z = \frac{y}{2\sqrt{D_{ab}t}} + \frac{2P}{\ell_f} \sqrt{\frac{t}{D_{ab}}} \quad (4.32)$$

To obtain the numerical solutions, one notes that for gases the diffusion coefficient

$$D_{ab} \approx 1 \text{ cm}^2/\text{sec} \quad (4.33)$$

and, that for permeability, the value for H_2 through various cellulose compounds as quoted by Barrer⁽⁷⁰⁾ can be used. This value is

$$P \approx 10^{-7} \text{ cm}^2/\text{sec} \quad (4.34)$$

Equations (4.28) and (4.30) are plotted in Figure 22 for various values of t . In the latter equation the value of $\ell_f = 200 \text{ }^{\circ}\text{A}$ was used. It can be seen that for relatively short times a thin film offers an excellent barrier to diffusion. It appears that in order to take advantage of the film the gases should be exposed to the film

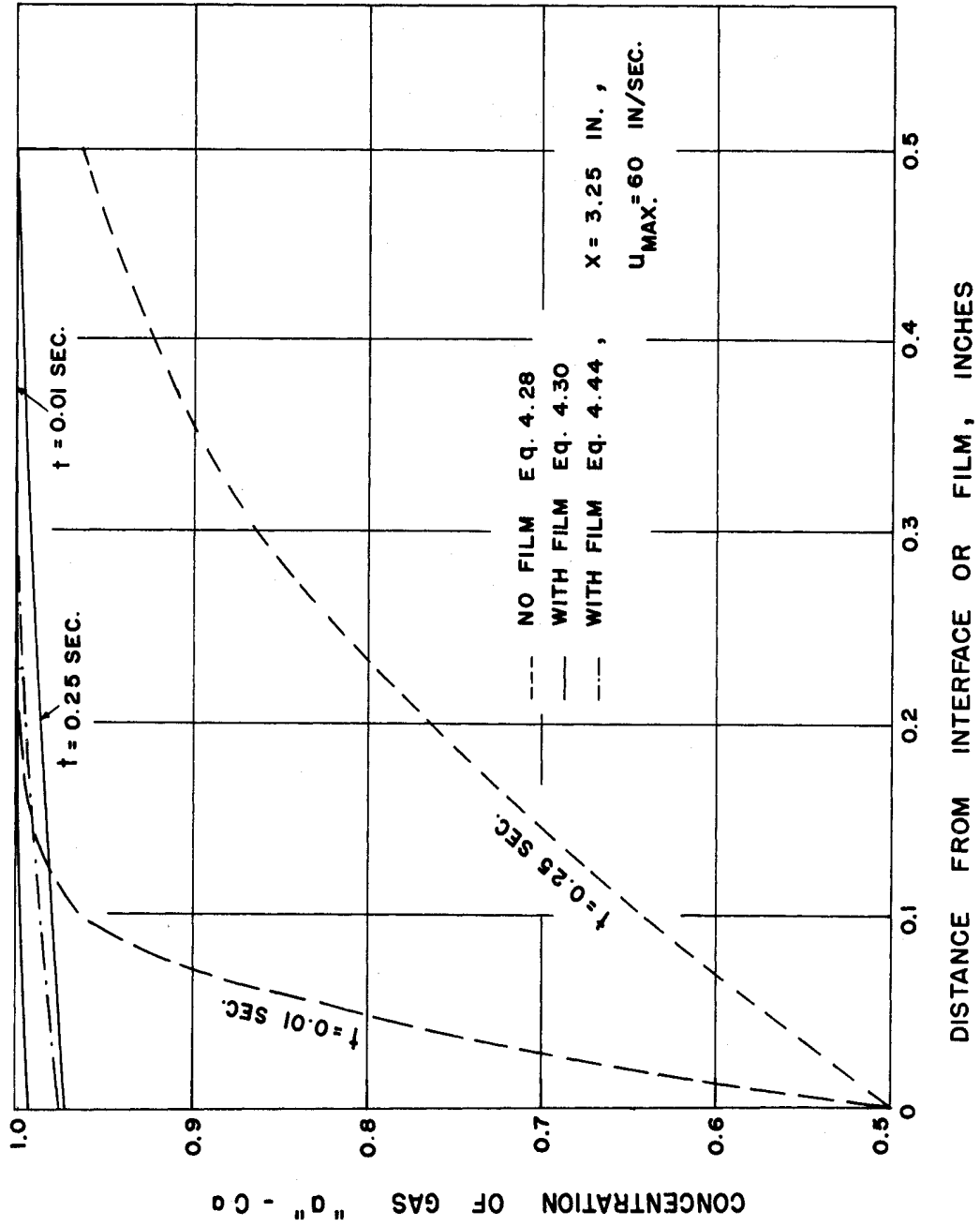


Figure 22. Concentration Distribution Due to Diffusion.

for a short time only. This can be accomplished by flowing the gases along the sides of the film and choosing a flow velocity that allows a reasonably short residence time.

It should be pointed out, however, that because of the no-slip condition of the two streams of gases at the film surface, the solution of the diffusion problem is somewhat more involved than that given by Equation (4.30). For the appropriate solution, the following analysis is offered.

Let both gases "a" and "b" be flowing in channels 1 and 2 respectively on either side of the film which is considered coincident with the x axis. By assuming incompressible steady flow and no change in density due to diffusion one can write the following conservation equations:

a) Continuity:

$$\frac{\partial u}{\partial x} + \frac{\partial v}{\partial y} = 0 \quad (4.35)$$

b) Momentum:

$$u \frac{\partial u}{\partial x} + v \frac{\partial u}{\partial y} = \nu \frac{\partial^2 u}{\partial y^2} - \frac{1}{\rho} \frac{dp}{dx} \quad (4.36)$$

c) Diffusion of "b"

$$u \frac{\partial c_b}{\partial x} + v \frac{\partial c_b}{\partial y} = D_{ab} \frac{\partial^2 c_b}{\partial y^2} \quad (4.37)$$

For a fully developed, parallel flow in a channel, $\partial u / \partial x = v = 0$. Therefore, Equation (4.36) reduces to that of a Poiseuille flow and Equation (4.37) becomes:

$$u \frac{\partial c_b}{\partial x} = D_{ab} \frac{\partial^2 c_b}{\partial y^2} \quad (4.38)$$

This equation is to be solved subject to the following boundary conditions:

$$c_b = 0, \quad x = 0, \quad y \geq 0 \quad (4.39)$$

$$c_b = 0, \quad x \geq 0, \quad y = \infty \quad (4.40)$$

and

$$\frac{P}{l_f} (c_{b2} - c_{b1}) + D_{ab} \frac{\partial c_b}{\partial y} = 0, \quad x \geq 0, \quad y = 0 \quad (4.41)$$

If the diffusion through the film is assumed to be constant and equal to the maximum possible diffusion, this boundary condition can be written as:

$$\frac{P}{l_f} = - D_{ab} \frac{\partial c_b}{\partial y}, \quad x \geq 0, \quad y = 0 \quad (4.42)$$

The system of Equations (4.38), (4.39), (4.40) and (4.42) is analogous to that obtained for the problem of heat transfer to a fluid flowing inside a tube when the heat flux at the wall is constant. If u is considered to change linearly with y , the solution is given in the book by Bird et al. ⁽⁷¹⁾ For a conservative answer one can write:

$$u = u_{\max} \frac{2y}{b} \quad (4.43)$$

where u_{\max} is the maximum velocity in a Poiseuille flow and b is the channel width. The solution involves a change of variables and is presented here without derivation:

$$c_b = 1 - c_a = \frac{P b}{2D_{ab} l_f} \left(\frac{36x D_{ab}}{u_{\max} b^2} \right)^{1/3} \left\{ \frac{e^{-x^3}}{\Gamma(\frac{2}{3})} - x \left[1 - \frac{\Gamma(\frac{2}{3}, x^3)}{\Gamma(\frac{2}{3})} \right] \right\} \quad (4.44)$$

where $x = \frac{2y}{b} \left(\frac{u_{\max} b^2}{36x D_{ab}} \right)^{1/3}$ and $\Gamma(2/3)$ is the "complete" gamma function and $\Gamma(2/3, x^3)$ is the "incomplete gamma" function.

Equation (4.44) is plotted in Figure 22 for a value of $u_{\max} = 60$ in/sec, $b = .5$ in and $x = 3.25$ in. corresponding to the conditions used in the experiments described in this work. The incomplete gamma function is obtained from the tables by Pearson⁽⁷²⁾. It is apparent from the plot that the diffusion is negligible under the experimental conditions used.

It should be added that taking $b = .5$ in. (the widest channel used) results in the most conservative answer, if the same average velocity is used in a narrower channel. This is so, because the concentration depends on the slope of the velocity profile at the film.

4.6 Experimental Arrangement and Procedure

The experimental apparatus is designed for obtaining two basic pieces of information: the critical explosive width and the velocity decrement of the detonation at explosive widths larger than the critical. For both of these measurements, the basic equipment for the preparation of the explosive and for charging the test section is the same. Figure 23 is a schematic diagram of the system. All lines are 1/4 in. stainless steel tubes except the 40 in. long flame tube which has an inside cross-section of 0.36 in. x 0.50 in. The glow plug is placed 8 ft ahead of the entrance to the flame tube to insure

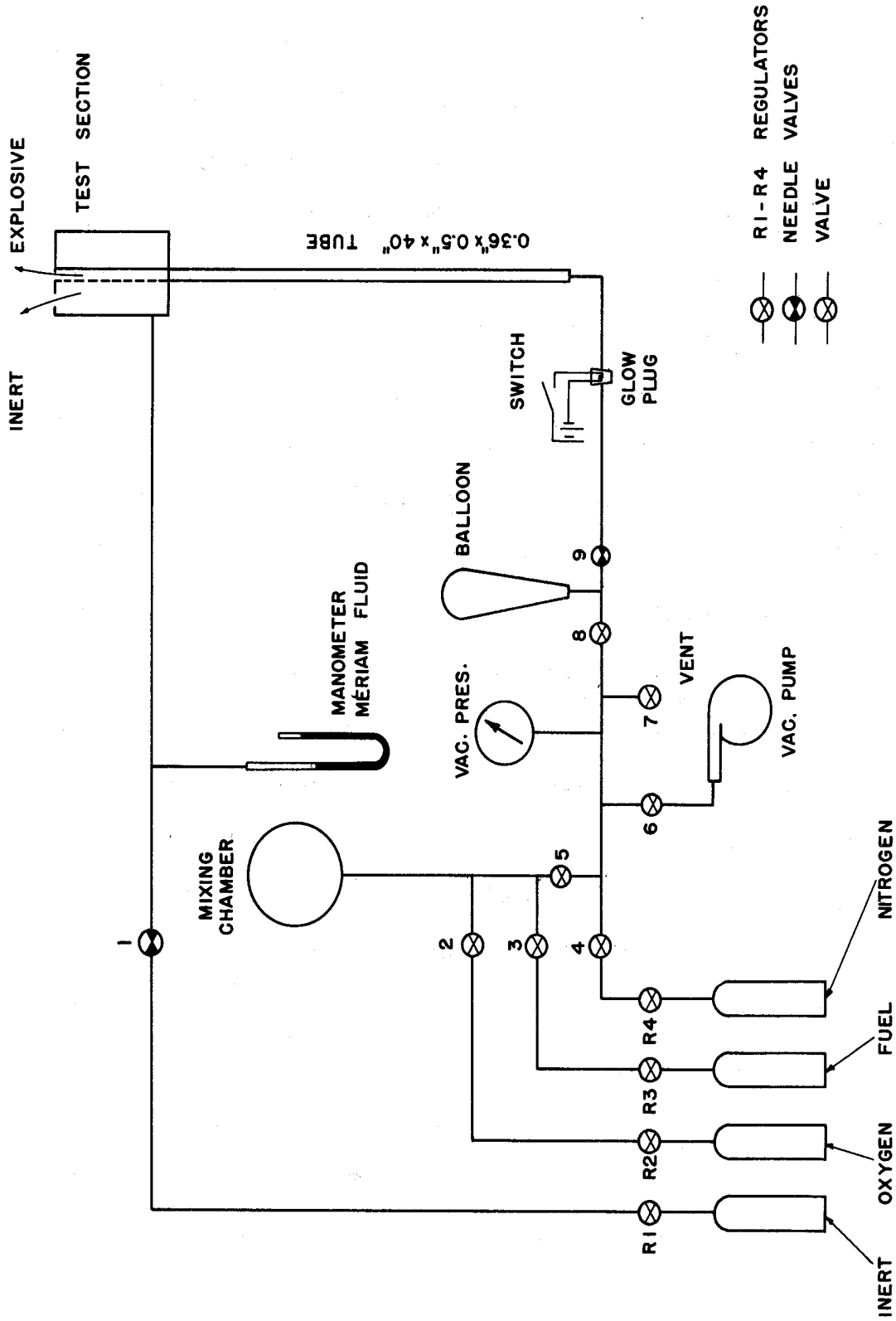
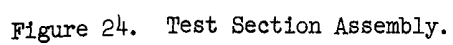


Figure 23. Schematic Diagram of Mixing and Charging System.

a fully developed wave before any measurements are taken. The flame tube is vertically mounted and is terminated by the test section shown in both Figures 24 and 25. . . The test section is provided with two 1/2 in. glass plates constituting the front and back walls, and each plate has .035 in. wide by .135 in. deep grooves for the film holder (Figure 20) to slide through. The depth of the explosive channel in the test section matches its depth in the flame tube, but its width can be easily changed from .5 in. to .1 in. at .05 in. intervals by suitable spacers and a wedge piece. While the detonation propagation velocity may be affected by the wedge on the inclined side as evidenced by the work of Nicholls, et al.⁽⁷²⁾ we shall see that this is not the case on the straight side.

To prepare the explosive mixture, the mixing chamber (see Figure 23) is evacuated and then filled consecutively with oxygen and fuel. The partial pressure method is used to obtain the desired mixture. The pressure is monitored by a Marsh guage, type 200-C, which can be read to less than 0.5 psi. The mixing chamber, which is a sphere one foot in diameter, is usually filled to about 60 psig total pressure. It is provided with a blow-off diaphragm for safety. Before a particular mixture is used a period of no less than two hours is allowed for complete mixing.

To prepare for a run, the expendible toy balloon is evacuated and then filled with the explosive mixture. This process is repeated once more to insure purity of the mixture in the balloon. Valves 5 and 8 are closed and the plumbing between them is evacuated. This



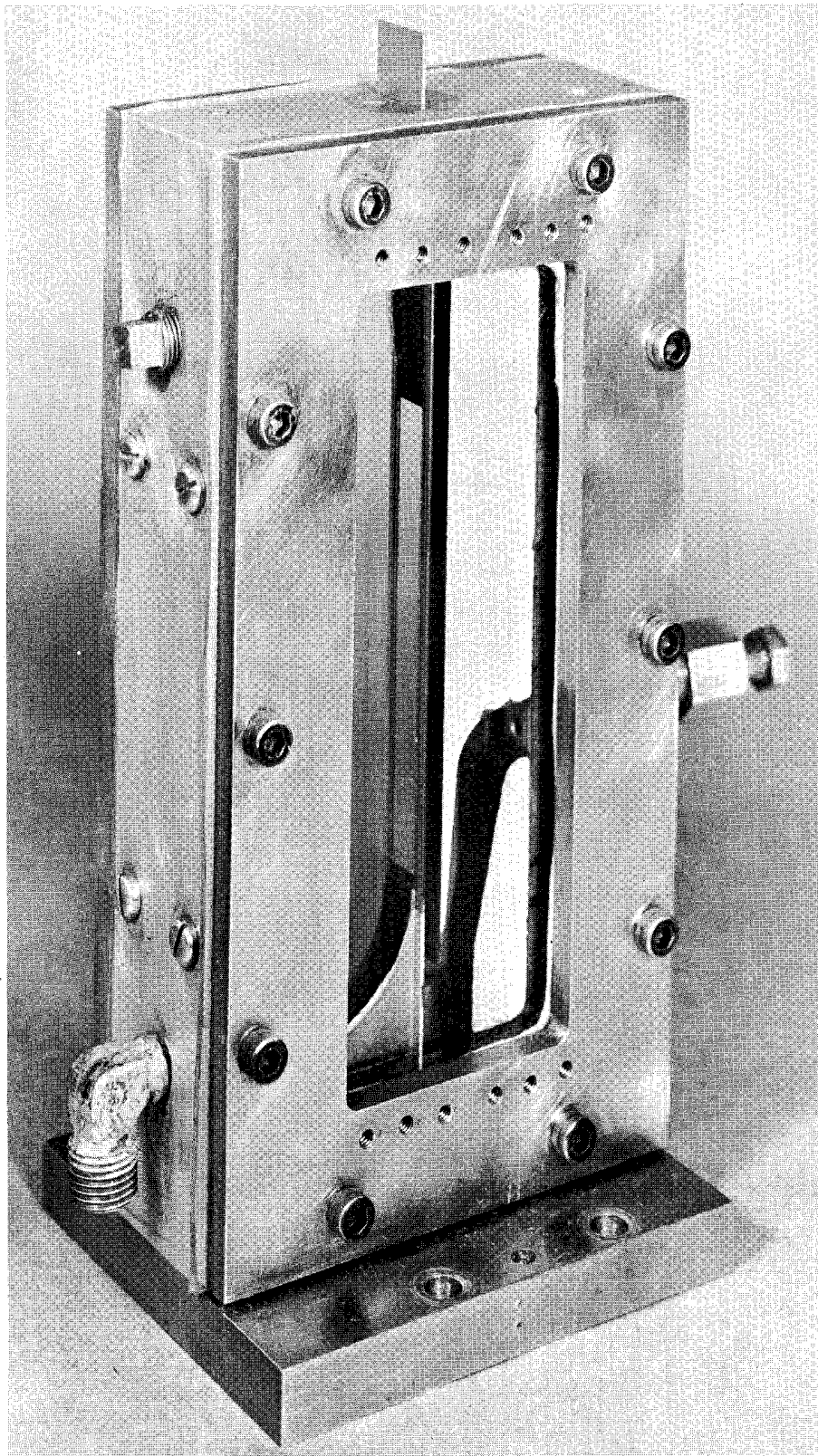


Figure 25. Photograph of the Test Section.

provides a buffer zone that blocks the detonation wave from travelling back to the mixing chamber.

The film holder on which a thin film has previously been mounted according to Section 4.4, is inserted into the test section, after its edges have been covered by a thin layer of vacuum grease. The purpose of the grease is to prevent any mixing and/or diffusion between the inert and the explosive via the grooves in the glass plates.

To make a run, valves 1 and 9 are opened slowly and simultaneously in such a way that pressures of the inert and the explosive are kept equal at all times until the balloon is nearly exhausted. To insure that the flame tube is purged of air, the balloon is filled again and this process is repeated. A simple but very sensitive check to insure equal pressures on both sides of the film at the test section is accomplished in the following manner. The filament of a small bulb is focused on a screen after reflection from the film. When the pressures are equal the film is plane and the image of the filament is sharp. At a slight unbalance in pressure the film becomes curved and the image of the filament shifts and becomes diffused. The direction of the shift indicates which side is higher in pressure so that corrections could be made. It was found that this method is sensitive to less than 1 mm of water of pressure difference. It should be added that maintaining equal pressures on both sides of the film is advantageous by itself in that it insures constant explosive width and prevents gross mixing.

All runs are made with test section over-pressures not less than 4 cm of water. The sizes of the exit orifices shown on the top of

the test section in Figure 24 are so chosen that the overall velocity in the test section is about 40 in/sec, corresponding to a maximum velocity of 60 in/sec if a Poiseuille flow is assumed. For such a velocity, the diffusion at the top of the test section is found to be negligible in Section 4.5.

When the balloon is nearly emptied the glow plug switch is closed momentarily thus starting two detonation waves, one going to the balloon and exploding it, and another travelling toward the test section. The sequence of events that take place as the latter travels down the flame tube depends on which of the two kinds of photographs is desired, as described next. It should be mentioned that a glow plug is found more satisfactory than a spark plug because the latter seems to affect the electronic instruments used in the experiment.

a. Equipment and Procedure for Spark Photography

The equipment for obtaining spark schlieren photographs of the detonation wave in the test section is shown schematically in Figure 26. Four ionization probes are used to detect the passage of the detonation wave in the tube resulting in the performance of certain functions which will be described shortly. Each probe is made up of two 20 gauge enameled copper wires 6 in. in length. The wires are twisted together for one inch and this part is inserted into a teflon tubing of equal length. The wire and the tubing are then housed into a 1/8 in. pipe thread Conax thermocouple fitting* resulting in a pressure tight assembly. The protruding teflon tube

*Manufactured by Conax Corporation, Buffalo, New York.

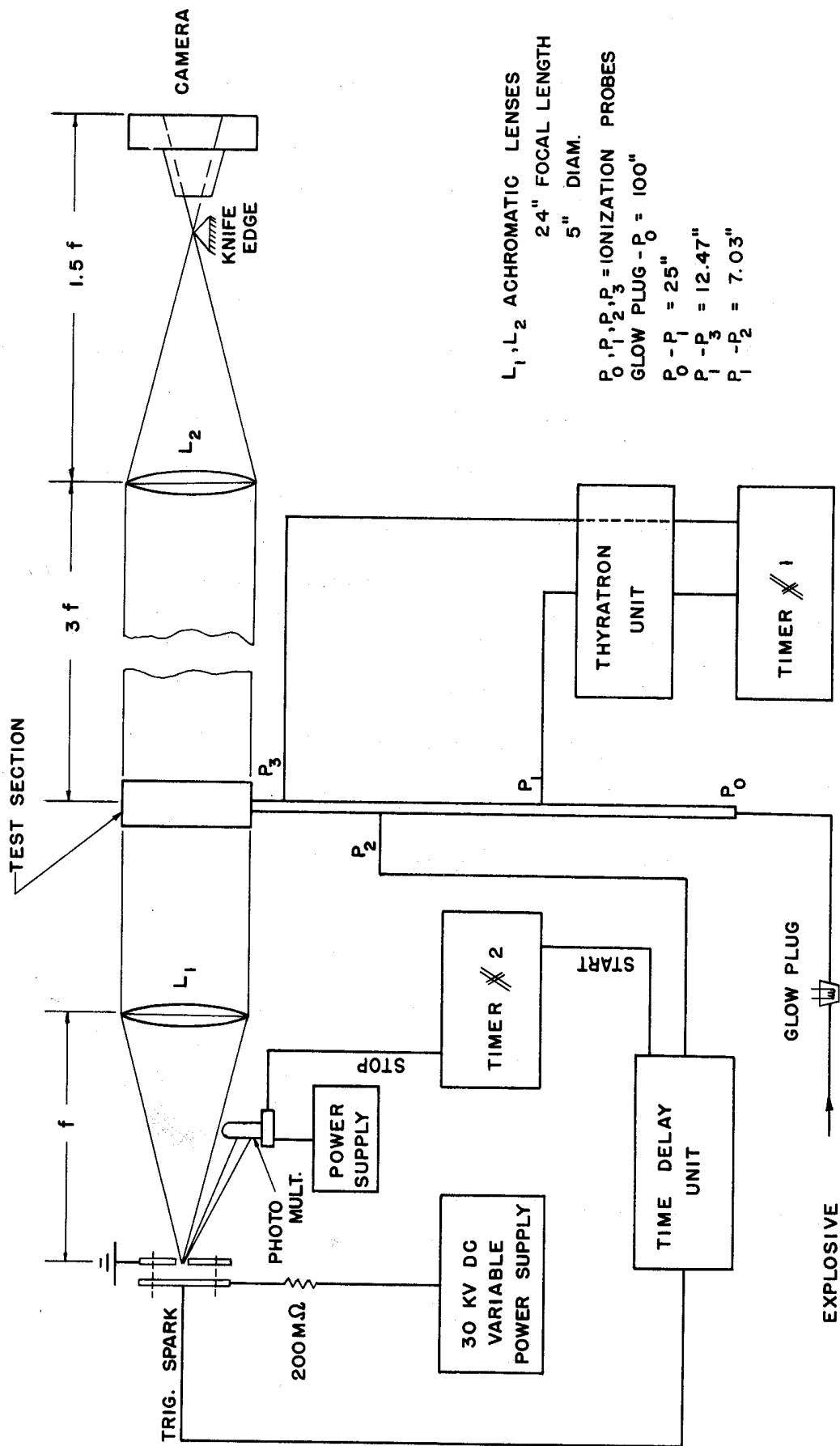


Figure 26. Schlieren System and Block Diagram of Instrumentation for Spark Pictures.

is cut and the wires are clipped to a length such that when the fitting is threaded into the tube, they will be flush with the tube wall. The clipped wires have pointed bare ends separated from each other by the two thin enamel layers thus constituting two conductors with a gap in between.

One wire of each probe is grounded and the other, in the case of probe 1 and 3, is connected to the grid of an 884 thyatron in the thyatron unit. A unit similar to the one used is described in the work of Morrison.⁽⁹⁾ The passage of the detonation wave, with attendant ionization, shorts the probe thus decreasing the grid bias of the thyatron causing it to fire and generate a voltage signal through the plate circuit. The voltage signal is fed to either the start or stop input of timer 1. In most runs a Berkley 1 megacycle counter, Model No. 5120, was used as timer 1. It is accurate to + 1 μ sec and it is used to measure the wave velocity.

In the case of probe 2 the ungrounded wire was connected to the grid of type 2050 thyatron in the time delay unit which is similar to the one described in Reference 9. The firing of this thyatron, in addition to providing a signal to the start input of timer 2, causes, after a predetermined time delay set by the potentiometer adjustment in the unit, a second 2050 thyatron to fire which in turn causes a spiked voltage signal to be induced in a coil. The output of the coil (about 15 kv) is used to trigger the spark source. A voltage signal due to the firing of the first thyatron is fed to the start of timer 2.

The spark source unit built by the Aircraft Propulsion Laboratory personnel consists essentially of two circular metal plates with 10 Sprague (type 20 DK-25) 500 μ farad capacitors spaced evenly in a circle. They are charged to 25 kv and discharged by the coil pulse from the delay unit. An orifice in one plate acts as a point light source during the duration of the spark which is of the order of 0.1 μ sec.

The light strikes the collimating lens of the schlieren system as well as a photomultiplier whose circuit generates a voltage signal used as an input to timer 2. Model 524 B Hewlett-Packard 10 megacycle which is accurate to $\pm 0.1 \mu$ sec is usually used as this timer. Its function in this case is to measure the time delay between the passage of the detonation of probe 2 and the spark discharge, i.e., when the spark picture is taken. It should be added that occasionally, Models 757 B and 727 BN timers made by Computer Measurement Company are used for checking purposes. They are accurate to $\pm 0.1 \mu$ sec.

b. Equipment and Procedure for Streak Photography

The essential features of the equipment used for schlieren streak photography are the same as those for spark photography. As the block diagram shows in Figure 27, probes 1 and 3 are again used for the measurement of the wave velocity. Probe 2 in conjunction with the time delay unit provides a triggering spark to initiate a flash of about 1 msec duration in the flash tube shown. The flash tube is housed in a box and again an orifice on one side acts as a point source. The optical system chosen was dictated by availability

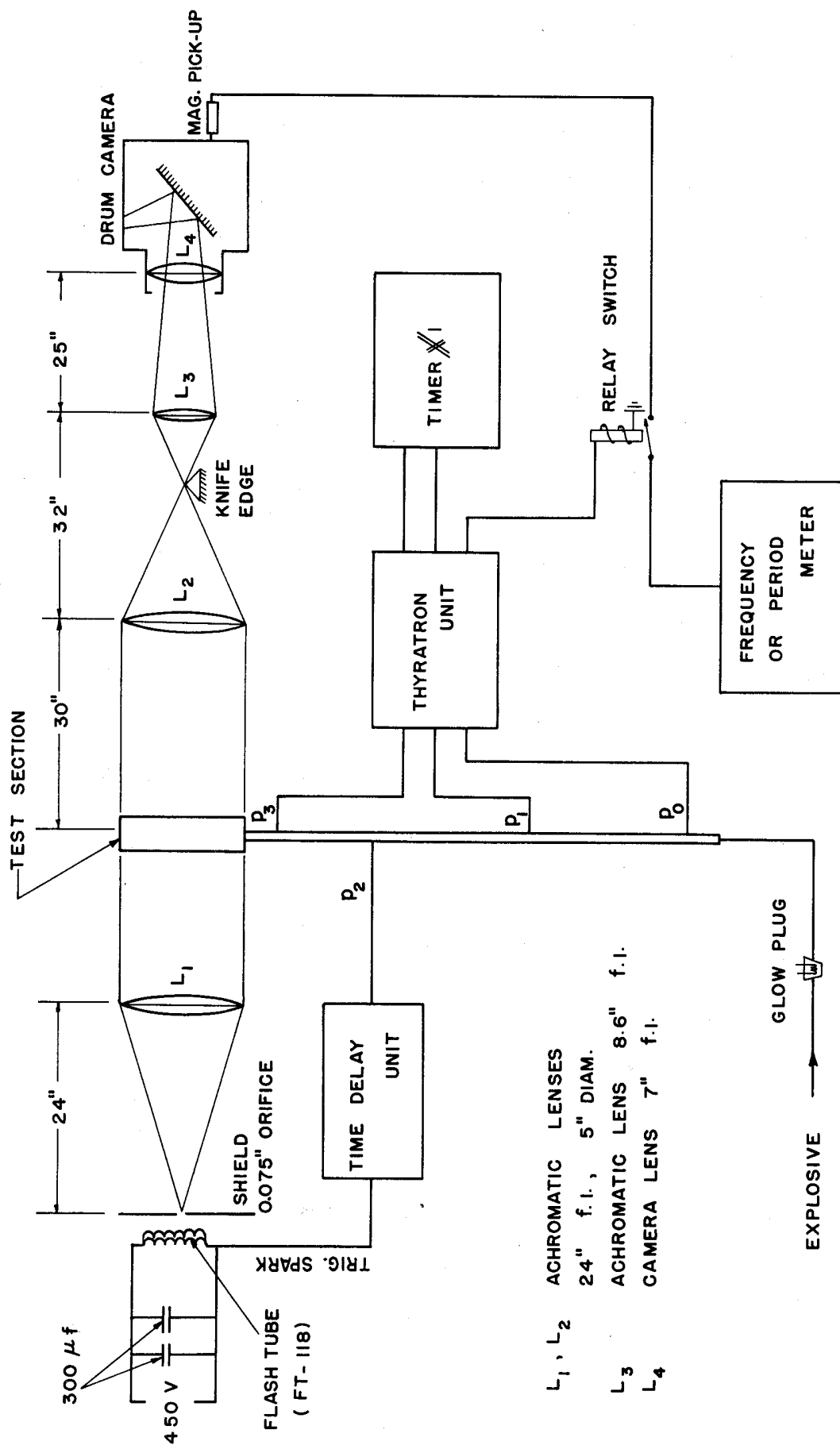


Figure 27. Schlieren System and Block Diagram of Instrumentation for Streak Pictures.

of components and space limitation. At the right hand side of the test section all light is blocked off except for a .010 in. slit along the explosive channel close to the solid wall side. One side of the slit has three notches providing increased exposure at the corresponding image points thus establishing the vertical spatial scale. The knife-edge was set horizontally in this schlieren system.

An Avco rotating drum camera was used to obtain the streak photographs. The drum is 4 in. in diameter and 3 in. long in inside dimensions. It is nitrogen or air driven with normal rotational speed being 600 rev/sec. Thus, its rotational period is longer than the flash duration and therefore no double exposure can occur. The camera is provided with a magnetic pick-up whose signal is fed to the Hewlett-Packard counter used as a period meter. The signal is interrupted by a normally open relay switch (Potter and Brumfield type KCP 11) whose energizing coil is part of the plate circuit of one thyatron in the thyatron unit. The switch thus closes only after the passage of the detonation wave by probe 0 with a time delay of 5 msec. This means that the period measured is for a cycle somewhat later than the one at which the picture is taken. However, the camera is usually brought to speed before a run is started and therefore the measurement is considered adequate.

Because of the comparatively slow linear speed of the film in the drum, it was found necessary to take pictures at .2 reduction. Such reduction results in a detonation streak at about 70° with the time axis.

Almost all film used for the streak pictures is Kodak plus-X on Estar base, which is a relatively curl resistant base. Further its dimensional changes due to processing, humidity or temperature variations are isotropic -- a quality which is essential for accurate determination of the velocity or the velocity change of the detonation wave.

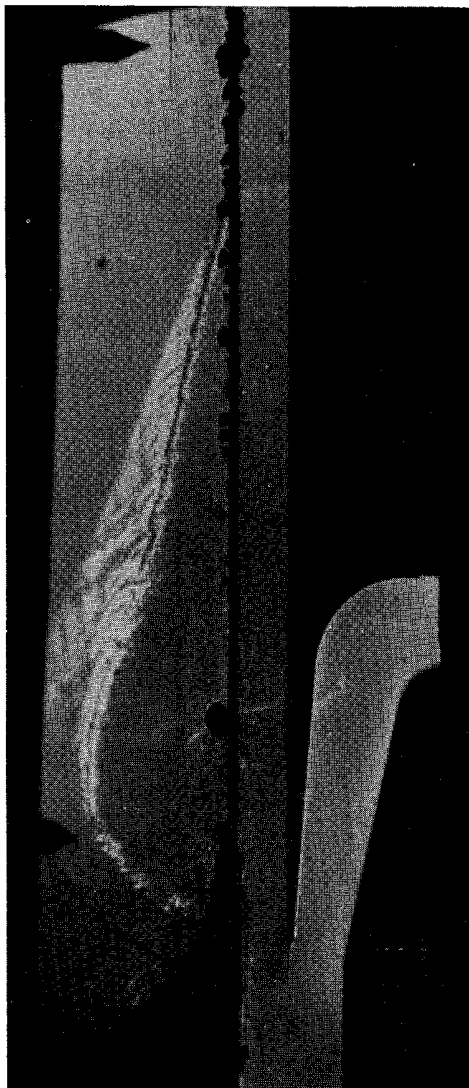
V. EXPERIMENTAL RESULTS AND DISCUSSION

5.1 Critical Channel Widths of H_2 - O_2 Mixtures When Bounded by Nitrogen

As was shown in Chapter III, the quenching criteria presented there are all based on the assumption that certain conditions have to be met in the post shock region of the detonation waves before the detonation could be considered self supporting. The different conditions could all be translated into a Mach number requirement which are shown in Figure 12. Before experimentally finding this critical Mach number for H_2 - O_2 mixtures, it is easier first to find the critical channel width for different mixture ratios when bounded by an inert gas and then determine the corresponding Mach number.

To do this, a series of go-no go type experiments were made where the mixture ratio as well as the channel width were varied. The boundary gas used was nitrogen in all cases. It was chosen because preliminary calculations indicated that quenching could be accomplished in a wide range of mixture ratios at channel widths compatible with the test section design.

In the experiments, a mixture ratio is chosen and a run is made with the test section set at the widest possible channel width (.5 in.). Spark schlieren photographs are taken when the detonation wave is about two or three inches past the point where the explosive is exposed to the inert. Examination of the photograph revealed whether the detonation is quenched or not. Typical photographs of an unquenched and a quenched detonation wave are shown in Figure 28.



(a)



(b)

Figure 28. Typical Spark Photographs of a Quenched and an Unquenched Detonation Wave.

- (a) Run No. 881, $b = 0.25$ in.
Unquenched, 60% H_2 - 40% O_2 with N_2 Boundary
- (b) Run No. 840, $b = 0.5$ in.
Quenched, 40% H_2 - 60% O_2 with N_2 Boundary

As was explained earlier, the quenched detonation wave is characterized by a "clean" shock front followed, at an appreciable distance, by a "turbulent" zone. Further, from a knowledge of the detonation velocity inside the tube as measured through probes 1 and 3 (see Figure 26) and the time delay at which the picture is taken, an estimate of the decrease in velocity of the quenched detonation wave could be made. It was found that the quenched detonation waves suffer an average of over 20% velocity decrement in 2-3 inches of exposure to the boundary gas.

To insure repeatability, four or five runs were made for each set of conditions (mixture ratio and channel width). If the detonation wave is unquenched, a smaller channel width is chosen and more runs are made. If the detonation wave is still unquenched, a further decrease in channel width is made until quenching is observed. Thus, a determination of the critical channel width could be made.

Figure 29 represents the results obtained on such a series of experiments. Within the capabilities of the test setup, the leanest possible mixture ratio for which a critical channel width could be determined is 45% H_2 -55% O_2 . Difficulties were encountered in starting a detonation wave in mixtures richer than 75% H_2 -25% O_2 . Thus, the results of Figure 29 are subject to these two limitations. However, they are extrapolated up to the experimental lean and rich composition limits of Table I as shown by the broken lines.

In some runs, it was difficult to decide whether the detonation wave is quenched or not. The reason was that in some cases only

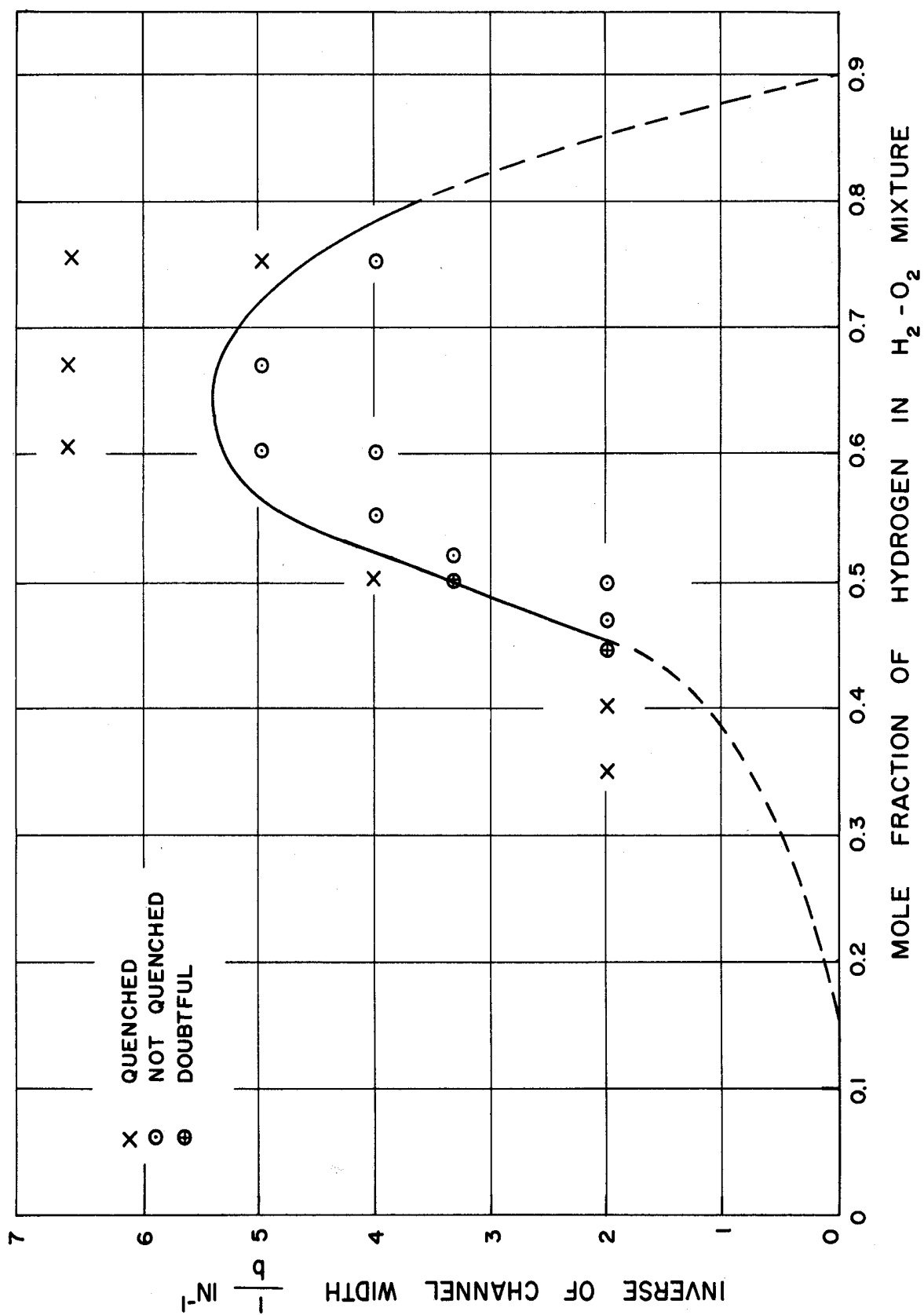


Figure 29. Critical Channel Widths of $\text{H}_2 - \text{O}_2$ Mixtures Bounded by Nitrogen.

considerable thickening of the reaction zone could be observed; in others, the pictures revealed 50-50 chance of quenching and non-quenching. The points corresponding to these situations are plotted in Figure 29 as "doubtful".

At this point, it is well to observe that Figure 28a reveals the same features of the assumed model of the interaction process shown in Figure 5. The absence of large curvatures in the detonation wave and the oblique shock as opposed to the curvature observed in Figures 4 and 16, is attributed to the reduction of diffusion offered by the separating film. Figure 29b shows that even in the quenched case, the interface is quite straight and thus adds more faith in the adopted model.

5.2 Velocity Decrement of Stoichiometric H_2-O_2 When Bounded by Nitrogen and Inferred Reaction Length

With the critical channel widths for various mixture ratios found, we now turn to the experimental determination of the effect of channel widths larger than the critical, on the propagation velocity of the detonation wave. In essence a check on the analytically calculated variation of the velocity with area increment, shown in Figure 11, is to be made.

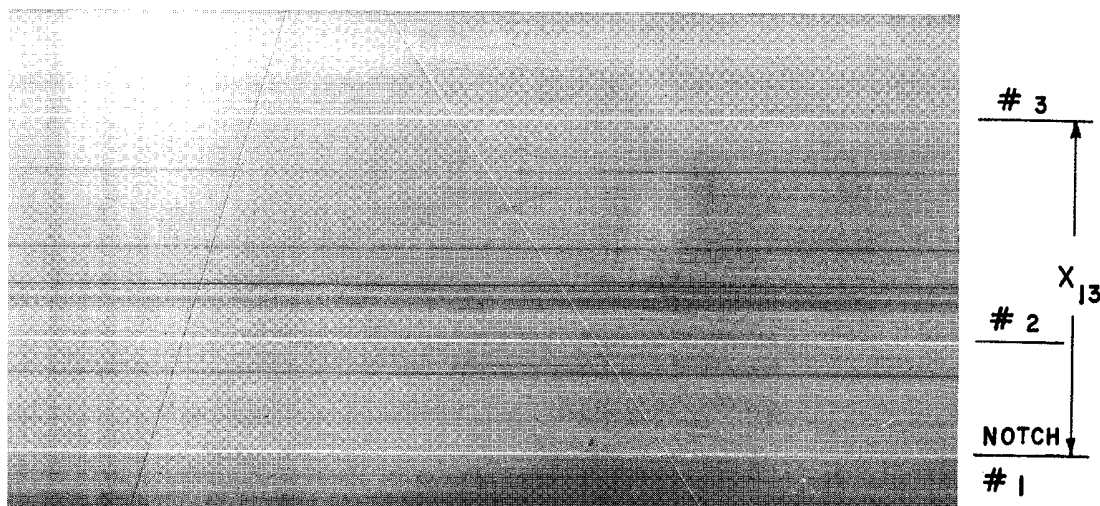
To carry out these experiments the stoichiometric hydrogen-oxygen was chosen for two reasons. One, it allows the widest range of channel widths that could be used within our experimental limitations, as can be seen from the results of Figure 29. Two, this mixture has been investigated extensively in the literature, and in particular, an

estimate of the reaction length which we shall need in our calculations, is available.

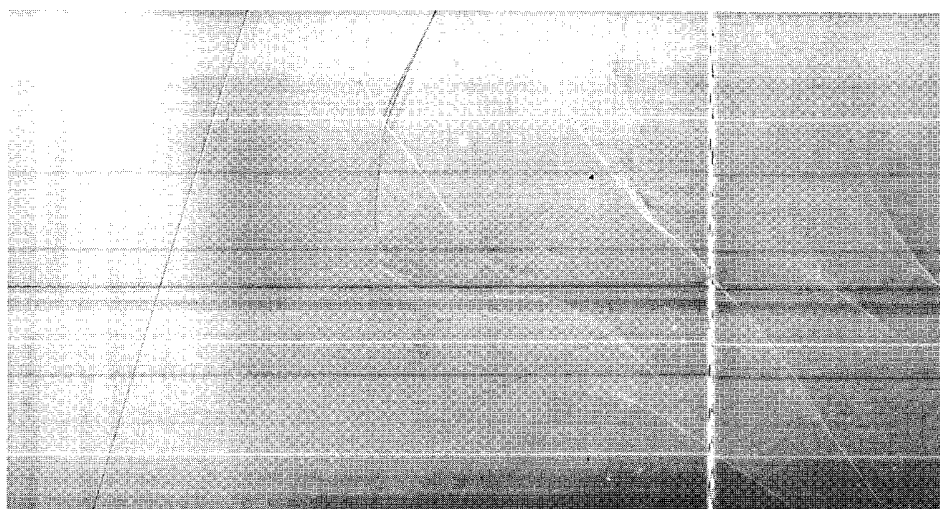
Tests were made according to Section 4.6 using streak photography. Four different channel widths were investigated, namely .2 in., .25 in., .3 in., and .5 in. From five to ten runs were made for each width. A run with a solid wall, instead of a thin film, was also made for each channel width. This was intended to confirm that any observed changes in the detonation velocity is not due to some peculiarities of the test section but due to the side relief.

Figure 30 shows typical streak photographs of the detonation wave, both with a solid wall and a thin film, for a channel width of .5 in. In the case of the solid wall, it can readily be seen that the slope of the detonation remains unchanged throughout the test section. A close examination of Figure 30b (the thin film case) shows that the detonation wave does slow down and indeed reaches a new steady state, indicating that it is not quenched. In all the streak pictures that will be presented henceforth, the detonation travels up and to the right. As a further guide to the identification of various streaks observed some pertinent dimensions are shown in Figure 31.

Figure 32 shows a streak photograph for the same conditions as those of Figure 30, except in this case the channel width is only .2 in. It can again be seen that in the case of a solid wall the detonation speed remains unchanged even though the wedge piece was present. In all similar cases the results were the same and, therefore show that the geometric arrangements in the test section does



- (a) Run No. 797
Solid Boundary
Vert. - $x_{13} = 2.996$ in.
Horz. - dist. equiv. to $x_{13} = 82.67$ μ sec



- (b) Run No. 796
Nitrogen Boundary
Vert. - $x_{13} = 2.996$ in.
Horz. - dist. equiv. to $x_{13} = 82.96$ μ sec

Figure 30. Streak Photographs of a Detonation Wave in Stoichiometric $H_2 - O_2$ ($b = 0.5$ in.).
(See Figure 31 for other dimensions.)

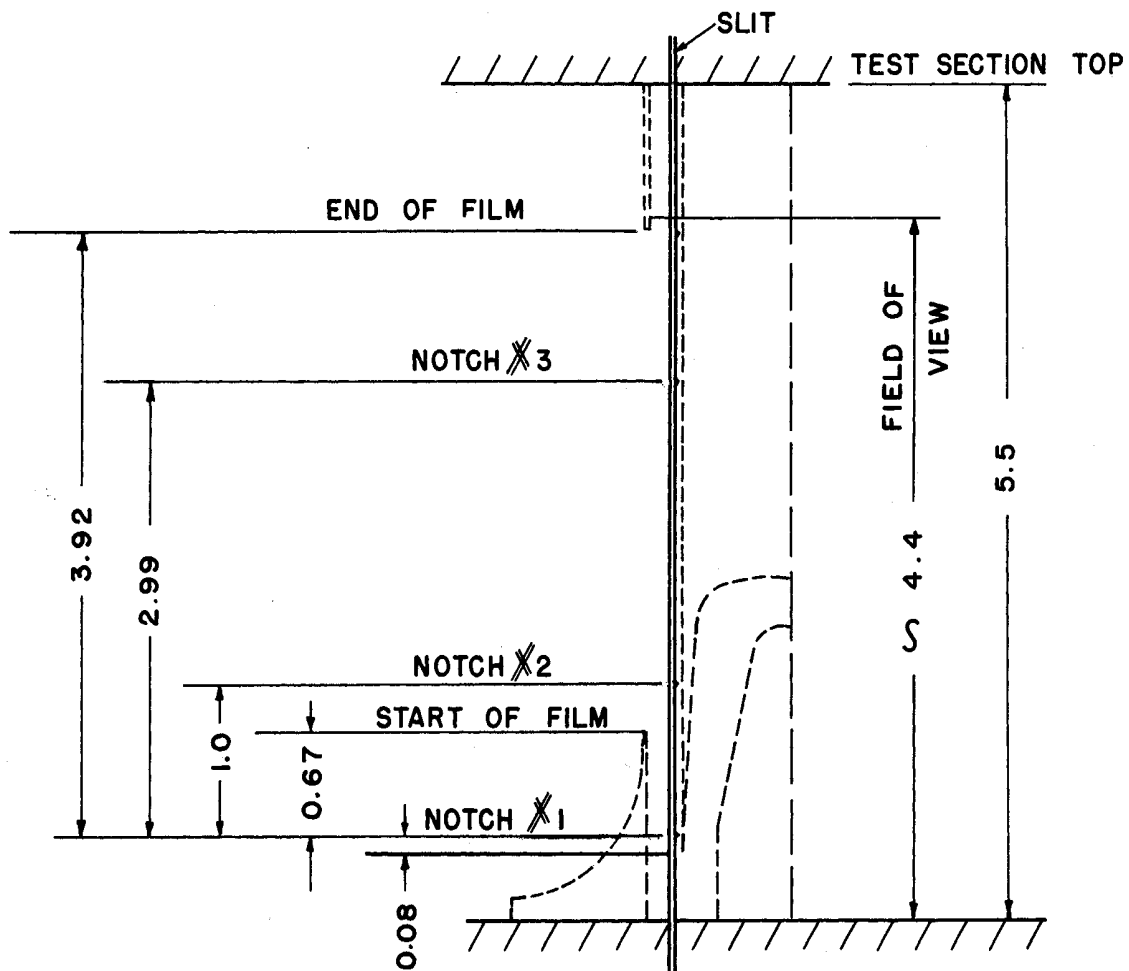
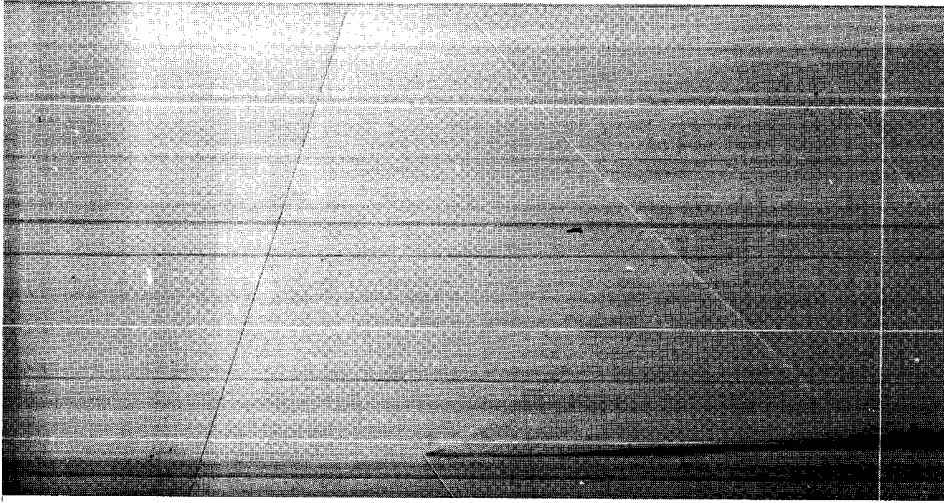
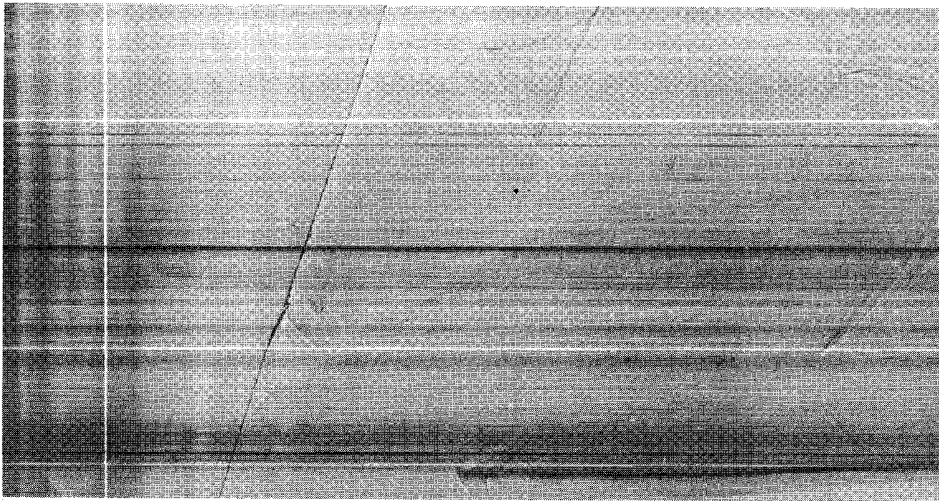


Figure 31. Pertinent Dimensions Helpful for the Interpretation of Streak Photographs.



- (a) Run No. 752
Solid Boundary
vert. - $x_{13} = 2.996$ in.
horz. - dist. equiv. to $x_{13} = 81.67 \mu\text{sec.}$



- (b) Run No. 992
Nitrogen Boundary
vert. - $x_{13} = 2.996$ in.
horz. - dist. equiv. to $x_{13} = 78.0 \mu\text{sec.}$

Figure 32. Streak Photograph of a Detonation Wave in Stoichiometric $H_2 - O_2$ ($b = 0.2$ in.).

not affect the detonation wave being studied. In the case of exposure to the side relief (Figure 32b), a close examination reveals again that a new steady state velocity is reached in a similar fashion to that of Figure 30b.

In addition to the incident detonation wave streak, some interesting patterns due to the reflected shock could be observed but these are of no consequence to our analysis. The striae observed in the case of channel widths less than .5 in. at the lower part of the photograph below the bottom white line is due to the reflection of the detonation wave in the small curved channel (see Figures 24 and 25).

Each run is followed by taking a picture of the slit on the same film strip. This was done for the purpose of accounting for any deviation in its perpendicularity from the time axis, as shall presently be seen. If the slit is at an angle α from the ordinate and the detonation trace makes an angle β with the time axis, it can be shown that the velocity of the detonation wave is

$$u_e \approx \frac{L}{\mu t_p} \frac{\tan \beta}{(1 - \tan \beta \tan \alpha)} \quad (5.1)$$

where L is the perimeter length of the drum, μ is the magnification and t_p is the time for one revolution of the drum. For small α and for $\beta > 45^\circ$, Equation (5.1) can be simplified to

$$u_e = \frac{L}{\mu t_p} \tan (\beta + \alpha) \quad (5.2)$$

Further, the change in velocity from u_e to a new steady-state velocity u_e' for which the corresponding slope angle is β' and the slit angle

is α' on the streak photographs, is simply:

$$\frac{\Delta u_e}{u_e} = \frac{u_e - u_e'}{u_e} = 1 - \frac{\tan(\beta' + \alpha')}{\tan(\beta + \alpha)} \quad (5.3)$$

The original streak photographs obtained with about 5:1 reduction were examined in a tool-maker's microscope and the pertinent angles and distances were measured for the purpose of calculating the velocity u_e at the entrance of the test section and the velocity decrement $\Delta u_e/u_e$ according to Equations (5.2) and (5.3) respectively. The velocity of the detonation wave also was calculated from knowledge of the distance between the ionization probes 1 and 3 and the time of passage of the detonation wave between them. Table IV shows a summary of the results.

Strictly speaking, the comparison between theory and experiment should be made using in the latter the velocity decrease from the theoretical velocity. However, it is shown in the appendix that the error involved in $\Delta u_e/u_e$ is about .8% of the detonation velocity, whereas the error in the measurement of the detonation wave velocity by either the ionization probes or the streak photographs, plus the error due to composition would amount to about 2% of the detonation velocity. If either column (4) or column (6) in Table IV were added to column (7) to obtain the decrement of velocity from the theoretical, then the results would be subject to an error of 2.8% of the velocity. Since the greatest decrement is about 11% such an error becomes an appreciable fraction of the decrement. It is therefore felt that $\Delta u_e/u_e$ without correction would be more reliable.

TABLE IV

SUMMARY OF THE EXPERIMENTAL RESULTS OBTAINED FOR THE
STOICHIOMETRIC H_2-O_2 BOUNDED BY N_2
 $[(u_e)_{th} = 9320 \text{ ft/sec (Ref. 46)}]$

(1)	(2)	(3)	(4)	(5)	(6)	(7)	(8)
Number of Runs	b	$\overline{(u_e)_{ion}}$	$\overline{\left[\frac{(\Delta u_e)_{ion}}{(u_e)_{th}}\right]}$	$\overline{u_{e\beta}}$	$\overline{\left[\frac{(\Delta u_e)_{\beta}}{(u_e)_{th}}\right]}$	$\overline{\left[\frac{\Delta u_e}{u_e}\right]}$	Range in $\frac{\Delta u_e}{u_e}$
	(in)	(ft/sec)		(ft/sec)			
9	.2	9074	.0264	9199	.0121	.070	.051 - .097
8	.25	9138	.0195	9090	.0245	.087	.063 - .111
5	.3	9224	.0103	9168	.0160	.072	.054 - .098
6	.5	9186	.0144	9209	.0120	.040	.0235 - .053

- (3) Average velocity obtained from ionization probes measurements.
- (4) Fractional average difference between (3) and the theoretical value.
- (5) Average velocity obtained from streak camera measurement, before wave reaches the side relief.
- (6) Fractional average difference between (5) and the theoretical value.
- (7) Average velocity decrement for wave with side relief obtained from streak pictures.
- (8) Range from which the average was obtained in (7).

On the other hand, the velocity decrement in the flame tube due to the effect of the boundary layer should be taken into account. This decrement, calculated by Fay's method⁽⁵³⁾, amounts to 1.8% for the tube size used in this investigation. It is added to columns (7) and (8) and the results plotted in Figure 33. Shown on the same plot is the theoretical curve deduced from Figure 11 where ξ is calculated according to Equation (2.53). The value of the reaction length \bar{x} is taken as .138 in. which is the value deduced by Fay⁽⁵³⁾ from the work of Kistiakowsky and Kydd.⁽⁷⁴⁾ The value of $\tan \delta$ was taken from Figure 8 to be .258 corresponding to the density parameter value of .353. Figure 33 shows that the experimental results are in reasonable agreement with the theory and therefore confirm that the value of the reaction length is .14 in. to within about 20%.

5.3 Behavior of Detonation Waves at Channel Widths Close to the Critical

At channel widths below the critical, it was seen in Section 5.1, that the detonation wave quenches and degenerates into a shock. A typical streak photograph of a quenching detonation wave shown in Figure 34, beautifully reveals the dynamics of the quenching process. At about two microseconds after the detonation meets the boundary gas, it starts slowing down. Then there is some thickening of the reaction zone and finally, it appears that a pure continuously decelerating shock (black curve) travels into the explosive followed by the interface of the shocked but unburned gas with the last layer of the gas that suffered combustion (light, comparatively thick curve), at an ever widening distance.

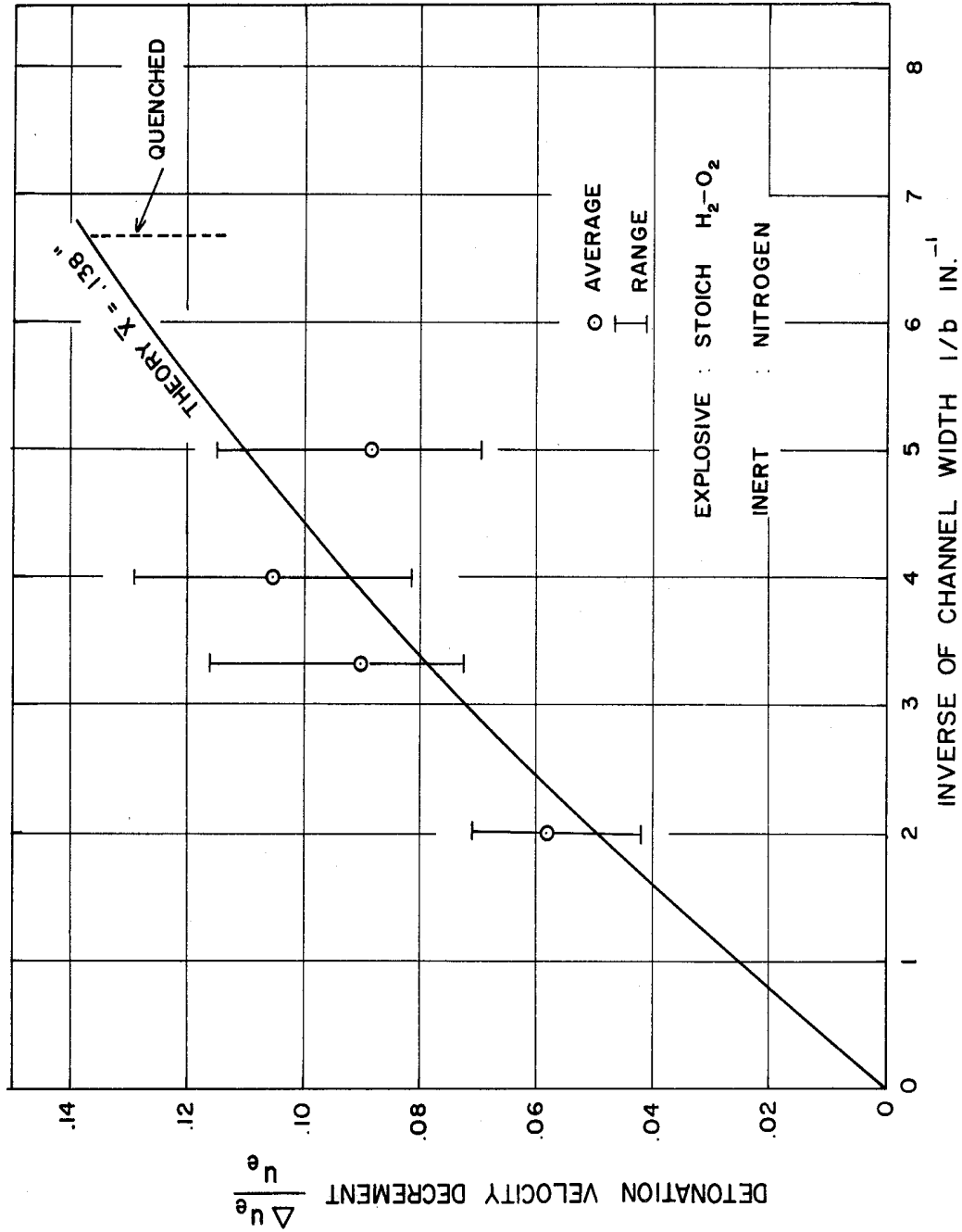


Figure 33. Variation of Detonation Velocity Decrement with Channel Width.

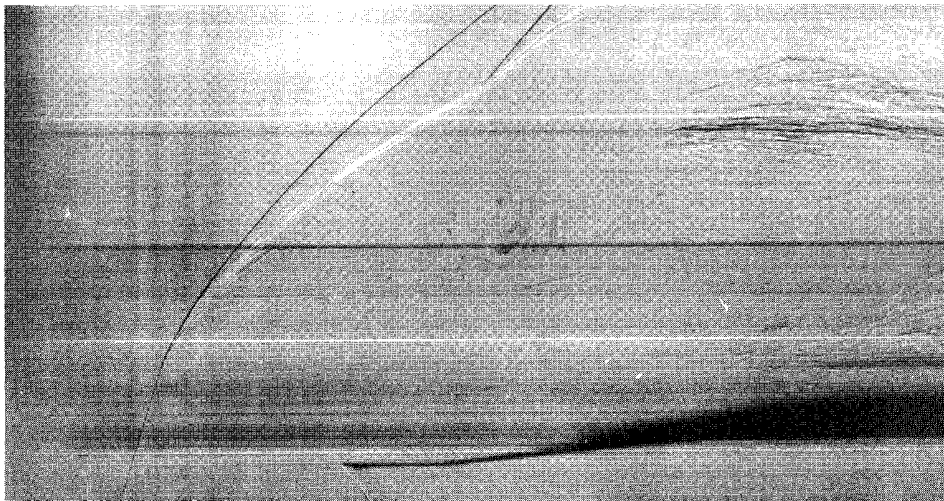


Figure 34. Streak Photograph of a Quenching Detonation Wave in Stoichiometric $H_2 - O_2$ with Nitrogen Boundary.

Run No. 760

$b = 0.1$ in.

Vert. - $x_{13} = 2.996$ in.

Horz. dist. equiv. to $x_{13} = 81.7 \mu\text{sec}$, approx.

At channel widths above the critical, it was maintained in the previous section that the detonation wave velocity reaches a new steady state value, as the various streak photographs revealed. To obtain a further proof of this, the velocity of the shock induced in the inert was checked. This was done by photographing the progress of the detonation wave through a slit close to the solid wall of the channel and the progress of the oblique shock in the inert through a slit at about .5 in. away from the separating film. Such a "double slit" streak picture is shown in Figure 35. A guide for the interpretation of such photographs is presented in Figure 36. Slit 2 is partially blocked off near the top of the test section, for the purpose of interrupting traces due to it, so that it would be possible to identify which trace belongs to which slit. The curved trace due to slit 2 near the bottom of the test section seen in Figure 35 is due to the cylindrical propagation of the shock from the point where the detonation wave first "sees" the boundary gas. After this initial curvature it can be seen that the trace of the oblique shock at points corresponding to where the detonation wave reaches a new steady state has the same inclination as that of the detonation wave trace. This is true of the interface trace also, although at first glance it does not appear to be so. However, this trace should be examined from the point where the initial curvature subsides to the point that corresponds to the detonation wave position when the latter hits the solid part of the film holder again. The distance corresponding to these two points is rather short.

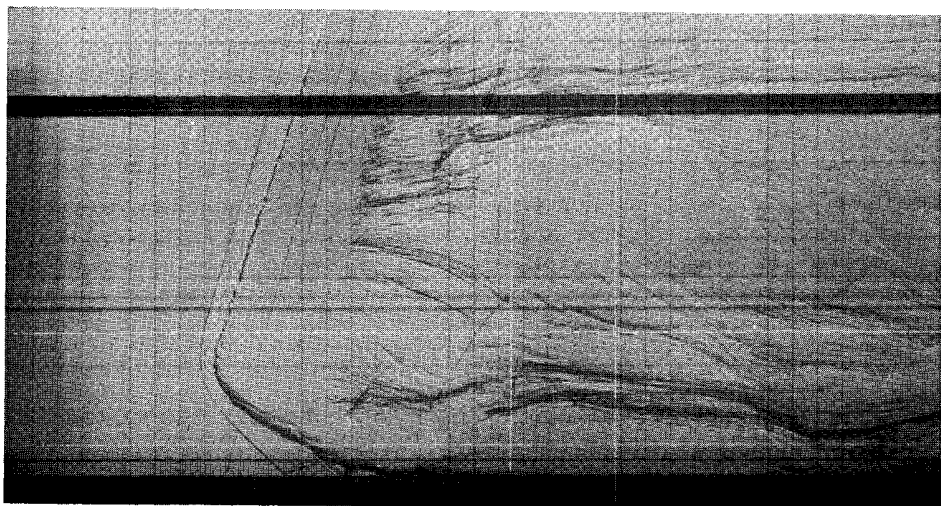


Figure 35. Streak Photograph of a Detonation Wave in Stoichiometric $H_2 - O_2$ and of Attendant Shock Wave in the Nitrogen Boundary (Double Slit).

Run No. 801

$b = 0.5$ in.

Vert. - $x_{13} = 2.996$ in.

Horz. dist. equiv. to $x_{13} = 91.86 \mu\text{sec}$

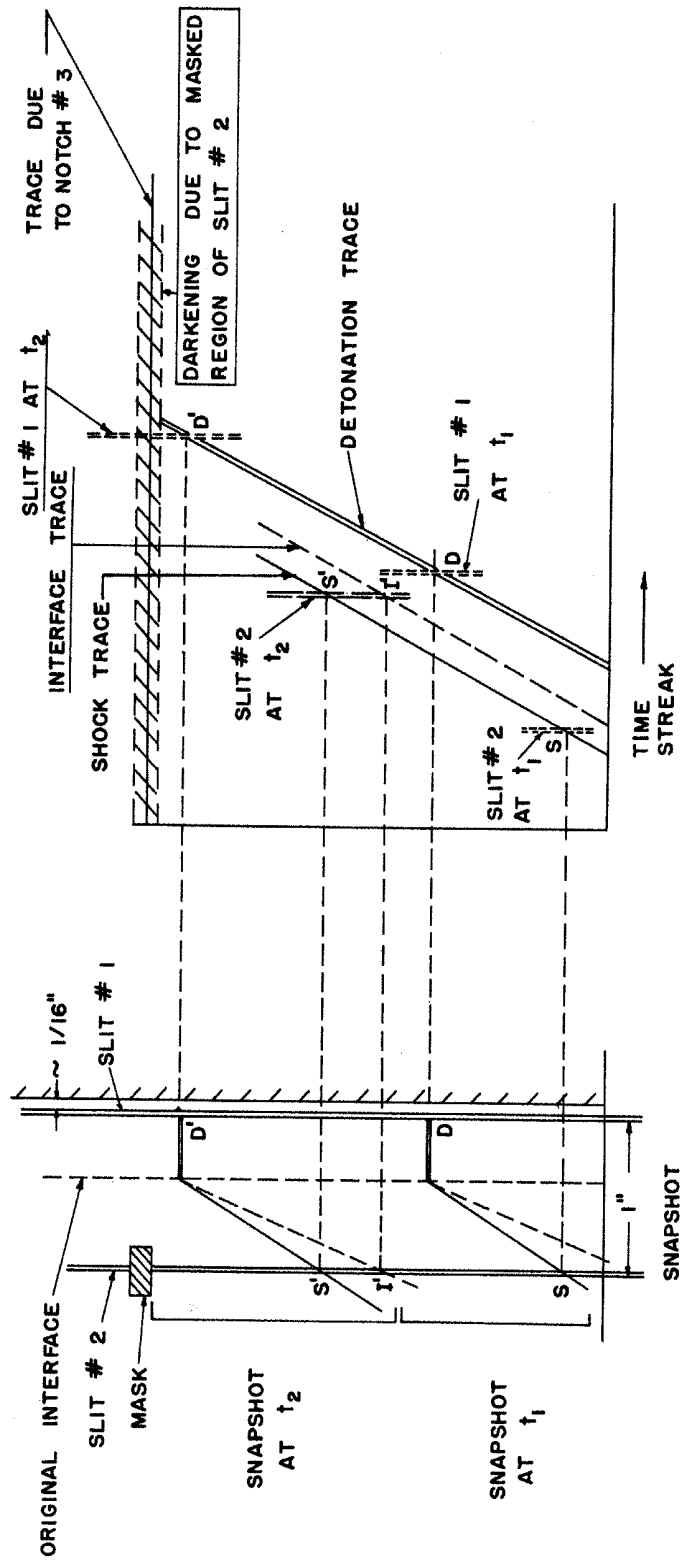


Figure 36. A Guide for the Interpretation of "Double Slit" Streak Photographs.

At channel widths close to the critical, the trace of the detonation wave in the streak picture showed, at times, some periodic waviness with the detonation wave remaining unquenched. An example of such a situation is shown in Figure 37 in which the appearance of the wave is very reminiscent of that of a "spinning detonation wave" (see, for example, Ref. 7). In a way, this is not surprising, for "spin" is usually associated with composition limits which in turn must necessarily depend on limits in the chemical reaction involved. That side relief imposes some limitation on the chemical reaction is demonstrated by the quenching behavior of the detonation wave.

The work of Fay⁽⁷⁵⁾ on spinning detonation wave showed that the waviness can reasonably be described as due to the transverse mode of vibration of the gas behind the shock front. It is, therefore, interesting to apply this theory to our work here. The sound frequencies of a column of gas in a rectangular channel with sides b and d, are:

$$v_{nm} = \frac{a}{2} \left(\frac{n^2}{d^2} + \frac{m^2}{b^2} \right)^{1/2} \quad (5.4)$$

with the fundamental frequency obtainable by setting $n = m = 1$. If the velocity of sound a, is taken as the average sound velocity behind the detonation wave then

$$\overline{a_{e2}} = a_{el} M_{el} \overline{\phi_2} \quad (5.5)$$

so that the theoretical fundamental frequency is

$$v_{th} = \frac{a_{el} M_{el} \overline{\phi_2}}{2b} \left(\frac{b^2}{d^2} + 1 \right)^{1/2} \quad (5.6)$$

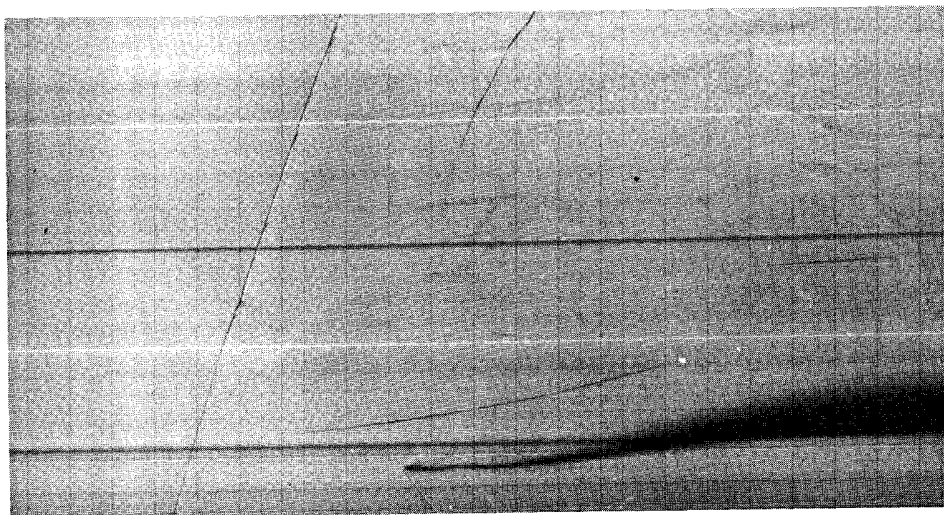


Figure 37. Streak Photograph of a Detonation Wave in
Stoichiometric $H_2 - O_2$ with Nitrogen
Boundary Showing Spin Characteristics.

Run No. 766

$b = 0.2$ in.

Vert. - $x_{13} = 2.996$ in.

Horz. - dist. equiv. to $x_{13} = 81.7 \mu\text{sec}$, approx.

The observed frequency can be obtained from the observed pitch length, x_p , as

$$\nu = \frac{u_{el}}{x_p} = \frac{a_{el} M_{el}}{x_p} \quad (5.7)$$

and therefore the ratio of the theoretical frequency to the observed is

$$\frac{\nu_{th}}{\nu} = \frac{\bar{\phi}_2}{2b} x_p \left(\frac{b^2}{d^2} + 1 \right)^{1/2} \quad (5.8)$$

From Figure 37 we find $x_p = .75$ in., and therefore, with $b = .2$ in., $d = .36$ in. and $\bar{\phi} = .52$ obtained from Table II, application of this equation gives

$$\frac{\nu_{th}}{\nu} = 1.12 \quad (5.9)$$

which indicates that the observed frequency is about 12% smaller than the theoretical. The order of the variation is the same as that observed in spinning detonation in tubes without side relief.

Fay's work does not delve into the origin of spin, nor has there been a satisfactory theory on this problem. Since our experimental work shows for the first time, that spin could be created at will by proper choice of the boundary gas and channel widths in explosive mixtures far away from their composition limits, further experimental study along these lines may well prove helpful in solving the initiation problem. As can be implied from the survey of Oppenheim et al.⁽⁷⁶⁾, spin initiation may very well have some bearing on rocket motor instability.

5.4 Velocity Decrement of H₂-O₂ Mixtures Bounded by Nitrogen Near Their Respective Critical Channel Widths

In order to establish which of the quenching criteria presented in Chapter III is most adequate in predicting the quenching limit, a series of runs were made with various hydrogen-oxygen mixtures bounded by nitrogen, at channel widths very close to the critical. The idea was to determine the maximum velocity decrement possible before quenching takes place and to compare the results with each of the three criteria. Again streak schlieren photography was used and examples of the results for the leanest and richest mixtures tested are shown in Figures 38 and 39 respectively. Table V below gives a summary of the results obtained on the measurement of the velocity decrement using the same method as Section 5.2.

To find the critical Mach number from the experimental data, the average velocity decrement column (9) was subtracted from the theoretical Mach number column (11) with the results shown in column (12). Column (13) shows the range in the critical Mach number based on the range in the velocity decrement. These results which were corrected by a velocity decrement of .018 due to the boundary layer effect (see Section 5.2) are plotted in Figure 12. They show best agreement with Belles' explosion limit criterion (with the old chemical kinetics data) not only in magnitude but in trend as well.

It might be argued that either Patch's constant temperature criterion or Shchelkin's instability criterion could be made to give a reasonable fit to the experimental data by simply adjusting the critical temperature in the former and the value of the activation

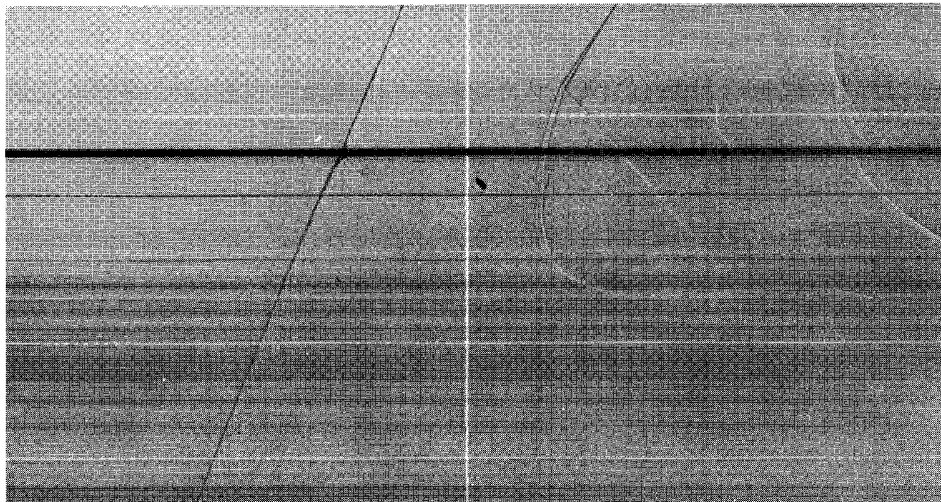


Figure 38. Streak Photograph of a Detonation Wave in
46.3% H₂ - 53.7% O₂, with Nitrogen Boundary.

Run No. 1014

b = 0.5 in.

Vert. - x_{13} = 2.996 in.

Horz. - dist. equiv. to x_{13} = 79.35 μ sec

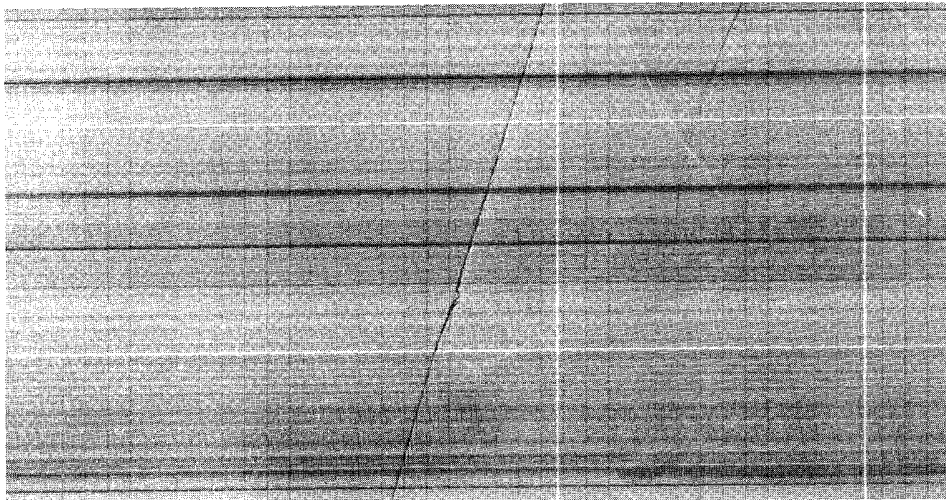


Figure 39. Streak Photograph of a Detonation Wave in
75% H_2 - 25% O_2 , with Nitrogen Boundary.

Run No. 976

$b = .25$ in.

Vert. - $x_{13} = 2.996$ in.

Horz. - dist. equiv. to $x_{13} = 78.60 \mu\text{sec}$

TABLE V

SUMMARY OF THE EXPERIMENTAL RESULTS OBTAINED FOR H_2-O_2 MIXTURES BOUNDED BY N_2

(1)	(2)	(3)	(4)	(5)	(6)	(7)	(8)	(9)	(10)	(11)	(12)	(13)
% H_2	No. of Runs	b (in.)	$(u_e)_{th}$ ft/sec	$\frac{(u_e)_{ion}}{(u_e)_{th}}$ ft/sec	$\frac{(\Delta u_e)_{ion}}{(u_e)_{th}}$	$\frac{u_{e\beta}}{u_{e\theta}}$	$\left[\frac{\Delta u_{e\beta}}{u_{e\theta}} \right]$	$\left[\frac{\Delta u_e}{u_e} \right]$	Range in $\frac{\Delta u_e}{u_e}$	$(M_e)_{th}$	M_{ec}	Range in M_{ec}
75	5	.25	10,430	10,285	.014	10,278	.015	.065	.053 .075	5.26	4.92	4.98-4.86
66.7	9	.2	9,320	9,075	.026	9,199	.012	.070	.051 .097	5.28	4.91	5.01-4.77
60	5	.2	8,560	8,436	.015	8,490	.008	.077	.052 .113	5.24	4.84	4.97-4.65
55	4	.25	8,050	7,690	.045	7,808	.031	.086	.078 .096	5.19	4.75	4.79-4.70
51.8	5	.35	7,770	7,481	.037	7,584	.024	.075	.054 .090	5.16	4.78	4.88-4.70
46.3	5	.5	7,320	7,035	.039	7,305	.020	.078	.059 .110	5.09	4.69	4.79-4.53

(4) Figure 47

(5), (6), (7), (8), (9) and (10): Similar to (3), (4), (5), (6), (7) and (8) respectively in Table IV.

$$(12) = (M_e)_{th} - \left[\frac{\Delta u_e}{u_e} \right]$$

$$(13) = (M_e)_{th} - \frac{\Delta u_e}{u_e}$$

energy E_2 used in the latter, since these are not known with considerable certainty. Doing this, however, would still give in both cases a constant critical Mach number and thereby the trend of the experimental data would not be followed. Further, the composition limits that would be predicted under these circumstances would be far removed from those observed.

In experiments conducted at lower than atmospheric pressures such as those on the standing detonation wave reported by Nicholls and Dabora⁽⁶²⁾ it was found that ignition did not take place except under conditions compatible with Belles' criterion. A further support to plausibility of the explosion limit criterion is the observation made by Lewis and von Elbe⁽⁷⁷⁾ that composition limits in H_2-O_2 can be widened if a special effort is made to dry the mixture. They point out that this is indicative of the role of the chain breaking reaction IV and the high efficiency of water as third body (see Equation 3.9) in this reaction. In this regard, the experimental results reported here which show that quenching takes place at lower Mach number decrement than the theory predicts can be interpreted to be due, in part, to the water contamination, as no special precaution was taken to pre-dry the gases any further than as supplied.

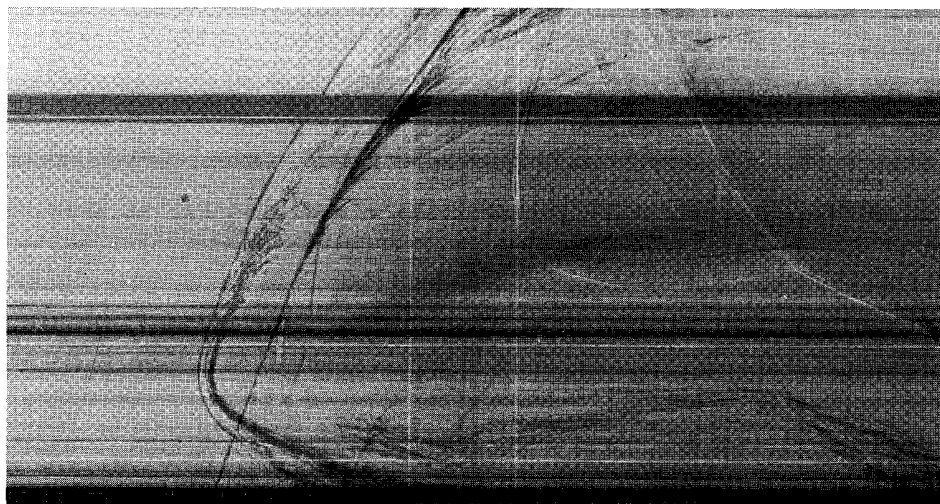
Neither Shchelkin's nor Patch's criteria take into consideration any composition effect. Further, Patch's criterion is probably applicable to mixtures which are initially at pressures near atmospheric, whereas Shchelkin's criterion is independent of pressure. Since the results presented here which show a definite composition

effect, and since the results in (62) for initial pressures much lower than atmospheric are in good agreement with the explosion limit criterion, it is concluded that it is basically adequate in describing the conditions under which detonation waves in H_2-O_2 mixtures could be self-maintained.

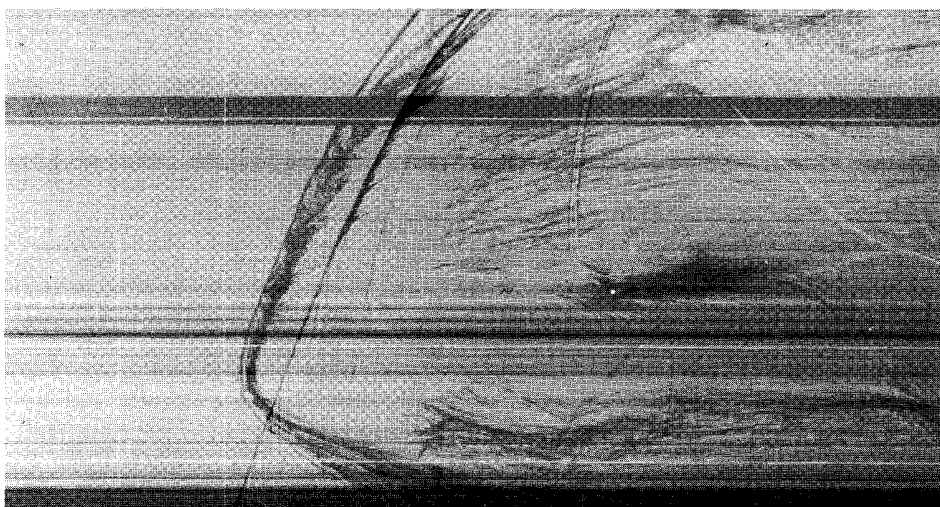
5.5 Estimation of the Reaction Length in the Stoichiometric Methane Oxygen Mixture

The theory presented in Chapter II indicates that if data on the velocity decrement of an explosive when confined by a known inert medium are available, they can be used to infer the reaction length of the explosive. This is what was done in Section 5.2 for the stoichiometric hydrogen oxygen mixture with encouraging results.

Stoichiometric methane oxygen was chosen as another explosive mixture for the purpose of calculating its reaction length. When the widest available channel width was used with nitrogen as boundary, it was found that the reaction zone thickened and the detonation wave tended to quench. As the theory predicts, the situation was improved when carbon dioxide, a gas heavier than nitrogen, was used. More improvement was experienced when butane was used as the confining gas. Typical streak photographs for the above three conditions are shown in Figure 40. In the butane case, the detonation wave still seemed to be thick but nevertheless it was considered unquenched because the velocity appeared constant near the top of the test section. The velocity decrement calculated from several photographs ranged from .081 to .093 with an average of .088. Thus the total velocity decrement becomes .106 after decrement due to boundary layer effect is added

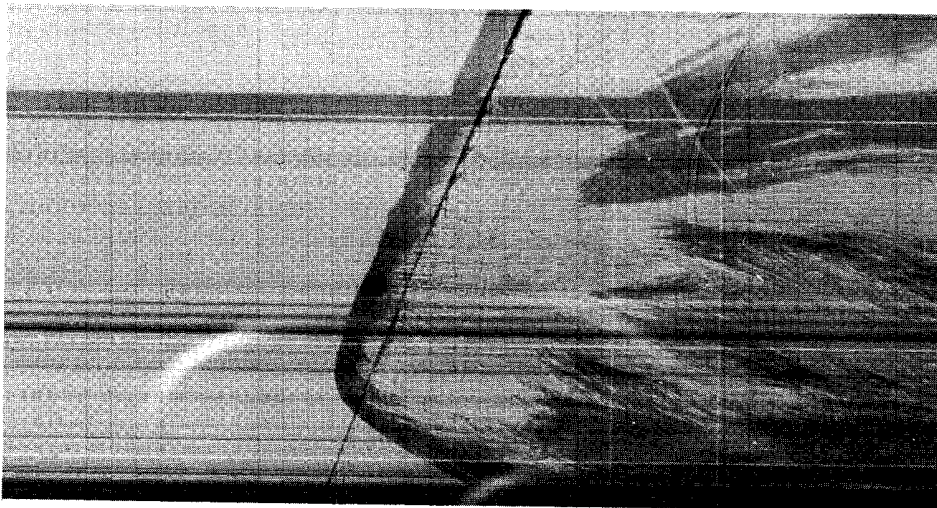


- (a) Run No. 1018
Boundary Gas: N_2
 $b = 0.5$ in.
Vert. - $x_{13} = 2.996$ in.
Horz. - dist. equiv. to $x_{13} = 77.92 \mu\text{sec}$



- (b) Run No. 1020
Boundary Gas: CO_2
 $b = 0.5$ in.
Vert. - $x_{13} = 2.996$ in.
Horz. - dist. equiv. to $x_{13} = 77.92 \mu\text{sec}$

Figure 40. Streak Photograph of Detonation Wave in Stoichiometric $CH_4 - O_2$ and of Attendant Shock Wave in the Boundary Gas (Double Slit).



(c) Run No. 1022
Boundary Gas: C_4H_{10}
Channel width = 0.5 in.
Vert. - x_{13} = 2.996 in.
Horz. - dist. equiv. to x_{13} = 79 μ sec

Figure 40. (Continued)

(as explained in Section 5.2). From Figure 11 such a velocity decrement corresponds to an incremental area increase ξ of .176. Using Equation (2.53), after finding $\tan \delta$ to be .272 from Figure 8 the value of .325 in. is obtained for the reaction length of the stoichiometric methane-oxygen, which is about twice that of the stoichiometric hydrogen-oxygen.

At this point, it is interesting to look at the results of Wagner⁽⁷⁸⁾ on detonations of mixtures of city gas* and oxygen conducted in paper tubes and examine them in the light of the findings on reaction lengths in this study. Wagner, by "specially treating" the paper tubes, was able to change the distance x_p , behind the detonation front at which they break. He finds that the detonation velocity in the paper tubes to be less than that in a solid tube with the decrement in velocity increasing with decreasing x_p , and quenching setting in when $x_p = .4$ in. His expression for the area increase due to the paper motion is

$$\xi = 10^{-3} t^2 \quad (5.10)**$$

where t is the time (in μsec) after the passage of the detonation wave. By assuming the time in which most of the reaction in detonation is completed is about 1 μsec , he concludes that the area increase, being thus very small, cannot alone explain the relatively large velocity decrements he obtains, and therefore the flow conditions behind the C-J plain must be influencing the propagation velocity.

*Composition not reported. Main constituent is assumed to be methane.

**Expression (5.10) corresponds to a paper thickness of about .001 in.

An alternative explanation of Wagner's findings is offered as follows. Because of some impurities in city gas, it is reasonable to assume that its reaction length is higher than that of methane. Such a reaction length would mean a reaction time of 6-9 μ sec, which in turn gives $\xi = .04 - .08$. Such an area increase corresponds to 2-5% velocity decrement which is what Wagner obtains at x_b slightly larger than .4 in. This explanation of Wagner's results seems to be very plausible as it does away with the unlikely postulation that perturbations behind the C-J plane can influence the propagation velocity of the detonation wave.

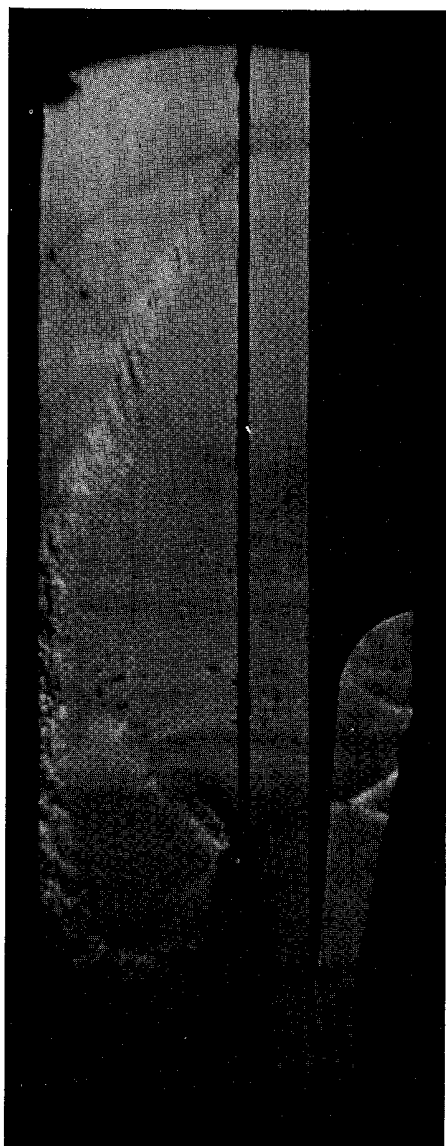
5.6 Behavior of Detonation Waves When the Density of the Boundary Gas is Much Lower Than That of the Explosive

In agreement with theory, it was demonstrated in the previous section that the denser the boundary gas the better the confinement of the detonation wave. The limit of course is a solid boundary, inside which a detonation wave travels without loss in velocity. The question arises as to what happens to a detonation wave when a gas much lighter than the explosive is used as the confining medium. Such a situation can usually arise in a rotating detonation wave rocket motor mentioned in the introduction. After the first cycle, the burned gas is pushed by the fresh charge thereby acting as a confining medium for the detonation wave in the next cycle. The burned gas is, of course, expanded from the Chapman-Jouguet pressure to some lower pressure; however, it would still be at a higher temperature than the injected charge and therefore would be much lighter than the charge.

Figure 9 which was derived using the shock tube analogy, indicates that when the density parameter is about 1.4, the shock angle in the inert becomes nearly 90° . Such a shock angle with flow deflection downstream of it is not possible unless the shock is detached from the leading edge of the deflection plane. In actuality, detachment arises at shock angles ranging between $62-78^\circ$ depending on the detonation Mach number and the density parameter. This situation was first recognized by Sommers⁽³¹⁾ who was able to show photographically that indeed when the inert gas is light enough a detached shock can develop.

The question that needs to be answered here is what effect, if any, has the condition of shock detachment on the quenching criterion. Some experiments were carried out with H_2-O_2 and CH_4-O_2 detonations bounded by either He or H_2 . Typical spark photographs are shown in Figures 41 and 42. In the case of 75% H_2 -25% O_2 bounded by He (Figure 41b), one can see that the shock is still attached, whereas, in the case of the same explosive bounded by H_2 (Figure 41a), the shock appears to lead the detonation wave. Finally, in the case of 33.3% CH_4 -66.7% O_2 bounded by H_2 (Figure 42) the shock is well ahead of the detonation wave and can be seen to be inducing an oblique shock into the explosive mixture. For all the conditions represented by these photographs calculations would indicate that quenching of the detonation wave in the explosive should have taken place. Why then do none of these photographs show any quenching?

A qualitative explanation can be offered as follows. When the shock is detached it runs ahead of the detonation wave. Now the



(a)



(b)

Figure 41. Spark Photographs of a Detonation Wave in
75% H_2 - 25% O_2 . ($b = 0.3$ in.)

- (a) Run No. 1148 - Hydrogen boundary
- (b) Run No. 1169 - Helium boundary

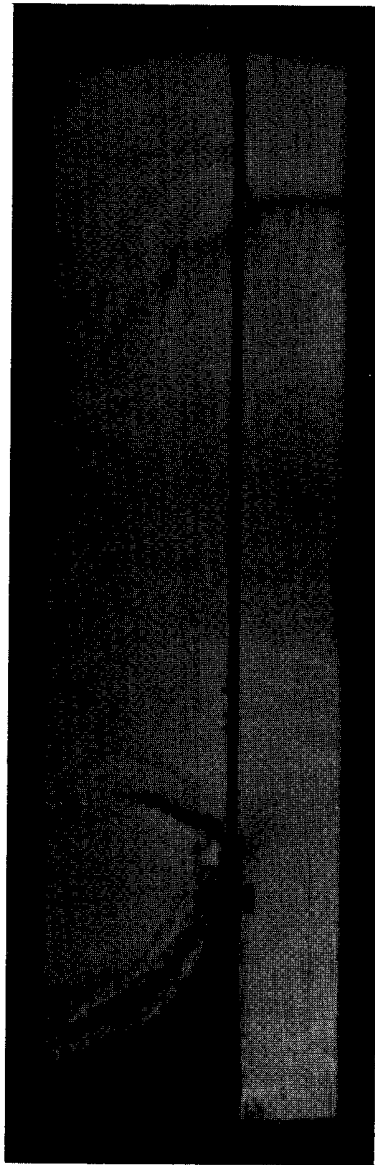


Figure 42. Spark Photograph of a Detonation Wave in
33% CH_4 - 67% O_2 with Hydrogen Boundary.
($b = 0.5$ in.) (Run No. 1107)

density of the inert gas behind the shock is higher of course than its initial density, so that what the detonation wave "sees" essentially, is this higher density gas. This in turn means a lower deflection angle and therefore a lower area increase and a lower Mach number decrement. Therefore, it is possible that the steady-state detonation Mach number could still be higher than the critical. Hence no quenching appears to take place.

Despite these circumstances it is still reasonable to assume that quenching could be accomplished if the channel width is sufficiently reduced. This was done in the case of 75% H_2 -25% O_2 bounded by hydrogen. A typical photograph is shown in Figure 43 where it can be seen that the shock in the boundary gas leads by an appreciable distance the reaction zone in the explosive. Further one can see the oblique shock induced by the shock into the explosive more clearly than could be seen in Figure 41. Also distinguishable is a new interface pushed into the explosive. Needless to say, the flow pattern is very complicated.

Unfortunately the rotating drum camera was not available when tests of conditions similar to those of Figure 43 were being conducted. However, tests where pictures at several time delays were taken when H_2 and He were used, showed a considerable decrease in the velocity of the detonation wave. The data is plotted in Figure 44, showing that the "reaction zone" propagation was at about 50% of the detonation velocity. Because the accuracy of the relative time delay is in question, it is not possible to say with certainty



Figure 43. Spark Photograph of a Detonation Wave in 75% H_2 - 25% O_2 Mixture with Hydrogen Boundary, Showing an Oblique Shock in the Explosive Resulting from a Leading Shock in the Inert. ($b = .02$ in.) (Run No. 1193)

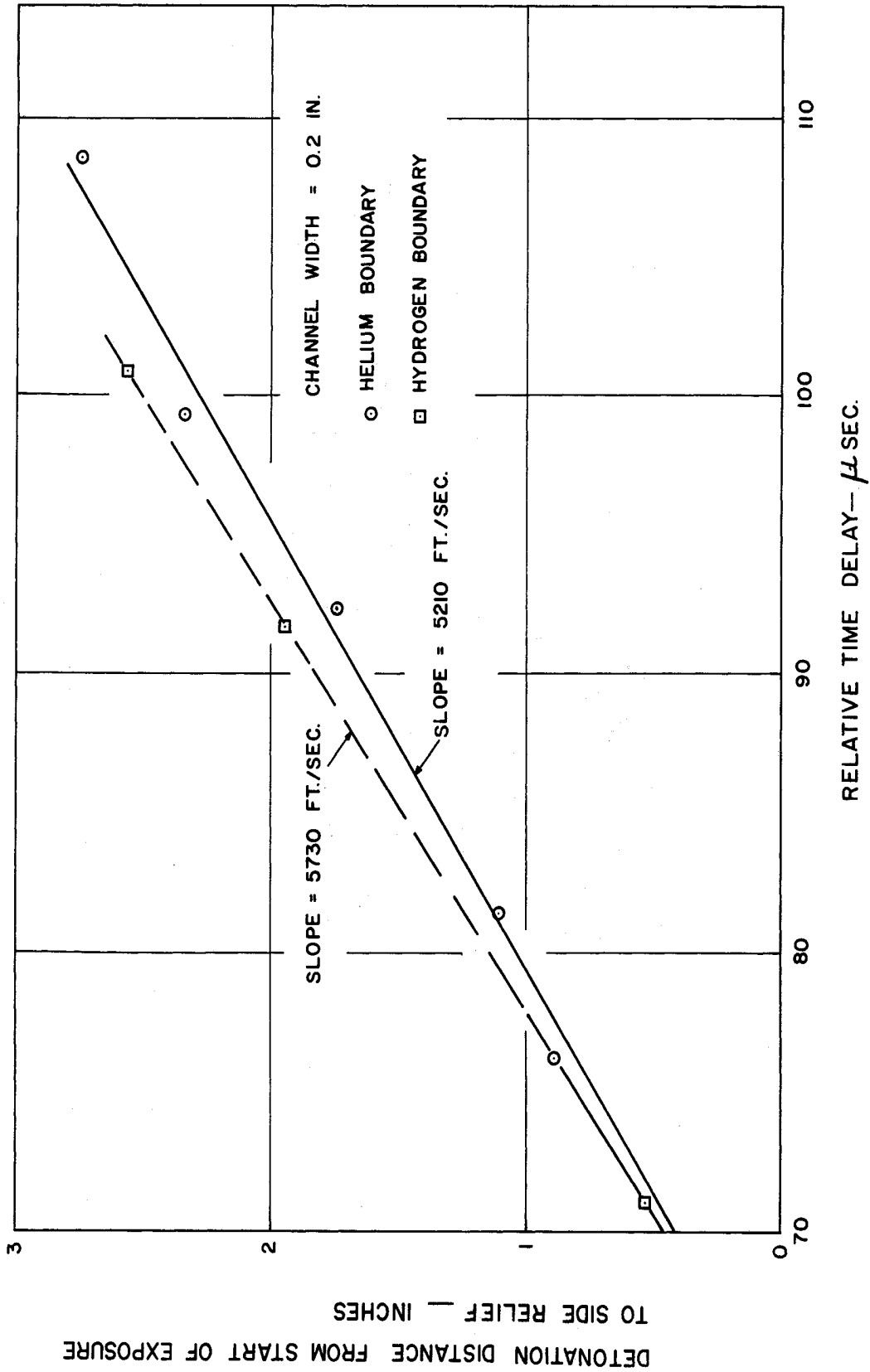


Figure 44. Detonation Wave Progress of 75% H₂ - 25% O₂ When Confined by Helium or Hydrogen.

at this point, whether the detonation is continuously decreasing in velocity or whether it reached a steady state. However, it is interesting to mention that Voitsekhovskii⁽³⁵⁾ reports a steady detonation velocity in an annular channel at half the C-J velocity. The situation in the annular channel is such that the burned gas is on the side of the fresh, unburned gas acting as a low density boundary.

If this is more than a mere coincidence, it must mean that a rather new and interesting mode of detonation wave is possible. It should be added that such a mode is not completely inconsistent with the quenching criterion, for by inducing an oblique shock into the explosive, the detached shock of the inert essentially increases both pressure and temperature of the explosive. This can mean that the explosion limit criterion can be attained at somewhat lower Mach number than would be needed when the explosive is not so "prepared". Thus it would appear that a low density gas, when used as an inert boundary, can provide a mechanism by which some of the energy of the detonation wave could be transferred ahead of the detonation front.

5.7 Experimental Interface Deflection Angles and Inert Shock Angles

As a check on the degree of accuracy with which the shock tube analogy can predict the interface deflection angles as well as the shock angles in the inert, measurements of these angles from spark schlieren photographs were made. The data for the deflection angles are plotted in Figure 45 where the theoretical deflection

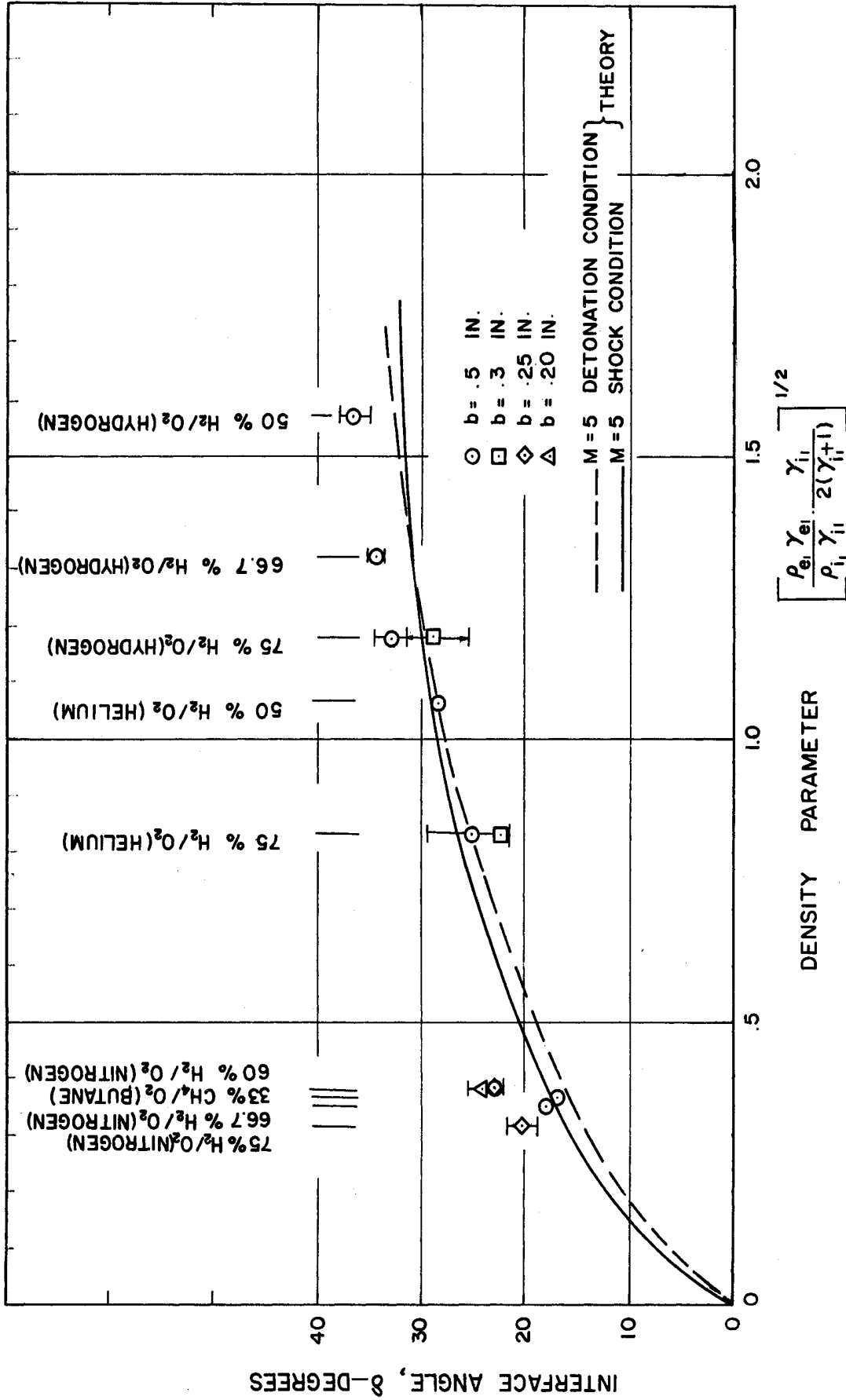


Figure 45. Experimental Results of Interface Deflection Angles.

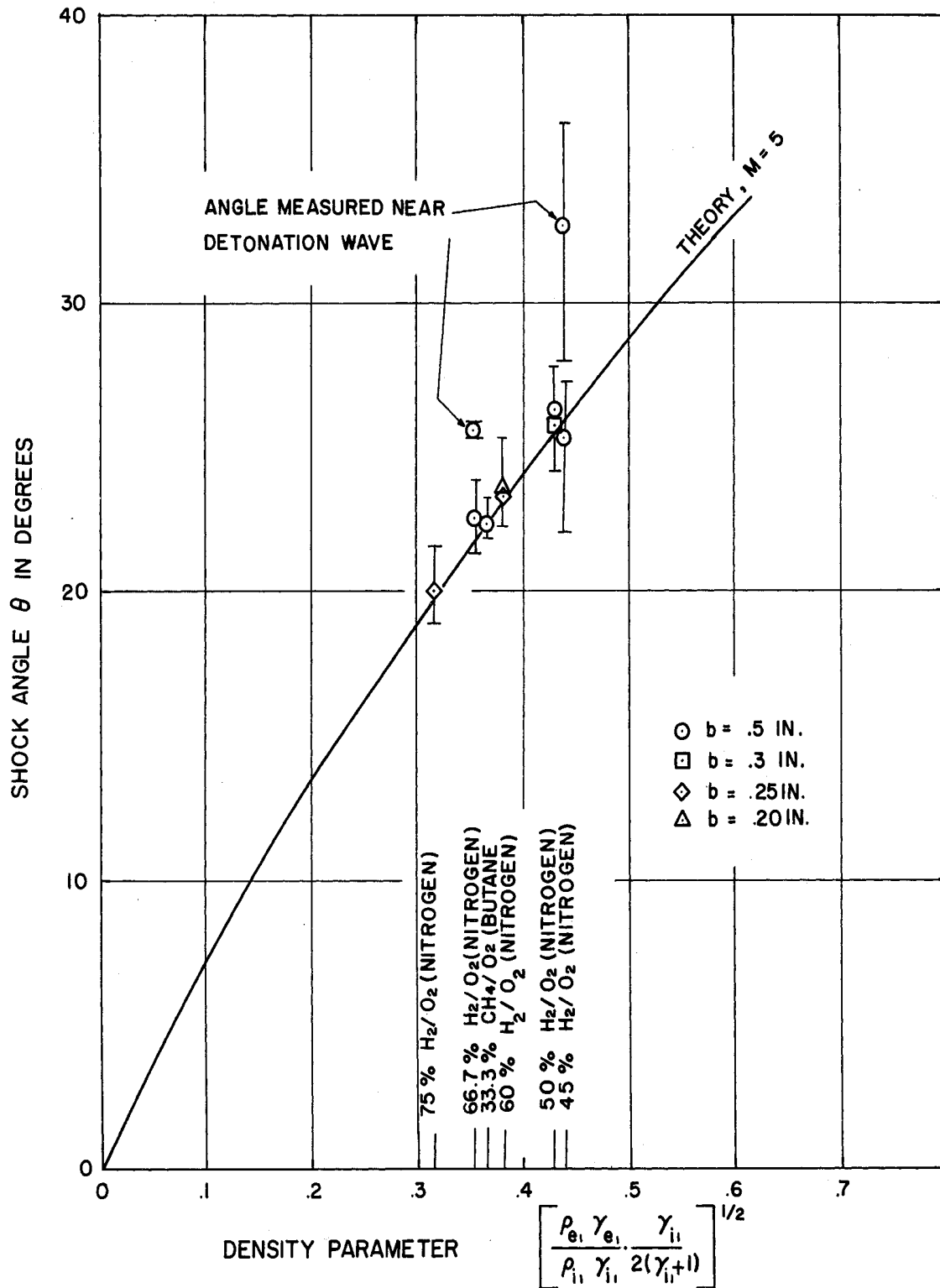


Figure 46. Experimental Results of Shock Wave Angles in the Inert Gas.

angle is also shown. Reasonable agreement is apparent throughout the range of conditions tested. Agreement appears, in general, to be excellent when the explosive channel width is large, i.e., when conditions are above and far away from the quenching limit.

The data for the shock angle in the inert for limited test conditions, are plotted in Figure 46. They indicate good agreement with theory again. Cases in which the shock leads the detonation wave are not plotted because the shocks were curved and it was impossible to determine an "average angle."

It is concluded on the basis of these measurements that estimation of area change near the detonation zone by use of the shock tube analogy results in a satisfactory agreement between theory and experiment.

VI. CONCLUSIONS

1. The shock tube analogy is successfully used to predict the shock angle induced by a gaseous detonation wave into the inert compressible medium that confines it. It can also predict the interface angle between the expanded burned gas behind the detonation wave and the shocked gas in the inert.
2. The parameter that controls the extent of the deflection angle contains essentially the ratio of the density of the explosive to that of the inert. The higher this ratio is, the larger the deflection angle.
3. The effective area change of each stream tube between the shock plane of the detonation wave and the Chapman-Jouguet plane, can be calculated from a knowledge of the deflection angle, the explosive channel width and the reaction length.
4. It is possible to predict that an area increase in the reaction zone reduces the detonation velocity. Thus, if the velocity decrement of a detonation wave in a known explosive of known channel width, confined in a known inert can be determined experimentally, the reaction length can be inferred. This is done in the case of a stoichiometric H_2-O_2 mixture and a stoichiometric CH_4-O_2 in which the reaction lengths are found to be .14 in. and .32 in. respectively. The inferred reaction length of the H_2-O_2 mixture agrees with the value reported in the literature.
5. Using Belles' explosion limit criterion it is possible to predict, for the H_2-O_2 mixtures, a critical detonation velocity below which

The detonation is expected to quench. Good agreement between this theory and the experimental results is obtained. It is found that a velocity decrement larger than 8-10% of the theoretical velocity can lead to the quenching of the detonation wave.

6. Near the quenching limit, the detonation wave propagates, at times, like a spinning detonation wave so common at composition limit. This is the first time that a "spin" could be induced in gas mixtures away from their composition limit and the method is therefore deemed convenient for the study of the origin of spin.
7. When the inert boundary gas is much lighter than the explosive, the induced shock is detached. In some instances, it appears that such a condition can provide a mechanism whereby energy from behind the detonation wave can be transferred ahead of it. In such situations, detonation waves traveling at about half the Chapman-Jouguet velocity have been observed experimentally.
8. A technique for minimizing diffusion between the boundary inert gas and the explosive gas by separating them by a thin film is developed. It is found that in order for the film itself to have a negligible effect on the interaction process being studied, the ratio of its thickness to that of the reaction length should be one-tenth the ratio of the explosive density to that of the film.

APPENDIX A

ERROR ANALYSIS

The calculation of the detonation velocity and the velocity decrement are subject to errors due to measurements as well as explosive composition. It is therefore necessary to assess the accuracy of the reported calculations.

According to Reference 79, the error in a quantity y , where

$$y = F(x_1, x_2, \dots, x_n) \quad (A-1)$$

and be calculated by the following equation:

$$\overline{(dy)^2} = \sum_{i=1}^n \left(\frac{\partial F}{\partial x_i} \right)^2 \overline{(dx_i)^2} \quad (A-2)$$

which will be used below.

A.1 Error in Velocity Measurement from Streak Photographs

The detonation velocity from streak photographs can be calculated according to Equation (5.1). This can be written, after assuming $\alpha = 0$ and noting that the magnification is obtained by measurements of two distances, as

$$u_e = \frac{L l_o}{l_i t_p} \tan \beta \quad (A-3)$$

where l_o = distance between two fixed points on the test section

l_i = distance between the corresponding points on the image.

Applying Equation (A-2) to (A-3), one obtains

$$\sqrt{\left(\frac{du_e}{u_e} \right)^2} = \left[\left(\frac{dL}{L} \right)^2 + \left(\frac{dl_o}{l_o} \right)^2 + \left(\frac{dl_i}{l_i} \right)^2 + \left(\frac{dt_p}{t_p} \right)^2 + \left(\frac{d \tan \beta}{\tan \beta} \right)^2 \right]^{1/2} \quad (A-4)$$

In using the tool maker's microscope for the measurement of angles and distances on the photographs, angles to within 0.1° and distances of $\sim .5$ in. to within .002 in. could be made. Since

$$\frac{d \tan \beta}{\tan \beta} = \frac{d\beta}{\sin \beta \cos \beta} \quad (A-5)$$

and since $\beta = 70^\circ$, then $d \tan \beta / \tan \beta = .0055$. Further with,

$$\frac{dL}{L} = .002 \quad (\text{ability to measure drum perimeter of } 2.5 \text{ in. to within } .025 \text{ in.})$$

$$\frac{d\ell_o}{\ell_o} = .001 \quad (\text{measurement of } 3 \text{ in. to within } .003 \text{ in.})$$

$$\frac{d\ell_i}{\ell_i} = .004 \quad (\text{ability to define fixed points on the photographs when viewed in the toolmaker's microscope})$$

and

$$\frac{dt_p}{t_p} = .003 \quad (\text{measurement of the drum camera period by the Hewlett-Packard timer as reported by the manufacturer})$$

one obtains

$$\sqrt{\left(\frac{du_e}{u_e}\right)^2} = .775\% \quad (A-6)$$

A.2 Error in Velocity Measurement from Measurement by Ionization Probes

The velocity in this case is calculated as

$$u_e = \frac{\ell_{13}}{t_{13}} \quad (A-7)$$

where ℓ_{13} is the distance between two probes which can be estimated to within $1/16$ in. in ~ 12 in., and t_{13} is the time for the detonation wave to pass from probe 1 to probe 3 as measured by the Berkley

timer, to an accuracy of 1 μ sec in 100 μ sec. Therefore,

$$\frac{d\ell_{13}}{\ell_{13}} = .0052 \quad \text{and} \quad \frac{dt_{13}}{t_{13}} = .01$$

which gives:

$$\sqrt{\left(\frac{du_e}{u_e}\right)^2} = 1.13\% \quad (\text{A-8})$$

A.3 Error Due to Composition

The hydrogen oxygen mixture is prepared by the partial pressure method. The accuracy of the gauge used combined with the accuracy of reading it is about .5 psi. Usually a total pressure of 70 psia is attained during the preparation of each mixture.

The mole fraction of H_2 is

$$f_{H_2} = \frac{p_{H_2}}{p_{tot}} \quad (\text{A-9})$$

For 40% H_2 - 60% O_2 mixture then

$$\frac{dp_{H_2}}{p_{H_2}} = \frac{.5}{70 \times .4} = .0178 \quad (\text{A-10})$$

and for 75% H_2 - 25% O_2 mixture

$$\frac{dp_{H_2}}{p_{H_2}} = \frac{.5}{70 \times .75} = .0095 \quad (\text{A-11})$$

But,

$$\frac{dp_{tot}}{p_{tot}} = \frac{.5}{70} = .0072 \quad (\text{A-12})$$

so that

$$\sqrt{\left(\frac{df_{H_2}}{f_{H_2}}\right)^2} = 1.92\% = 1.19\% \quad (\text{A-13})$$

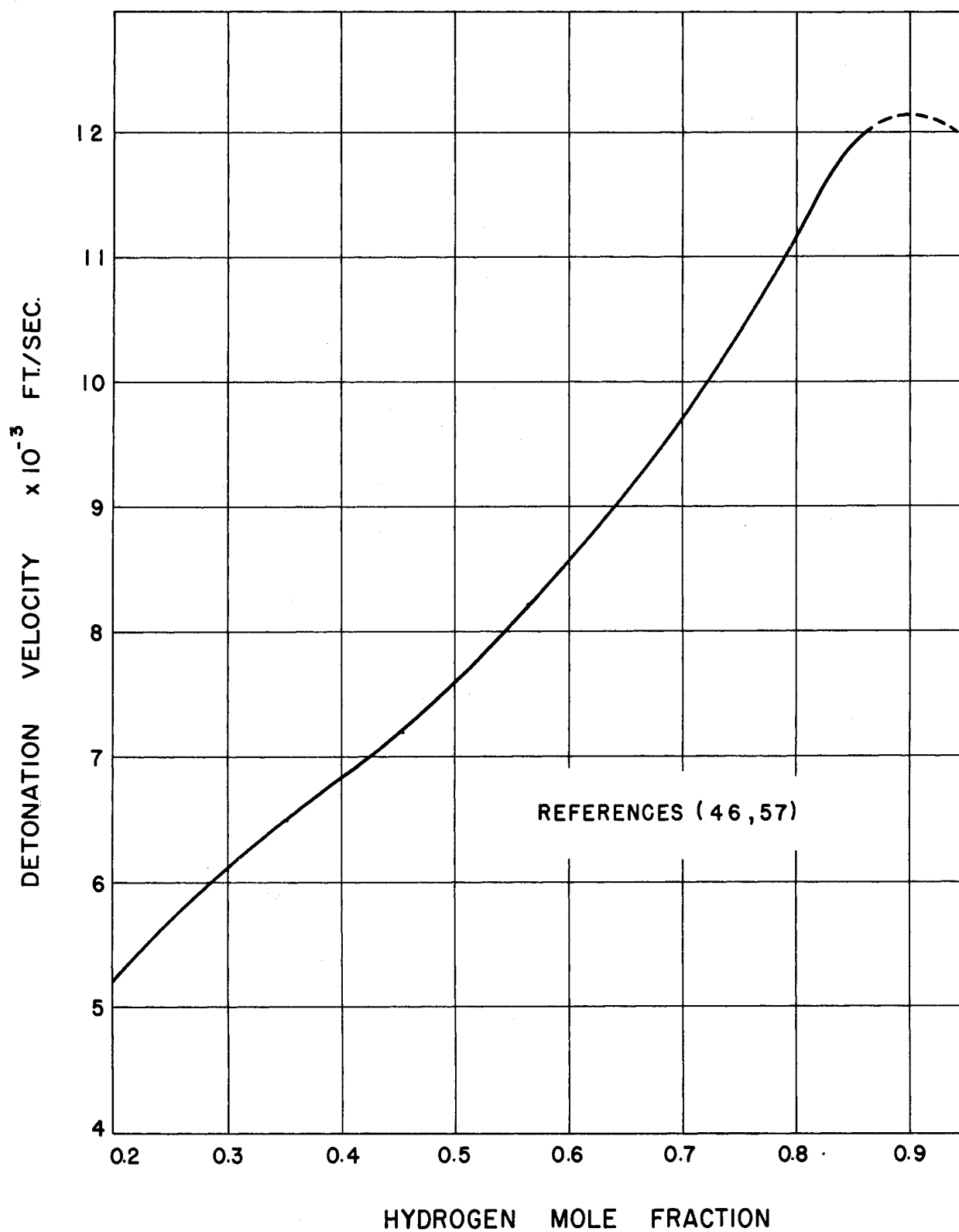


Figure 47. Theoretical Detonation Wave Velocity of $H_2 - O_2$ Mixtures at One Atmosphere and $535^\circ R$.

The theoretical detonation wave velocity as calculated by Gordon⁽⁵⁷⁾ is shown in Figure 47 as a function of the hydrogen mole fraction. From this figure and the possible error in the mole fraction of H_2 one can deduce that the possible variation in detonation velocity can be:

$$\sqrt{\left(\frac{du_e}{u_e}\right)^2} = .9\% - 1.3\% \quad (A-14)$$

A.4 Error in the Velocity Decrement as Measured from Streak Photographs

When $\alpha' = \alpha = 0$, the velocity decrement in Equation (5.3) becomes:

$$\frac{\Delta u_e}{u_e} = 1 - \frac{\tan \beta'}{\tan \beta} \quad (A-15)$$

Applying Equation (A-2) and noting that $\tan \beta \cong \tan \beta'$, one obtains the following expression for the error in the velocity decrement:

$$\sqrt{d\left(\frac{\Delta u_e}{u_e}\right)^2} = \sqrt{2\left(\frac{d \tan \beta}{\tan \beta}\right)^2} \quad (A-16)$$

With the value of the error in $\tan \beta$ calculated to be .0055 in Section A.1, this becomes

$$\sqrt{d\left(\frac{\Delta u_e}{u_e}\right)^2} = .78\% \quad (A-17)$$

BIBLIOGRAPHY

1. Berthelot, M. and Vieille, P. "Sur la Vitesse de Propagation des Phenomenes Explosifs dans les gaz." Comptes Rendus, de l'Academie des Sciences, Paris, 93 (1881), 18-22.
2. Mallard, E. and LeChatelier, H. "Sur la Vitesse de Propagation de L'inflammation dans les Melanges Explosifs." Comptes Rendus, de l'Academie des Sciences, Paris (July 18, 1881), 145-148.
3. Chapman. "On the Rate of Explosion in Gases." Phil. Mag., 47, (1899), 90.
4. Jouguet. "Sur la Propagation des Reaction Chimiques dans les Gaz." J. Mathematique, 6, No. 1 (1905), 347; 6, No. 2 (1906), 6.
5. Morrison, R. B., Adamson, T. C., Jr. and Weir, A., Jr. "Detonative and Deflagrative Combustion." Advances in Chemistry Series No. 20, Amer. Chem. Soc., 1958.
6. Gross, R. A. and Oppenheim, A. K. "Recent Advances in Gaseous Detonation." ARS Journal, 29 (1959), 173.
7. Wagner, H. Gg. Fundamental Data Obtained from Shock-Tube Experiments, edited by A. Ferri, Chap. IX, Pergamon Press, 1961.
8. Evans, M. W. and Ablow, C. M. "Theories of Detonations." Chem. Rev., (April, 1961), 129.
9. Morrison, R. B. A Shock Tube Investigation of Detonative Combustion. Univ. of Mich. Report UMM-97, January, 1952.
10. Lewis, B. and von Elbe, G. Combusion, Flames and Explosions of Gases. New York: Academic Press Inc., (1951), 579-627.
11. Scoriah, R. L. "Thermodynamic Theory of Detonation." J. Chem. Phys., 3 (1935), 425.
12. Siestrunk, R., Fabri, J. and LeGrives, E. Some Properties of Stationary Detonation Waves. Fourth Symposium on Combustion, William and Wilkins Co., Baltimore, 1953.
13. Rutkowski, J. and Nicholls, J. A. Considerations for the Attainment of a Standing Detonation Wave. Proc. Gas Dynamics Symposium on on Aerothermochemistry, Northwestern Univ., August, 1955.

14. Nicholls, J. A., Dabora, E. K. and Gealer, R. L. Studies in Connection with Stabilized Detonation Waves. Seventh Symposium on Combustion, London, Butterworths, Sci. Pub., (1959), 766-772.
15. Gross, R. A. Exploratory Studies of Combustion in Supersonic Flow. AFOSR TN 59-587, ASTIA AD 216 769, 1959.
16. Gross, R. A. "Research on Supersonic Combustion." ARS Journal, 29 (1959), 63.
17. Rhodes, R. P. and Chriss, D. E. A Preliminary Study of Stationary Shock Induced Combustion with Hydrogen-Air Mixtures. AEDC-TN-61-36 (July, 1961).
18. Kirkwood, J. and Wood, W. "Structure of a Steady State Plane Detonation Wave with Finite Reaction Rate." J. Chem. Phys., 22 (Nov., 1954), 1915-1919.
19. Wood, W. and Kirkwood, J. "On the Existence of Steady State Detonation Supported by a Single Chemical Reaction." J. Chem. Phys., 25 (Dec., 1956), 1276-1277.
20. Wood, W. and Kirkwood, J. "Present Status of Detonation Theory." J. Chem. Phys., 29 (1958), 957-958.
21. Hirschfelder, J. O. and Curtiss, C. F. "Theory of Detonations. I. Irreversible Unimolecular Reaction." The J. Chem. Phys., 28 (1958), 1130.
22. Linder, B., Curtiss, C. F. and Hirschfelder, J. O. "Theory of Detonations. II. Reversible Unimolecular Reaction." The J. Chem. Phys., 28 (1958), 1147.
23. Curtiss, C. F., Hirschfelder, J. O. and Barnett, M. P. "Theory of Detonations. III. Ignition Temperature Approximation." The J. Chem. Phys., 30 (1959), 470.
24. Adamson, T. C., Jr. "On the Structure of Plane Detonation Waves." Phys. of Fluids, 3 (1960), 706.
25. White, D. "Turbulent Structure of Gaseous Detonations." Physics of Fluids, 4 (1961), 465.
26. Oppenheim, A. K. and Stern, R. A. Development and Structure of Plane Detonation Waves. Fourth AGARD Combustion and Propulsion Colloquium, Milan, Italy, April, 1960.
27. Fay, J. A. The Structure of Gaseous Detonation Waves. Eighth Symposium on Combustion, The Williams and Wilkins Co., Baltimore (1962), 30.

28. Duff, R. E. "Calculation of Reaction Profiles Behind Steady-State Shock Waves. I. Application to Detonation Waves." The J. Chem. Phys., 28 (1958), 1193.
29. Schott, G. L. and Kinsey, J. L. "Kinetic Studies of Hydroxyl Radicals in Shock Waves. II. Induction Times in the Hydrogen-Oxygen Reaction." The J. Chem. Phys., 29 (1958), 1177.
30. Nicholls, J. A. Stabilization of Gaseous Detonation Waves with Emphasis on the Ignition Delay Zone. Univ. of Mich., Ph.D. Thesis, Feb., 1960.
31. Sommers, W. P. The Interaction of a Detonation Wave with an Inert Boundary. Ph.D. Thesis, The Univ. of Mich., 1961.

Sommers, W. P. and Morrison, R. B. "Simulation of Condensed-Explosive Detonation Phenomena with Gases." Phys. of Fluids, 5, No. 2, Feb., 1962.
32. Campbell, A. W., Malin, M. E. and Holland, T. E. Detonation in Condensed Explosives. Second ONR Symposium on Detonation, Feb. 9-11, 1955.
33. Medard, L. "Dispositif pour l'Arrêt d'une Onde de Detonation du Nitromethane." Memorial des Poudres, 39, 1957.
34. Nahmani, G. and Manheimer, Y. "Detonation of Nitromethane." J. Chem. Phys., 24 (1956), 1074.
35. Voitsekhovskii, B. V. "Maintained Detonations." Soviet Physics Doklady, 4, No. 6. Translated from: Doklady Akad. Nauk SSSR, 129, No. 6 (Nov.-Dec., 1959), 1254-56.
36. Morrison, R. B. and Cosens, G. L. Rotating Detonation Wave Rocket Engine. Paper to be submitted to AIAA.
37. Nicholls, J. A., et al. The Feasibility of a Rotating Detonation Wave Rocket Motor. Univ. of Mich. Quarterly Report 05179-1-P, Aug., 1962.
38. Nicholls, J. A., et al. The Feasibility of a Rotating Detonation Wave Rocket Motor. Univ. of Mich. Quarterly Report 05179-2-P, Dec., 1962.
39. Nicholls, J. A., et al. The Feasibility of a Rotating Detonation Wave Rocket Motor. Univ. of Mich. Quarterly Report 05179-3-P, March, 1963.
40. Adamson, T. C., Jr. and Morrison, R. B. "On the Classification of Normal Detonation Waves." Jet Propulsion, 25 (1958), 400.

41. Adamson. Class notes. Course on "Flame Propagation," 1958.
42. Moyle, M. P., Morrison, R. B. and Churchill, S. W. "Detonation Characteristics of Hydrogen-Oxygen Mixtures." A.I.Ch.E. Journal, 6, (March, 1960), 92-96.
43. Gealer, R. L. and Churchill, S. W. "Detonation Characteristics of Hydrogen-Oxygen Mixtures at High Initial Pressures." A.I.Ch.E. Journal, 6 (Sept., 1960), 501-505.
44. Dunn, R. and Wolfson, B. T. Generalized Equations and Procedures for the Calculation of Detonation Parameters. WADC TN 54-13, March, 1956.
45. Eisen, C. L., Gross, R. A. and Rivlin, T. J. Theoretical Calculations in Gaseous Detonations. AFOSR Report No. TN-58-326, March, 1958.
46. Zeleznik, F. J. and Gordon, S. "Calculation of Detonation Properties and Effect of Independent Parameters on Gaseous Detonations." ARS Journal, 32, No. 4 (April, 1962), 606.
47. Doering, W. and Burkhardt, G. Contribution to the Theory of Detonation (translation from German). Technical Report No. F-TS-1227-IA (GDAM A9-T-46), Wright-Patterson Air Force Base, Dayton, Ohio (May, 1949), 209-219.
48. Zeldovich, Y. B. "Theory of Propagation of Detonations in Gaseous Systems." J. Exper. and Theoret. Phys. (USSR), 10 (1940), 542.
49. von Neumann, J. Theory of Detonation Waves. Progress Report 238, to April 1, 1942, OSRD Report 549, 1942, Ballistic Research Lab. File No. X-122, Inst. for Adv. Study, May 4, 1942.
50. Doering, W. "Uder den Detonationsvorgang in Gases." Annalen de Physik, 43 (1943), 421.
51. Hornig, D. F. Energy Exchange in Shock and Detonation Waves. Tech. Report 4, Frick Chemical Laboratory, Princeton Univ., October, 1962.
52. White, D. R. Structure of Gaseous Detonation. III. Density in the Induction Zone of Hydrogen Detonation. G.E. Research Lab. Report No. 63-RL-3288C, Schenectady, April, 1963.
53. Fay, J. A. "Two-Dimensional Gaseous Detonations: Velocity Deficit." Phys. of Fluids, 2 (1959), 283.
54. Liepman, H. W. and Roshko, A. Elements of Gasdynamics. John Wiley and Sons, Inc., New York, 1957.

55. Gvozdeva, L. G. "The Refraction of Detonation Waves Incident on the Boundary Between Two Gas Mixtures." Soviet Physics, Tech. Phys., 6, No. 6, December, 1961.
56. Shchelkin, K. I. "Two Cases of Unstable Combustion." Soviet Phys. JETP, 36 (9), No. 8, August, 1959.
57. Gordon, S. Private Communication.
58. Belles, F. E. Detonability and Chemical Kinetics: Prediction of Limits of Detonability of Hydrogen. Seventh Symp. (Int'l) on Combustion, Butterworths Scientific Publications, London, (1959), 745.
59. Lewis, B. and von Elbe, G. Combustion, Flames and Explosions of Gases. New York: Academic Press Inc., 1951, Chap. I and II.
60. Clyne, M. A. A. Rates of Some Atomic Reactions Involving Hydrogen and Oxygen. Ninth Symposium on Combustion, Academic Press, New York, (1963), 211.
61. Baldwin, R. R. Comments on Reference 60, p. 218. See also p. 667.
62. Nicholls, J. A. and Dabora, E. Recent Results on Standing Detonation Waves. Eighth Symposium on Combustion, The Williams and Wilkins Co., Baltimore, Md., 1962.
63. Patch, R. W. "Prediction of Composition Limits of Hydrogen-Oxygen-Diluent Mixtures." ARS Journal (1961), 46-51.
64. Gordon, W. E., Mooradian, A. J. and Harper, S. A. Limit and Spin Effects in Hydrogen-Oxygen Detonations. Seventh Symposium on Combustion, Butterworths Scientific Publication, London (1959), 752-759.
65. Breton, M. J. "Recherches sur la Detonations des Mélanges Gaseux." Annales de l'Office National des Combustibles Liquides, 11 (1936), 487-548.
66. Lafitte, P. F. "Flames of High Speed Detonation." Science of Petroleum, IV, Oxford Univ. Press, London (1938), 2995-3003.
67. Hall, C. E. Introduction to Electron Microscopy. McGraw-Hill Book Co., Inc., New York, 1953, Chap. 11.
68. Peachy, L. D. "Thin Sections I. A Study of Section Thickness and Physical Distortion Produced During Microtomy." J. Biophysic and Biochem. Cytol., 4 (1958), 233.
69. Carslaw, H. S. and Jeager, J. C. Conduction of Heat in Solids. 2nd Ed., Oxford Univ. Press. (1959), 87-89.

70. Barrer, R. M. Diffusion In and Through Solids. Macmillan Co., New York (1941), 398.
71. Bird, R. B., Stewart, W. E. and Lightfoot, E. N. Transport Phenomena. John Wiley and Sons, Inc., New York (1960), 363-364.
72. Pearson, K., (Editor) Tables of the Incomplete Γ -Function. His Majesty's Stationery Office, London, 1922.
73. Nicholls, J. A., Morrison, R. B. and Cullen, R. E. Measurements on Gaseous Detonation Waves. Second ONR Symposium on Detonation (1955), 148-163.
74. Kistiakowsky, G. B. and Kydd, P. H. "The Reaction Zone in Gaseous Detonations." J. Chem. Physics, 22 (1954), 1940.
75. Fay, J. A. "A Mechanical Theory of Spinning Detonation." J. Chem. Phys., 20, No. 6 (1952), 942-950.
76. Oppenheim, A. K., Manson, N. and Wagner, H. Gg. "Recent Progress in Detonation Research." AIAA Journal, 1 (Oct., 1963), 2243-52.
77. Lewis, B. and von Elbe, G. Combustion Flames and Explosion of Gases. 2nd Edition, Academic Press, New York (1961), 538.
78. Wagner, H. Gg. Reaction Zone and Stability of Gaseous Detonations. Ninth Symposium (International) on Combustion, Academic Press, New York (1963), 454-460.
79. Wilson, E. B., Jr. An Introduction to Scientific Research. McGraw Hill Book Co., Inc., New York (1952), 272.

